RL-TR-95-181
Final Technical Report
September 1995

BISTATIC CLUTTER MEASUREMENT PROGRAM - PHASE 3

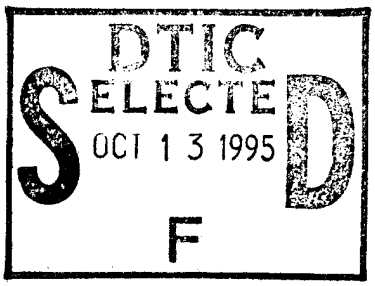

Decision-Science Applications

John Clancy (Decision-Science Applications)
Joseph Len (Syracuse Research Corporation)

APPROVED FOR PUBLIC RELEASE; DISTRIBUTION UNLIMITED.

Rome Laboratory
Air Force Materiel Command
Griffiss Air Force Base, New York

This report has been reviewed by the Rome Laboratory Public Affairs Office (PA) and is releasable to the National Technical Information Service (NTIS). At NTIS it will be releasable to the general public, including foreign nations.

RL-TR-95-181 has been reviewed and is approved for publication.

APPROVED: Robert F. Ogrodnik

ROBERT F. OGRODNIK
Project Engineer

FOR THE COMMANDER: Donald W. Hanson

DONALD W. HANSON
Director of Surveillance & Photonics

If your address has changed or if you wish to be removed from the Rome Laboratory mailing list, or if the addressee is no longer employed by your organization, please notify RL (OCSM) Griffiss AFB NY 13441. This will assist us in maintaining a current mailing list.

Do not return copies of this report unless contractual obligations or notices on a specific document require that it be returned.

REPORT DOCUMENTATION PAGE

Form Approved
OMB No. 0704-0188

1. AGENCY USE ONLY (Leave Blank)	2. REPORT DATE	3. REPORT TYPE AND DATES COVERED
	September 1995	Final Nov 93 - Jan 95

4. TITLE AND SUBTITLE

BISTATIC CLUTTER MEASUREMENT PROGRAM - PHASE 3

5. FUNDING NUMBERS

C - F30602-93-D-0081, Task 2
PE - 63226E
PR - 3540
TA - QF
WU - 02

6. AUTHOR(S)

John Clancy (Decision-Science Applications)
Joseph Len (Syracuse Research Corporation)

7. PERFORMING ORGANIZATION NAME(S) AND ADDRESS(ES)

Prime Contractor:
Decision-Science Applications
1300 Floyd Ave.
Rome NY 13440

Sub-Contractor:
Syracuse Research Corp.
Merrill Lane
Syracuse NY 13210

8. PERFORMING ORGANIZATION REPORT NUMBER

N/A

9. SPONSORING/MONITORING AGENCY NAME(S) AND ADDRESS(ES)

Rome Laboratory (OCSM)
26 Electronic Pky
Griffiss AFB NY 13441-4514

10. SPONSORING/MONITORING AGENCY REPORT NUMBER

RL-TR-95-181

11. SUPPLEMENTARY NOTES

Rome Laboratory Project Engineer: Robert F. Ogrodnik/OCSM/(315) 330-4431

12a. DISTRIBUTION/AVAILABILITY STATEMENT

Approved for public release; distribution unlimited.

12b. DISTRIBUTION CODE

13. ABSTRACT (Maximum 200 words)

Under the Bistatic Clutter Measurement Program, Syracuse Research Corporation designed and performed experiments that collected bistatic clutter from different sources over a variety of terrain types and geometries. This report describes the testing and results of data collection performed in the Florida Keys with the fixed position, aerostat-based, airborne S-band transmitter at Cudjoe Key, and with the moving airborne receiver. Data is reduced to clutter cross sections per unit area (Sigma Zero) values, which are statistically analyzed as a function of out-of-plane angle, transmit grazing angle, receive grazing angle, and terrain type. Testing during this program also used the moving airborne receiver with a moving airborne S-band transmitter (TS-3). The details are covered in a separate report.

14. SUBJECT TERMS	15. NUMBER OF PAGES
Bistatics, Clutter radar cross section, Backscatter, Geometrics, Polarmetric data	240
	16. PRICE CODE

17. SECURITY CLASSIFICATION OF REPORT	18. SECURITY CLASSIFICATION OF THIS PAGE	19. SECURITY CLASSIFICATION OF ABSTRACT	20. LIMITATION OF ABSTRACT
UNCLASSIFIED	UNCLASSIFIED	UNCLASSIFIED	UL

TABLE OF CONTENTS

TABLE OF CONTENTS (Cont.)

LIST OF FIGURES

LIST OF FIGURES (Cont.)

LIST OF TABLES

1.0 INTRODUCTION

1.1 HISTORY, PROBLEM STATEMENT AND OBJECTIVE

As bistatic radar technology progresses, we find that almost all of the same issues facing monostatic radar must be faced by bistatic radar, but with added complications. Receiver design, signal processing techniques, tracking algorithms, interference rejection - all of these must be readdressed for bistatic radar mainly by modifying techniques developed for monostatic radar. In addition, various synchronization problems must be solved in order for the bistatic radar's performance to be optimized.

Under the Adaptive Multimode Bistatics (AMBIS) program, SRC is now developing techniques for moving-baseline bistatic radar operation. Specifically, we have a stationary transmitter and moving (airborne) receiver. A major issue for any airborne radar is non-stationary clutter. In a stationary monostatic or bistatic radar, the clutter does not move (except for some slight internal motion due to wind, for example). This property becomes a primary clutter discriminant. We can therefore use MTI, zero Doppler excision (for coherently-processed, constant-PRF waveforms) and clutter mapping to very effectively control clutter and reduce false alarms and tracks.

When the receiver becomes mobile, our primary discriminant no longer exists, and we must modify our techniques for clutter rejection appropriately. To do this, we need to understand the structure and properties of the clutter. Under the Airborne Surveillance Technology II (AST II) program, SRC developed a detailed clutter simulation. But, while simulations are good, they must be backed up with measured data. Unfortunately, there is very little good bistatic clutter data available, generally, and even less for the frequencies AMBIS normally operates at. This dearth of data is due to the fact that in a bistatic radar, both antennas must be pointed at the same patch of ground to obtain useful clutter data. This has historically been a very difficult task requiring costly solutions. One aspect of previous solutions is the use of cooperative transmitters. This was done to facilitate antenna beam overlap. They also, however, add significantly to the cost of the program.

AMBIS is uniquely qualified to make low-cost bistatic clutter measurements. First, it is non-cooperative. It can be made to synchronize itself to a wide variety of mechanically-rotating radar transmitters. Second, it is able to perform pulse chasing, thus solving the antenna beam synchronization problem. Third, it can be installed in a commercial Cessna 402 aircraft using simple horn antennas mounted in the nose and cabin. Fourth, it is able to semiautomatically collect either raw I, Q data at the output of the A/D converters, or range-Doppler (ambiguity) surfaces of the clutter for complete analysis.

Under previous tasks, SRC has demonstrated the ability to collect calibrated low-cost bistatic clutter data at various bistatic angles and derive a per unit area of clutter cross-section (σ_o) data base to address the diffuse-jammer-multipath or "hot clutter" problem.

If we consider the scenario of Figure 1-1, we see that there is a standoff jammer radiating towards the radar. In addition to the direct path jammer signal, which is received in the radar sidelobes and can presumably be cancelled spatially, the radar will also receive jammer power reflected off the ground into both the radar sidelobes and mainlobe. The power scattered into the radar mainlobe is a potential problem since it can't readily be cancelled. These "hot clutter" levels are, therefore, of great interest, especially those at high bistatic angles. The levels can become very large as the scattering becomes less diffuse and more specular in nature.

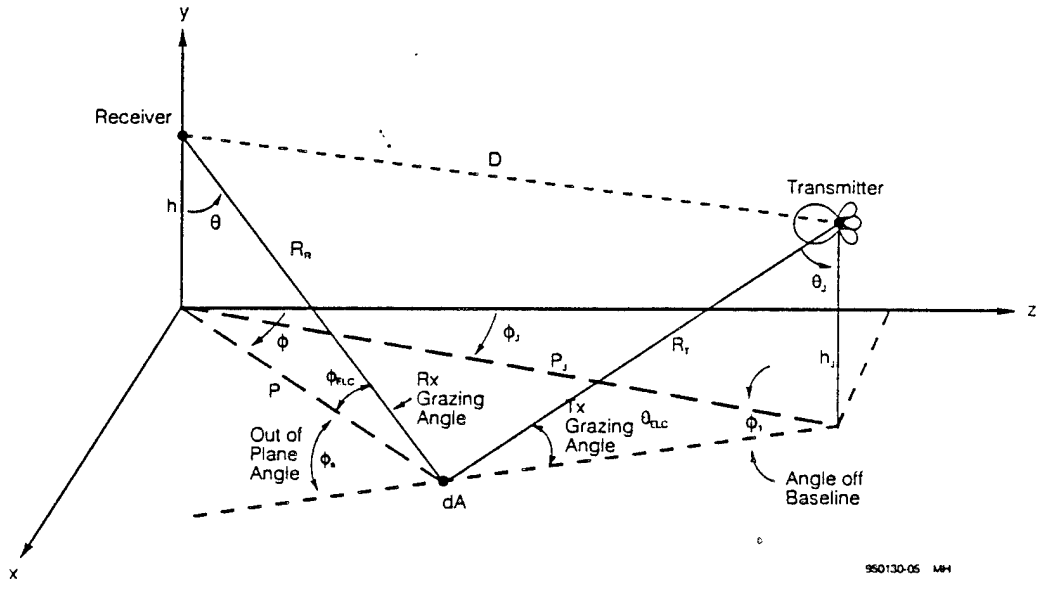

FIGURE 1-1. RELATIVE LOCATIONS OF THE JAMMER AND RADAR

The problem of hot clutter is presently of great interest to the Air Force, and in particular Rome Laboratory. To address this, SRC has collected bistatic clutter data against three sources to provide a data base to evaluate the impact of hot clutter. Two of the sources were ground-based and provided data at only very small grazing angles and had a relatively large uncertainty. The third source, AWACS TS-3, was a moving platform with a highly range ambiguous waveform.

Under this test effort, SRC collected data against SEEK SKYHOOK, an aerostat-borne DPS-5 radar stationed at Cudjoe Key, Florida. SEEK SKYHOOK will be in a fixed position and operate at S-band with a waveform that is not range ambiguous with respect to clutter returns. The data will be non-coherently processed (the radar uses a staggered PRF) and clutter cross sections will be estimated.

2.0 SYSTEM OVERVIEW

2.1 BISTATIC RADAR SUBSYSTEM

This section is an introduction to the development and function of the Bistatic Radar system and a general overview of passive bistatic radars.

Current electronic technology has permitted solutions to many of the traditional shortcomings of bistatic radar surveillance, such that the bistatic radar is comparable in performance to its monostatic counterpart. Some of these technology developments will be presented, as well as some of the advantages and fundamental differences between bistatic and monostatic radars.

A bistatic radar, by definition, is any radar where the transmitter and receiver do not share the same antenna aperture. A non-cooperative bistatic radar can be defined simply as a bistatic radar in which the operator has no direct control over either the operation or availability of the transmitter. The operator of the non-cooperative bistatic radar system must configure the receiver to exploit transmitters that are already radiating for purposes of their own.

The eccentricity of the bistatic radar system is defined by its bistatic angle, with respect to a particular target location. The bistatic angle is the angle formed between two line segments extending from the target to the receiver and from the target to the transmitter.

Bistatic angles vary from zero (monostatic geometry) to 180 degrees (target on the bistatic baseline). The resolution of the bistatic radar in range or Doppler varies inversely with the cosine of half the bistatic angle.

The Bistatic Equivalence Theorem (BET) states the bistatic radar cross section (RCS) of a target can be predicted by evaluating the monostatic RCS at the bisector of the bistatic angle, and at the operating frequency reduced by the cosine of half the bistatic angle. Both theory and experiment indicate that the BET prevails over the entire domain of bistatic angle, except the direction directly along the baseline (the forward-scatter region). However in pulsed waveform applications, this region is typically gated out in the time domain, analogous to T/R gating in a monostatic radar.

Since the inception of monostatic radar, the concept of bistatic radar surveillance has been vulnerable to three criticisms:

1. In order to match the performance of its monostatic counterpart, the bistatic receiver must be supplied with the necessary information to achieve time and phase synchronization with the transmitter.

2. The bistatic receiver is unable to achieve efficient volume surveillance coverage when operating with a directional scanning transmitter.

3. The bistatic receiver uses its antenna pattern once, instead of twice. This creates sidelobe clutter problems, vulnerability to jamming, and difficulties in rejecting sidelobe target echoes.

Most of these objections are countered by operation of the receiver as a non-cooperative sensor, whether or not the transmitter is cooperative. Time, phase, and scan synchronization are all derived by processing the line-of-sight signal from the transmitter. To control interference and multipath, a separate receive channel is dedicated to this function. Otherwise, no additional

hard wiring or broadband communication is necessary to establish complete receiver synchronization. The receiver can realize all of the benefits of coherent signal processing; pulse compression, clutter cancellation, and target Doppler indication. Using an electronically-steered antenna, a single agile receive beam can be continually directed to the point in space where the transmitted pulse is illuminating targets, thus achieving efficient volume coverage. Limitations of the non-cooperative sensor concept include the difficulty of fully synchronizing with transmitters that are either beam-agile or frequency agile.

2.1.1 PRINCIPLES OF BISTATIC RADAR

2.1.1.1 TARGET LOCALIZATION

Figure 2-1 illustrates the non-cooperative bistatic radar (NCBR) concept, where, again, the term "non-cooperative bistatic radar" refers to a system concept where the receiver exerts no direct control over the transmitter. All necessary synchronization and coherent signal information is derived by intercepting the line-of-sight signal from the transmitter. Although the transmitter may be a friendly, or even a dedicated asset, whose parameters are well defined, no auxiliary communication or control is required between transmitter and receiver for proper system operation. Likewise, the non-cooperative sensor employs no atomic clocks or other precision synchronization equipment. By simply receiving the direct-path signal, the receiver can establish time synchronization for bistatic range measurement and phase lock for coherent signal processing.

In the bistatic radar system, the transmitter and receiver are separated by a distance D, called the bistatic baseline. For each transmitted pulse, time begins at the receiver when the pulse is received via line of sight from the transmitter. The passive receiver operates by measuring the target echo delay, relative to the time of arrival of the direct-path signal. The receiver thus measures the quantity (R_1+R_2-D), as shown in Figure 2-2. This places the target on the surface of an ellipsoid that has the transmitter and receiver as foci. The instantaneous transmit azimuth angle is known to the receiver, via scan synchronization.

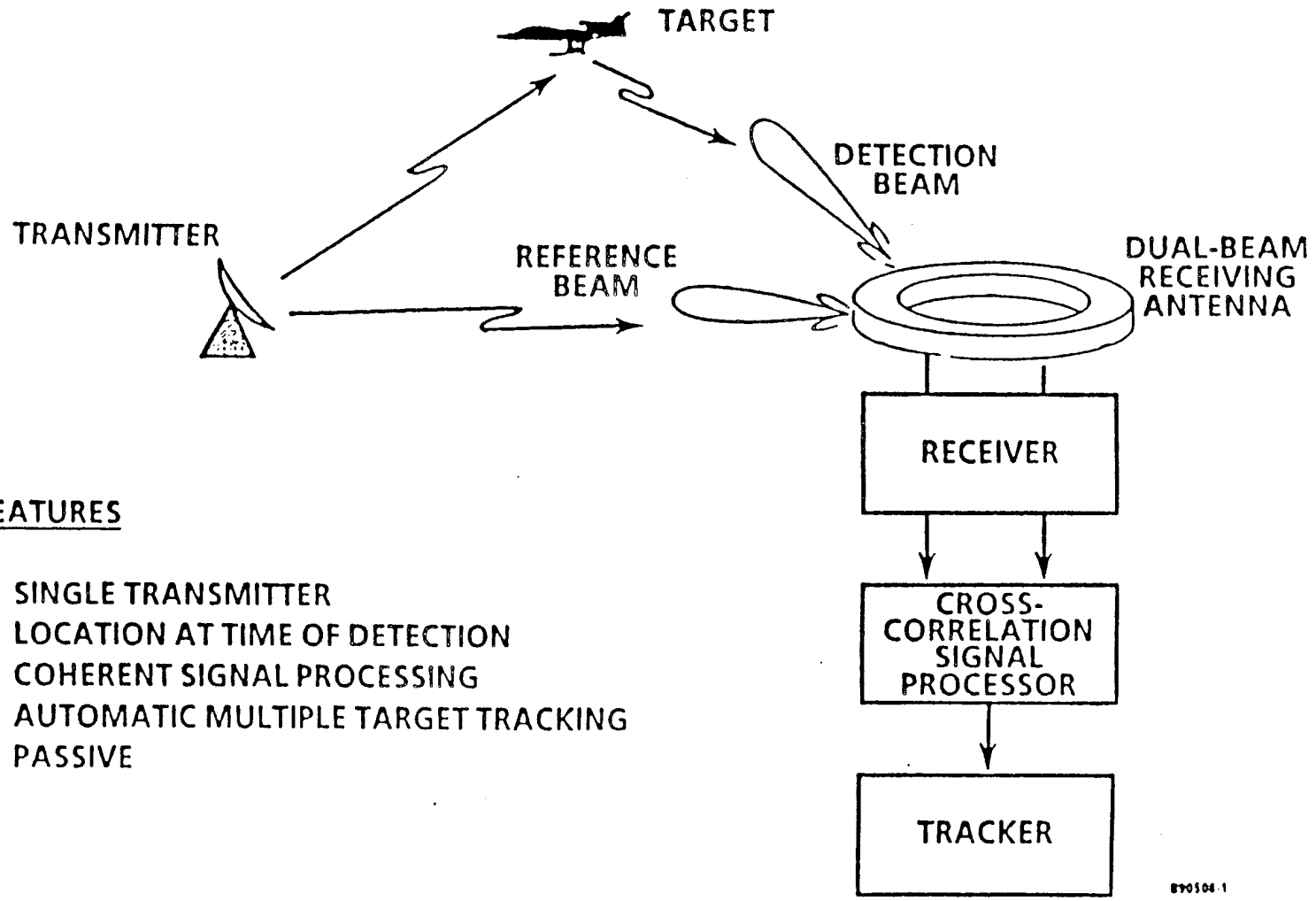

FIGURE 2-1. NON-COOPERATIVE BISTATIC RADAR CONCEPT

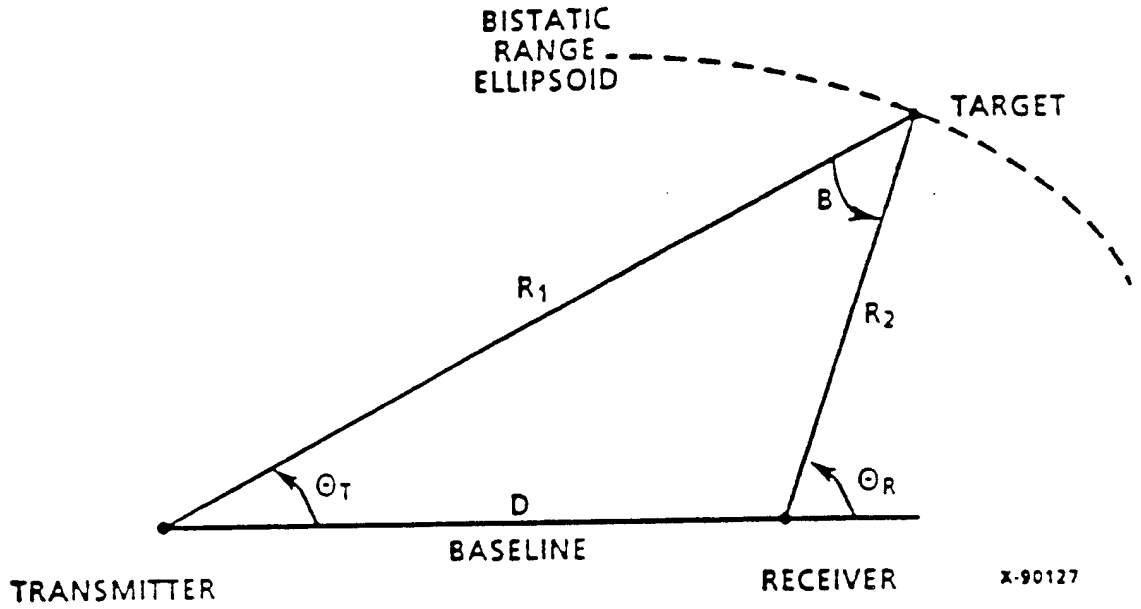

FIGURE 2-2. BISTATIC LOCALIZATION

Knowledge of both the transmitter and receiver location is necessary, to properly localize targets. In non-cooperative operation, it is often the case that the transmitter location is only known approximately; possibly its direction is known, but not its range. If the transmitter is scanning, then the extra information obtained by scan synchronization can be used to solve for the transmitter location, each time a target detection occurs. If not, then the transmitter must be located by some external means.

The angle B in Figure 2-2 is called the bistatic angle, and is a measure of the degree of distortion of the bistatic localization system, relative to that of a monostatic radar. When B is small, the system is near-monostatic, and the baseline is small, compared with the target range. When B is large (near 180 degrees), the target lies near the bistatic baseline. The resolution of the bistatic radar in range or Doppler is given by the monostatic radar resolution, divided by the cosine of half the bistatic angle. Note that as B approaches 180 degrees, range and Doppler resolution become infinite. Bistatic range and Doppler both go to zero along the baseline.

In a conventional radar, the minimum range at which targets can be detected is limited by the radar T/R time, plus whatever time is necessary for the near-range clutter to subside to manageable levels. The monostatic radar detection space is thus a circular annulus. A similar limitation prevails for a bistatic radar, except that the annulus is elliptical, and excludes the entire baseline and some area around it. In other words, normal radar T/R timing typically excludes the regions with large bistatic angles from the coverage. This coverage limitation is of interest because of two peculiarities of bistatic radar operation, that are widely discussed in the technical literature; bistatic radar cross-section enhancement and specular clutter. Both of these are forward-scattering effects that occur near the baseline for large bistatic angles. As such, these effects are excluded by normal radar timing. In bistatic radar surveillance applications neither of these phenomena is considered important; bistatic RCS and clutter cross-sections are generally similar to those encountered by a monostatic radar.

2.1.1.2 SENSITIVITY and COVERAGE

The sensitivity of the bistatic radar is predicted by the bistatic radar range equation:

$$\frac{S}{N} = \frac{P_T G_T}{4\pi R_1^2 L_T} \sigma \frac{G_R \lambda^2 T_I}{(4\pi)^2 R_2^2 KTFL_R} \qquad (1)$$

where:

S/N	=	Pre-detection signal/noise ratio
P_T	=	Average transmit power
G_T	=	Transmit antenna gain
L_T	=	Transmit losses
σ	=	Target cross-section
G_R	=	Receive antenna gain
λ	=	Carrier wavelength
T_I	=	Coherent dwell period
KT	=	Boltzmann noise (= -174 dBm/Hz, at 20 deg C)
F	=	Receiver noise figure
L_R	=	Total receive losses, including signal processing
R_1 , R_2	=	Defined in Figure 2-2

The three terms of the range equation can be associated with the transmitter, the environment, and the receiver. Note that the bistatic equation differs from the monostatic range equation only in the separate definition of the transmit and receive antenna gains and system losses. Also, we have $R_1^2 R_2^2$ rather than R^4.

For a monostatic radar, the contour of constant detection sensitivity is a circle of radius R, centered at the radar. The equivalent contour for a bistatic radar is a curve called an Oval of Cassini, which is obtained when the quantity $(R_1R_2)^2$ is held constant. This contour approaches a circle for short baselines relative to $(R_1R_2)^{1/2}$. As the baseline length increases, the contour becomes elongated, as shown in Figures 2-3 and 2-4, and finally separates into two contours about the transmitter and receiver. The total coverage volume of a bistatic radar can never exceed that of its monostatic counterpart. However, the actual coverage can extend beyond that of the monostatic radar, in certain directions.

2.1.1.3 SIGNAL PROCESSING

To perform coherent signal processing, the bistatic receiver must employ the intercepted transmit waveform as a coherent processing reference. The canonical form of such a signal processor is shown in Figure 2-5. Here, the reference pulse from the transmitter is cross-correlated with the signal from the receive surveillance antenna. The coherent cross-correlation process accomplishes pulse compression and bistatic range gating of the received signal. Phase coherence is also established, to support subsequent Doppler processing and clutter cancellation.

Once the cross-correlation has been successfully accomplished, the remainder of the bistatic receiver, including Doppler processing, detection, and target tracking, is very similar to a monostatic radar. In some respects, the processing fidelity is higher, since most conventional radars do not normally trouble themselves to establish a new processing reference on each transmitted pulse. Pulse-by-pulse synchronization tends to cancel transmitter phase noise, and yield better sub-clutter visibility. The complementary disadvantage is that the bistatic radar is intolerant of distortion in the reference waveform, as might be caused by jamming or local multipath. Usually, if the receiver siting is suitable for a monostatic radar, it will be suitable for minimizing reference signal distortion.

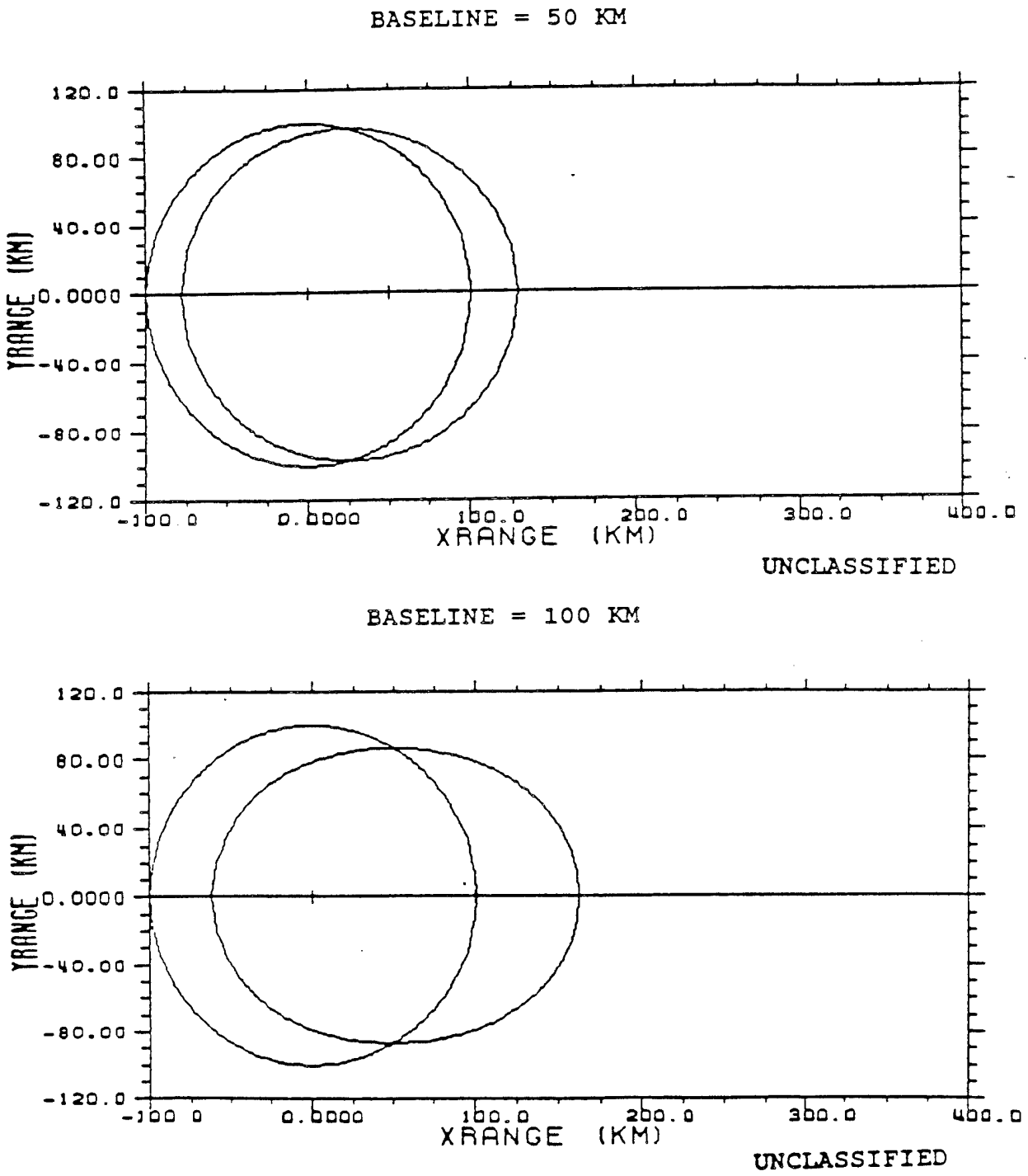

Figure 2-3. (U) Comparison of Monostatic and Bistatic Radar Coverage (Monostatic Range = 100 KM)

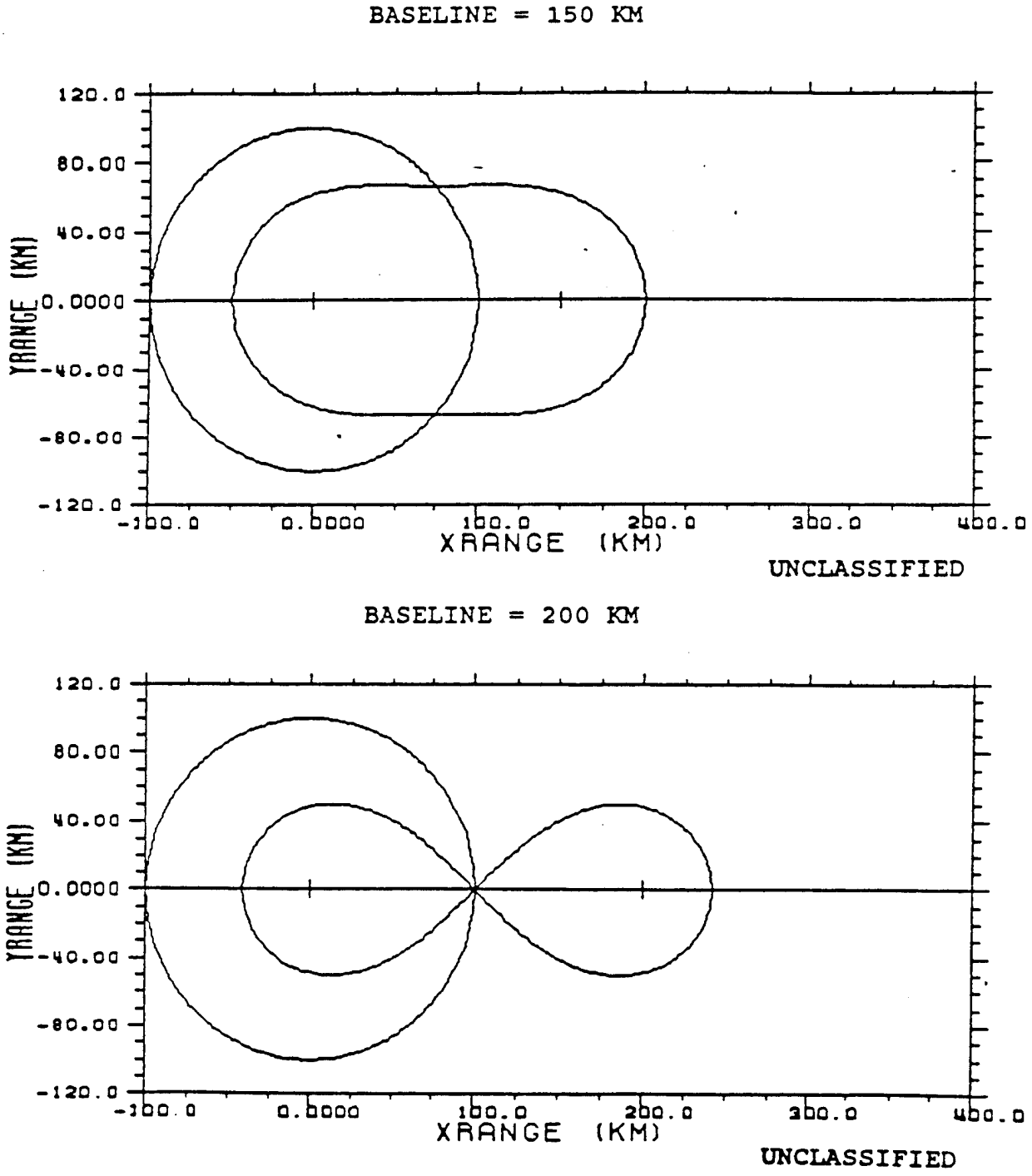

Figure 2-4. (U) Comparison of Monostatic and Bistatic Radar Coverage (Monostatic Range = 200 KM)

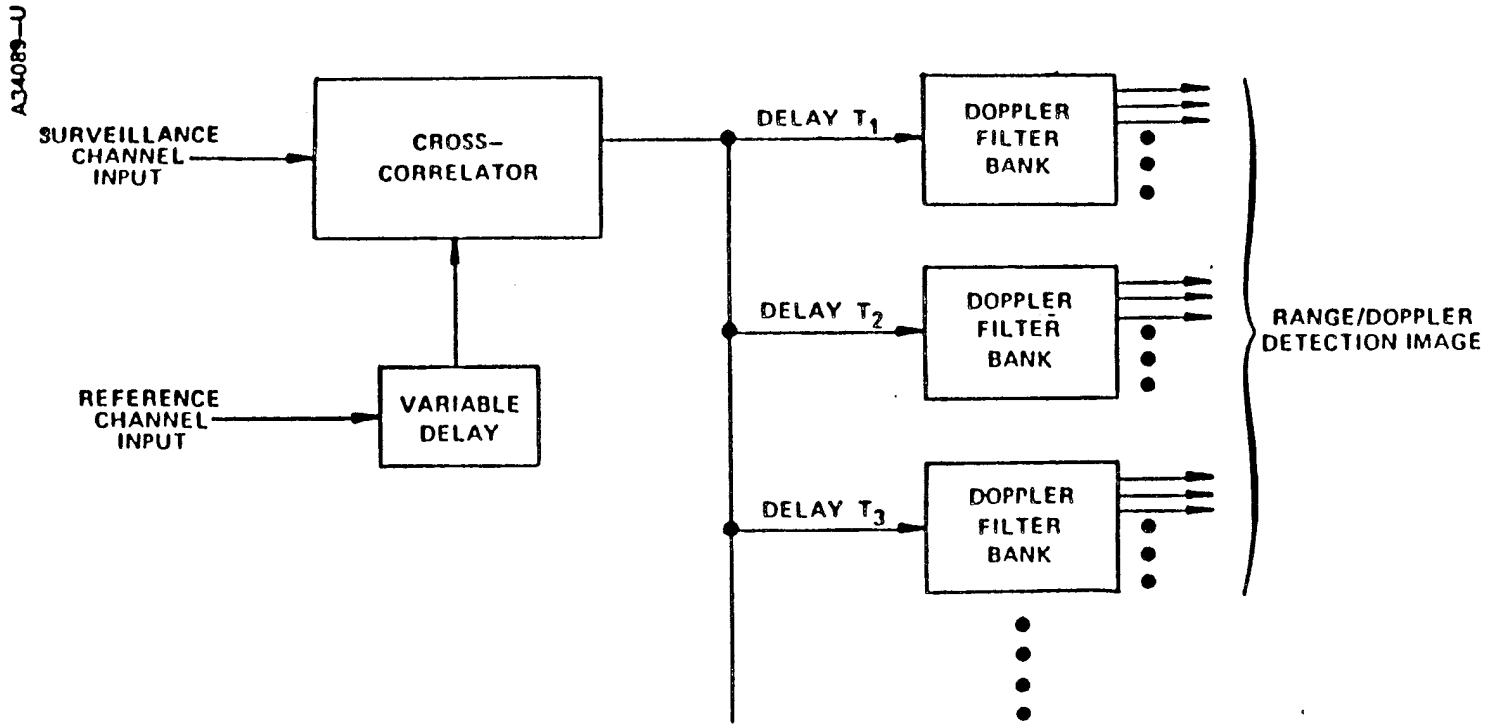

Figure 2-5. (U) Bistatic Radar Signal Processor

In principle, the transmit and receive local oscillators need to be matched only closely enough that the transmitted signal falls within the receiver signal bandwidth; ie., tens of kilohertz. The cross-correlation process is capable of removing these frequency and phase differences. Practical difficulties occur, however, when the receive and transmit oscillators differ by this amount. High-level clutter signals pass through the receiver at non-zero frequencies, and generate Doppler image components in the correlator that are detectable at the output of the signal processor. To control these problems, it is highly desirable that the frequencies of transmitter and receiver track within the Doppler resolution of the system; usually 10 to 100 Hz. In a cooperative system, this amount of synchronization can be achieved with good crystal oscillators, without resorting to atomic clocks.

A non-cooperative sensor must tune to the transmitter frequency in real time, and ordinarily will not achieve a precision better than tens of kilohertz. This means that the receivers must be designed for excellent image rejection, to suppress the clutter images discussed above.

2.1.1.4 SCAN SYNCHRONIZATION

A traditional criticism of bistatic radars is the difficulty of achieving efficient area surveillance using a directional transmitter. Since target detection can occur only at the intersection of the transmit and receive beams, a means must be found for steering the receive beam, in real time, to the exact location of the transmitted pulse. Consider Figure 2-6, which shows a narrow transmit beam illuminating a small part of a desired surveillance sector. Suppose the receiver is processing signals in only one of the indicated receive beam positions. Then target detection can occur only at the beam intersection, a relatively small area. All the rest of the area illuminated by the transmitter is lost.

The simple solution is to employ a floodlight transmitter, possessing 90 degrees or more of azimuth coverage. The receiver can then scan the illuminated surveillance sector without any constraints. However, this approach is very inefficient; at any instant of time, most of the transmitted power is illuminating areas where the receiver is not receiving.

Furthermore, the transmitter power must be increased to compensate for the reduction in transmit antenna gain; possibly by an order of magnitude or more. To correct these problems, a multibeam receiver must be supplied, in order to process the entire surveillance sector simultaneously. This is a very expensive solution, hence an inefficient solution.

The efficient solution is called synchronous beamsteering, or single-beam pulse chasing. Suppose the transmitted waveform has a pulse repetition frequency of 1 kHz, appropriate for a range coverage of 150 kilometers, and the system is operated with a coherent dwell period of 50 milliseconds, or 50 pulses. During the dwell period, the transmit beam of Figure 2-6 will be fixed (or assumed fixed) in the indicated position. As each pulse is transmitted, it will propagate in succession through receive beam positions 1, 2, 3, etc. The times at which the pulse enters and leaves each beam position are known, if the transmit angle and the time of pulse arrival at the receiver are known. The receiver can set up a steering program for its antenna that causes the receive beam to "chase" the transmit pulse down the transmit beam on each transmission. On the next dwell, the scanning transmit beam will have moved to the adjacent transmit beam position for the next 50 pulses. Now, the receive beam schedule is somewhat different, because of the change in transmit beam angle. The precomputed beam steering schedule must, therefore contain a different beam versus time table for each transmit beam angle.

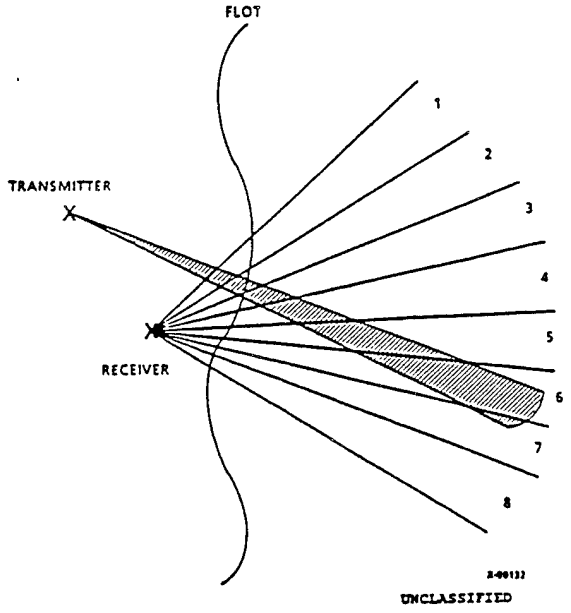

FIGURE 2-6. AZIMUTH COVERAGE

The procedures for implementing this kind of antenna control are relatively simple and well documented. Clearly, the bistatic receiver must be equipped with an electronically steered antenna, since the beam position must change several times during each pulse period. The receiver also requires two real-time control signals, in order to properly address the beamsteering table:

1. Detection of each direct-path pulse as it arrives at the receiver. This is also required for normal signal processor operation, as discussed above.

2. Knowledge of the current transmit beam angle. The receiver must maintain a scan synchronization with the transmitter.

Note that pulse chasing is not possible, unless the receiver can predict the next position of the transmit beam. Such a prediction can be made reliably for most mechanically scanning transmitters. A beam-agile transmitter, however, cannot be synchronized, unless the receiver is informed of transmit angle by some external means, such as cues.

For data collection performed during this task, pulse-chasing was not employed. We are not as concerned with volume surveillance as we are with clutter collection in specific regions. Therefore a wide receive beam is used to stare in one direction while the transmitter beam moves through the covered region.

2.1.1.5 DIRECT-PATH SIGNAL

The direct-path signal is essential in deriving the NCBR coherent processing reference, and in establishing synchronization with directional transmitters. A separate receiver channel, and often a separate antenna beam are dedicated to handling this signal properly. However, the direct-path signal represents a potentially serious source of interference when received in the main surveillance channel of the NCBR. In a pulsed radar application, there is typically no problem in rejecting the direct-path signal, since it is gated out in the time domain, as in a monostatic radar. With high duty cycle or CW transmitters, however, the direct path is present at the same time as the desired target echoes. In these cases, the direct-path signal can be viewed as the largest constituent of the radar clutter.

With a simple calculation, the magnitude of the direct-path problem can be estimated. Consider a bistatic system with the following parameters:

P_TG_T	=	Transmitter effective radiated power (ERP)
λ	=	Carrier wavelength
σ	=	Target radar cross-section
D	=	Bistatic baseline length
R1	=	Range (transmitter to target)
R2	=	Range (target to receiver)

The isotropic direct-path signal level at the receiver is given by:

$$P_{DP} = \frac{P_T G_T \lambda^2}{(4\pi)^2 D^2} \qquad (2)$$

Note that this expression assumes that the full gain of the transmit antenna is directed at the receiver, as would be the case for an omnidirectional illuminator. For a directional transmitter, the main beam will be directed at the target, not the receiver. The isotropic target echo level at the receiver is given by:

$$P_S = \frac{P_T G_T \sigma \lambda^2}{(4\pi)^3 R_1^2 R_2^2} \qquad (3)$$

Therefore, the isotropic ratio of direct-path to desired signal is:

$$\frac{P_{DP}}{P_S} = \frac{4\pi R_1^2 R_2^2}{\sigma D^2} \qquad (4)$$

For a near-monostatic geometry, where the baseline is short compared with the target range, the direct-path/signal ratio can clearly become almost arbitrarily large. For a more ordinary bistatic surveillance geometry, suppose that the baseline and the two range values are all approximately equal. Then:

$$\frac{P_{DP}}{P_S} \approx \frac{4\pi R^2}{\sigma} \qquad (5)$$

In other words, the direct-path/signal ratio is the ratio of the surface area of a sphere whose radius is the target range, to the effective area of the target. For a 0 dBsm target and a range of 100 kilometers, this ratio is 111 dB. Since a 13 to 16 dB signal/interference ratio is needed for detection, the direct-path signal must be suppressed approximately 125 dB in the surveillance receiver if normal detection performance is to be achieved. There are several methods for accomplishing this rejection:

1. Conventional antenna sidelobes: The target signal is received in the surveillance antenna mainlobe, while the direct-path signal is received in the sidelobes. For a typical antenna, a direct-path suppression of 30 dB can be achieved.

2. Sidelobe cancellation: This is a good application for a coherent sidelobe canceller, which effectively creates an antenna pattern null in the direction of the transmitter, for an additional 30 db of direct-path suppression.

3. Signal processing: Since the direct-path signal is neither time- nor Doppler-coincident with the target, the two signals are discriminated by the radar signal processing gain. This gain is the product of the waveform bandwidth and the signal processor coherent integration time, less signal processing losses. For typical radar surveillance systems, signal processing gain varies from 40-60 dB.

Adding up the numbers, it seems unlikely that the desired direct-path suppression will be achieved in the typical situation. Recall that the necessary suppression becomes even greater for shorter bistatic baselines. There are two remaining possibilities for improving the rejection of the direct path. First, the transmitted waveform may have significant intrinsic clutter cancellation capability. Usually, this means that the waveform envelope is highly periodic in the time domain. In this case, the direct path and clutter energy will tend to collect at discrete Doppler frequencies, distinct from those of the target. Second, it may be possible to site the receiver such that a certain amount of horizon diffraction or terrain screening occurs along the baseline. The general conclusion is that siting and terrain may become critical system parameters in high duty cycle situations, where the transmitted waveform is expected to overlap the receiver "on" time.

For this test the direct path was not recorded separately. A single channel was used to record both the direct path signal as well as short time delay clutter or multipath returns. A reference signal was synthesized from direct path data since those tests were performed at close

ranges and significant receiver and transmitter heights so as to minimize any possibility of multi-path corruption. Direct path collection tests were made specifically for the purpose of determining a direct path level which could be used to calibrate out uncertainties in the measurable parameters of the transmitter and receiver. Section 4.1.3.3 describes this procedure in more detail.

2.1.2 PERFORMANCE PREDICTION

In Section 2.1.1.2, the bistatic radar range equation was introduced as the basic rule for defining sensitivity and radar coverage. In this Section, the bistatic range equation will be manipulated to predict performance with non-cooperative radar transmitters.

A monostatic radar performance prediction is made by assembling all of the radar parameters, target characteristics, and loss budgets, to produce an estimate of maximum detection range or tracking accuracy. In general, the performance of the radar can be characterized in fairly simple terms. When conducting the same exercise with a non-cooperative bistatic sensor, a different level of performance must be defined for each of a number of potential host transmitters. Instead of a single maximum detection range, there is a maximum detection range for each transmitter. The issue of coverage is an additional complication. For any level of performance, the monostatic radar coverage is ideally a circular annulus, centered at the radar. At the same level of performance, the coverage of the bistatic sensor is completely dependent on the relative siting of transmitter and receiver. Thus, the performance predicted for a bistatic sensor will be restricted to a particular host transmitter and a particular geometry. A compromise approach will be to compute coverage for each transmitter in a monostatic geometry, thus deferring the geometry question until some specific siting is to be analyzed.

2.1.2.1 BISTATIC RANGE EQUATION

The bistatic radar range equation presented in Section 2.1.1.2 can be expressed in an altered form, as follows:

$$R_1^2 R_2^2 = \frac{P_{AV} G_T}{4\pi L_T} \sigma \frac{A_R T_I}{4\pi (S/N) KTFL_R} \qquad (6)$$

and, to eliminate bistatic geometry, an equivalent monostatic range can be defined:

$$R_0^4 = \frac{P_{AV} G_T T_I}{L_T} \frac{\sigma}{(4\pi)^2 KT} \frac{A_R}{(S/N) F L_R} \quad (7)$$

where:

P_{AV}	=	Average Transmit Power
G_T	=	Transmit Antenna Gain
T_I	=	Coherent Integration Time, or Dwell Period
L_T	=	Transmitter Losses
KT	=	Boltzmann Noise (-174 dBm/Hz, at 20 deg C)
σ	=	Target Cross-Section
A_R	=	Effective Receive Antenna Aperture
S/N	=	Minimum Signal/Noise Ratio for Detection
F	=	Receiver Noise Figure
L_R	=	Receiver Losses

The dwell period is usually established by the transmitter, and is the amount of time that the scanning transmit beam can be expected to illuminate a point target. The average transmit power and the dwell period can be rewritten as follows:

$$P_{AV} = P_P T_P (PRF) \quad (8)$$

and where:

$$T_I = \frac{T_S B}{360} \quad (9)$$

P_P	=	Peak Transmit Power
T_P	=	Transmit Pulse Width
PRF	=	Pulse Repetition Frequency
T_S	=	Transmit Antenna Scan Period
B	=	Transmit Antenna Azimuthal Beamwidth

and, the final version of the range equation becomes:

$$R_0^4 = \frac{P_P G_T T_P (PRF) T_S B}{360\ L_T} \frac{\sigma}{(4\pi)^2 KT} \frac{A_R}{(S/N) F L_R} \tag{10}$$

The three terms of this equation can be viewed as a transmitter figure of merit, a receiver figure of merit, and a term involving target cross-section and some constants. This is a handy representation; a single receiver can be evaluated with respect to a number of potential host transmitters, simply by computing new transmitter figures of merit. Note that the transmitter figure of merit has units of energy, and could be viewed as available detection energy from the transmitter.

2.2 ESM SUBSYSTEM

There is an ESM subsystem which monitors the electromagnetic environment in the radar bands of interest. For radar signals, it then estimates a number of radar parameters including pulsewidth, PRI and scan time. This is useful when searching for unknown illuminators or for determining if a known illuminator is on the air and strong enough for radar use. The ESM subsystem played only a minor role in the clutter data collection.

2.3 NAVIGATION SUBSYSTEM

The navigation subsystem consists of an on-board Global Positioning System receiver and compass. The GPS receiver provides both position (latitude, longitude, altitude) and time reference to the radar system. The compass provides heading information. Taken together, the position and heading information is used by the system to perform beamsteering and real-time target location. The navigation data is sent to the radar approximately every one second.

2.4 INSTALLATION DESCRIPTION

The AMBIS equipment is installed in a Cessna 402B aircraft owned and operated by Griffiss Aero Club. The general setup is illustrated in Figure 2-7. The AMBIS hardware is contained in three racks as shown. These are connected via switch to three L/S - band horn antennas and one 50 ohm load. The coverage of the antennas is shown more clearly in Figure 2-8. Two horns are mounted in the nose of the aircraft and cover approximately ±-22 to 67.5° relative to nose-on. Antenna 2 is located inside the aircraft and points out the starboard window, covering 45° - 135° off of nose-on.

A photograph of the Cessna is given in Figure 2-9. The AMBIS equipment, mounted in the Cessna is shown in Figure 2-10. The nose-mounted antennas are shown in Figure 2-11 and the side antennas are shown in Figure 2-12.

2.5 I-Q DATA RECORDER SUBSYSTEM

The I-Q Data/Recorder Subsystem is a single 6U x 220 VME wire wrap board which receives data and control signals from the Bistatic Radar subsystem and GPS time information from the time-frequency processor board.

The software which controls the execution of data collection runs on a Radisys PC (486 processor) connected to the I, Q data recorder subsystem via the VME backplane. The processor has both an 80 Mbyte and 40 Mbyte hard disk which are used to store the recorded data.

The recording system is configurable by operator selection during execution or by software changes which require compilation prior to being executed. Data collection is specified by transmitter scan position, number of pulses, and number of samples between pulses (time delay relative to transmitted pulse).

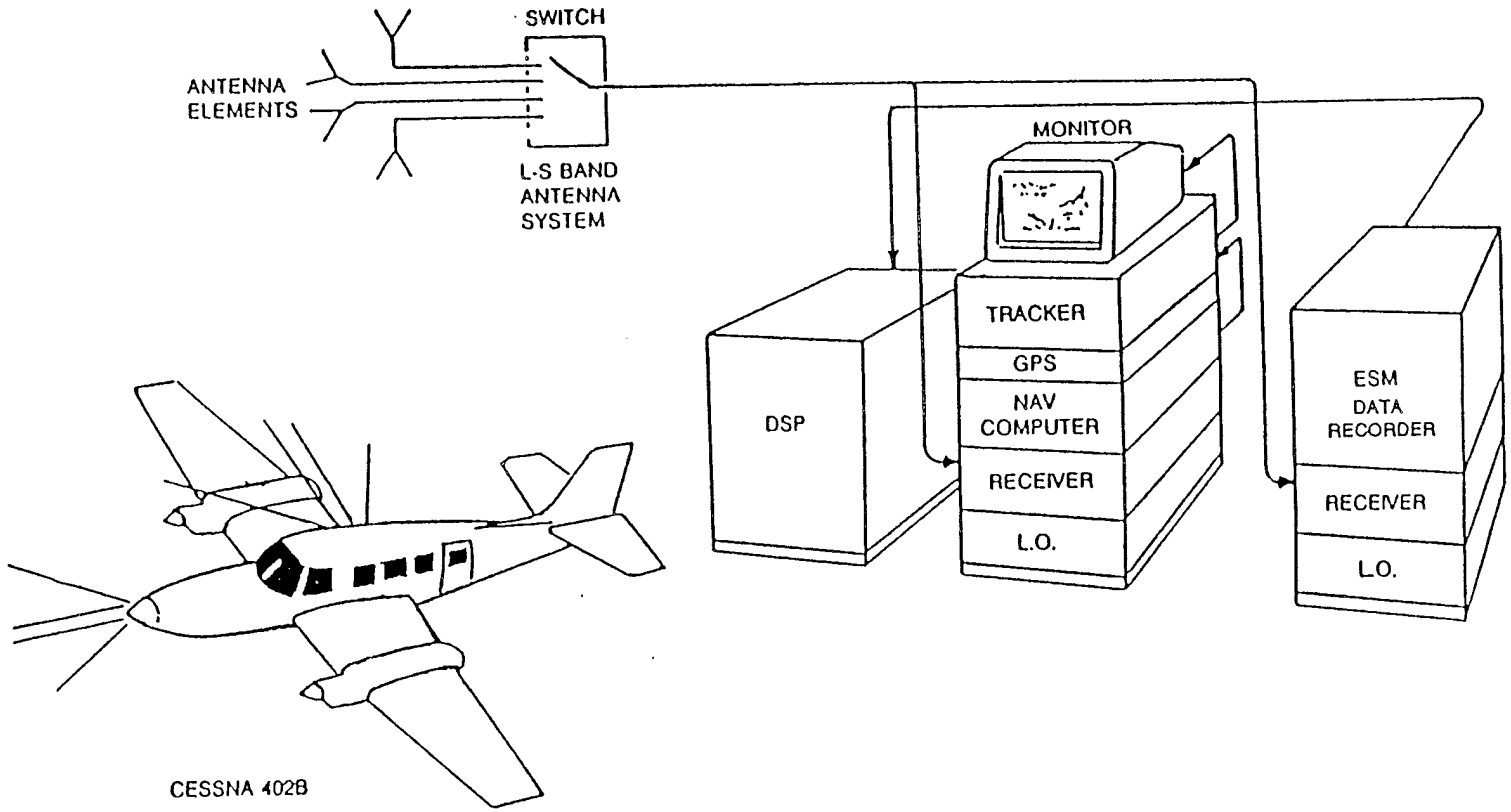

FIGURE 2-7 AMBIS AIRBORNE TEST SETUP

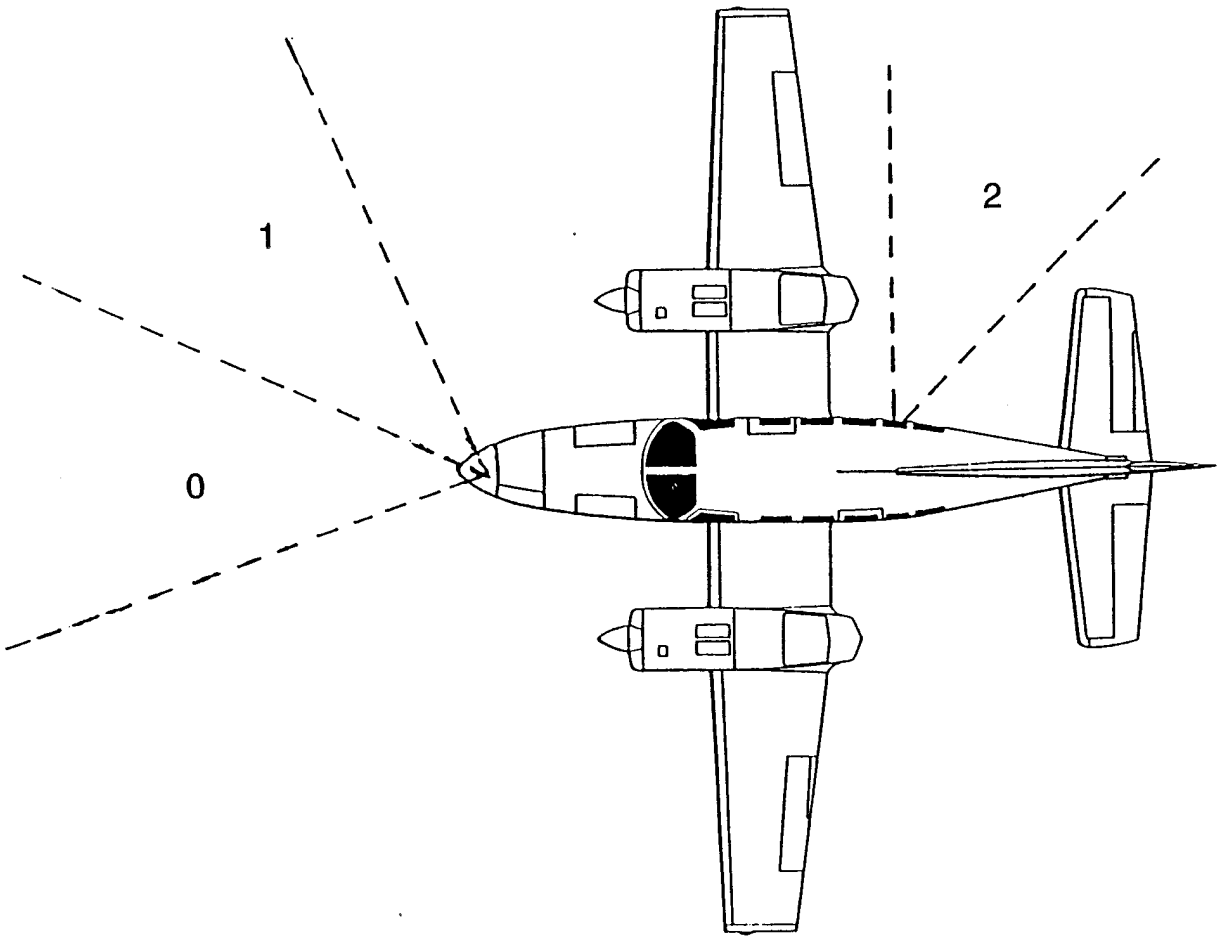

FIGURE 2-8 CESSNA ANTENNA ARRANGEMENT CUDJOE KEY FLIGHTS

FIGURE 2-9 CESSNA 402B AIRCRAFT

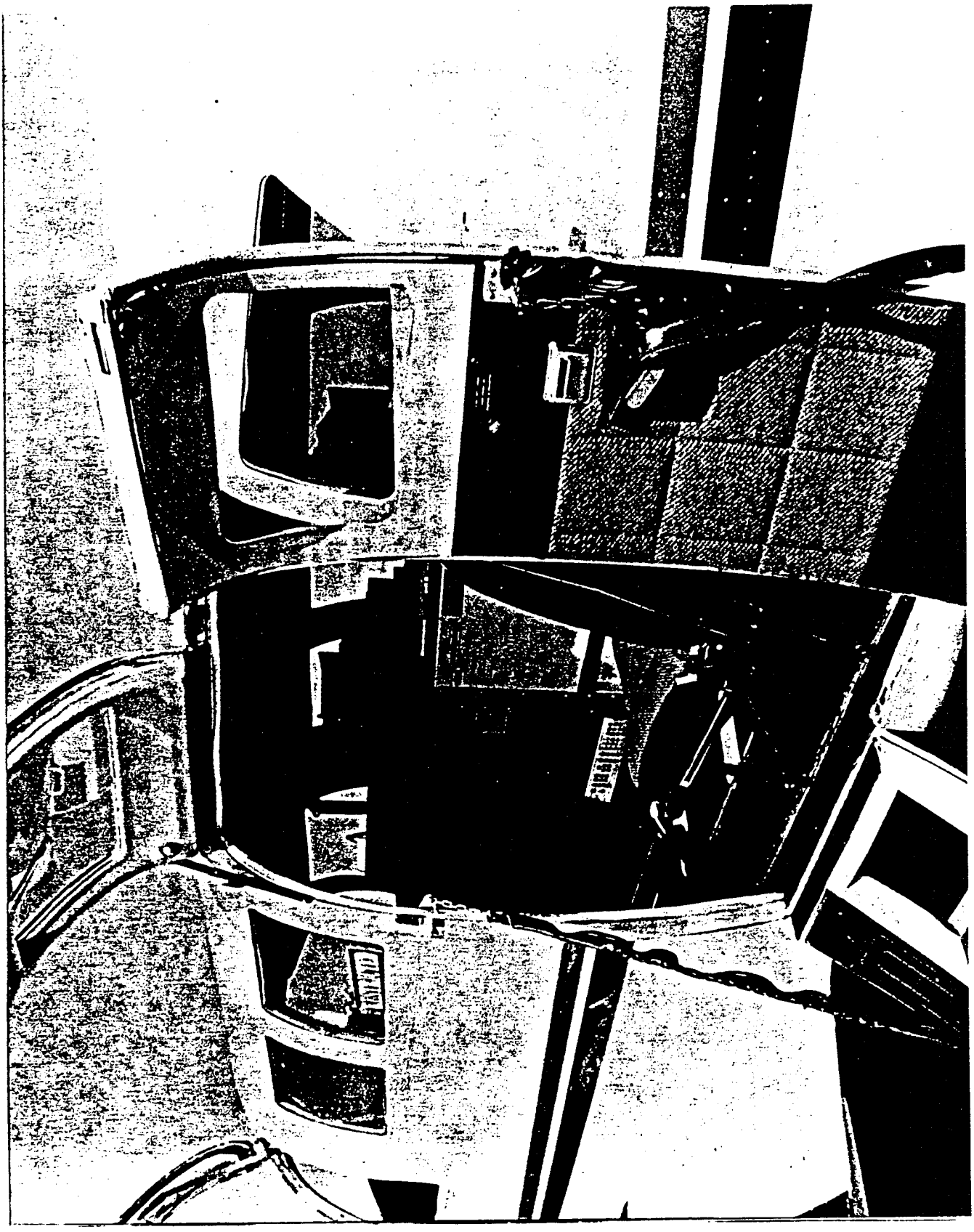

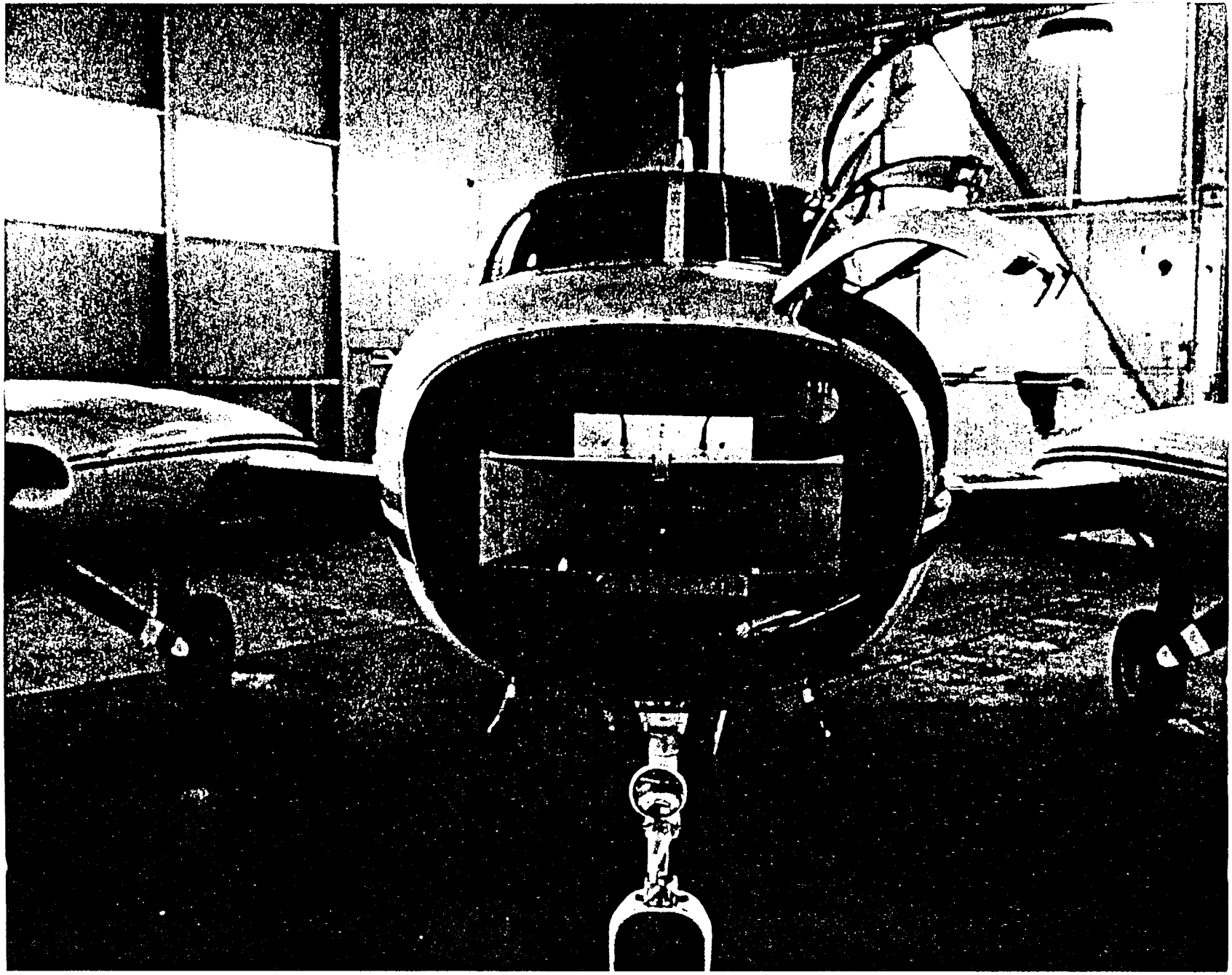

FIGURE 2-11 NOSE-MOUNTED AMBIS HORN ANTENNA

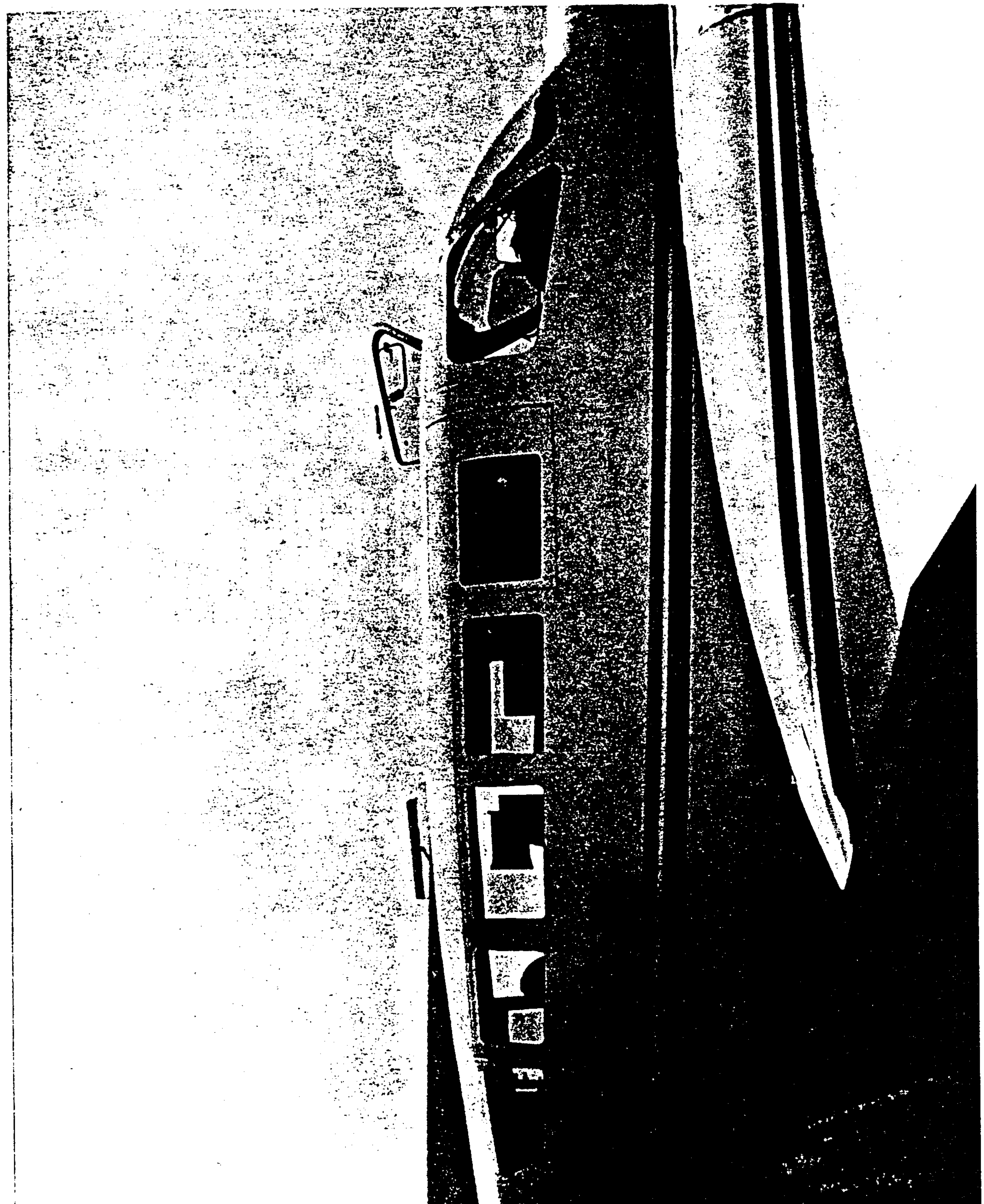

The collection system operates in one of two modes; continuous or gated. Continuous mode simply collect an entire buffer of data (32K 32-bit samples) at the system sampling rate the moment the selected angular region is reached. Gated mode collects a specified number of pulses (programmed in PROM M.T.), with each pulse containing an operator selectable number of samples (time delay or bistatic range). The pulses will be continuous as long as the total amount of data (pulses * samples) does not exceed the buffer size described above. The angular region is specified by an azimuth starting angle and duration (the angle is the transmitter pointing angle relative to the baseline).

The I-Q recorder board contains independent 23K 16-bit FIFO's which collect data from the I and Q A/D converters. When the desired amount of data has been collected, the FIFOs are read and the data written to a file on the hard disk. The I-Q recorder is then M.T. ready to collect the next set of data. Each of these FIFO writes to disk are considered a block of data. The operator selects the number of blocks to be written to a single file. The time of the start of collection for each block is latched into an onboard register. After writing the block of data to disk, the time is decoded and stored in a buffer. After an entire file has been recorded the times for all blocks in the file are written as a header to that file.

3.0 BISTATIC CLUTTER

3.1 DESCRIPTION

Bistatic clutter can be characterized by its per unit area cross section σ_0, just as monostatic clutter. The bistatic radar cross section is therefore $\sigma_c = \sigma_0 A_c$ where A_c is the clutter cell area. In a monostatic radar, σ_0 depends upon the incidence angle for a given frequency and terrain. In a bistatic radar, the situation is more complex. The value of σ_0 will depend upon the incidence angles relative to both the transmitter and receiver as well as the out-of-plane angle. These are denoted by θ, θ_j, and ϕ_s in Figure 1-1. In particular, we are interested in the clutter as the out-of-

plane angle approaches 0°. In this case, the clutter is becoming more and more specular, depending upon the terrain. This will typically be the worst-case clutter. An example of σ_0 vs. out-of-plane angle is given in Figure 3-1. Notice that σ_0 is relatively flat over much of the range of out-of-plane angles surrounding monostatic (out-of-plane angle = 180°). It does peak up about 20 dB as you approach the specular scattering geometry (out-of-plane angle = 0°). This is a region of interest for modeling.

A general picture of the bistatic clutter geometry is given in Figure 3-2. Three regions can be defined. The mainbeam - mainbeam clutter region occurs where the mainbeams of both transmitter and receiver overlap on the ground for an illuminated range cell. The mainbeam sidelobe region occurs where the mainbeam of the receiver intersects the ground range cell that the transmit sidelobes are illuminating. The sidelobe - sidelobe region comprises the rest of the range cell. For a properly designed receive antenna, there should be no ground region illuminated by the transmitter which is not also illuminated by the receiver. This is true for our tests, in which the receive antenna beams are quite large: ≈45°.

Bistatic Clutter Data

Referring back to Figure 2-5, we see that the output of the signal processor is a range / Doppler detection image which can be thought of as an estimate of the ambiguity surface for the radar waveform. It extends approximately from 0 to PRI * (3 x 10^8 m/s) in bistatic range and from 0 to PRF in Doppler. The amplitude values of this image were the data being collected under previous tasks. A typical airborne bistatic clutter data plot is shown in Figure 3-3. This is data collected using the Remsen ARSR-60M as a transmitter. A number of distinguishing features can be observed. The surface estimates the ambiguity function for the lowest bistatic ranges (0-143 km) and all of Doppler (16 cells), normalized to show clutter-plus-noise-to-noise (C+N)/N ratios in dB. The peak response for any given range is due to mainbeam-mainbeam, mainbeam-sidelobe and sidelobe -sidelobe clutter, as well as sample rate-PRF mismatch modulation sidelobes, and various correlator products.

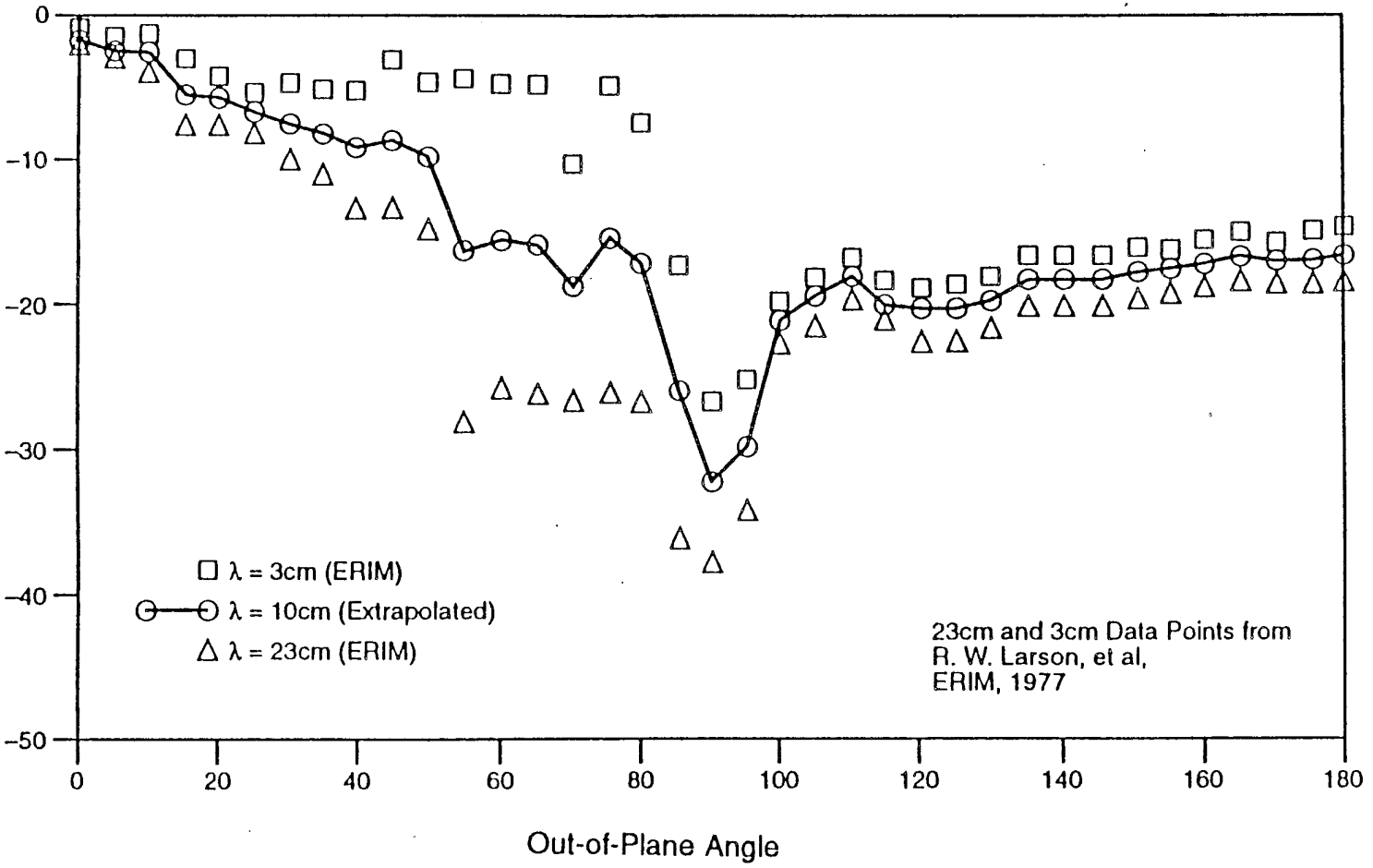

Figure 3-1. Out-of-Plane Angle Dependence of Mean Clutter Cross Section per Unit Area for Tall Weeds and Scrub Trees (HH Polarization) When $\theta = \theta_J = 1.4$ Radian (80°)

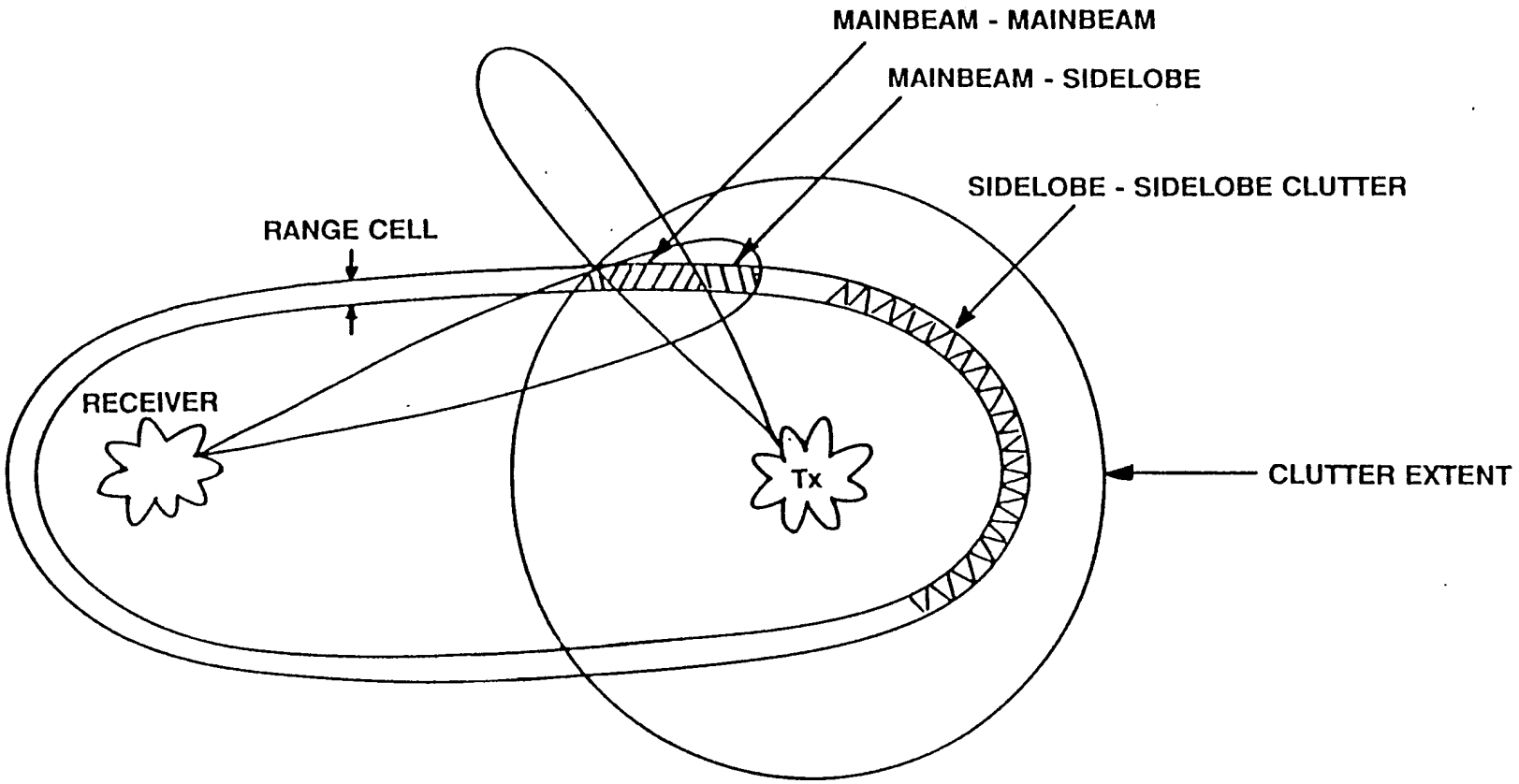

Figure 3-2. Bistatic Clutter Geometry

910905-28

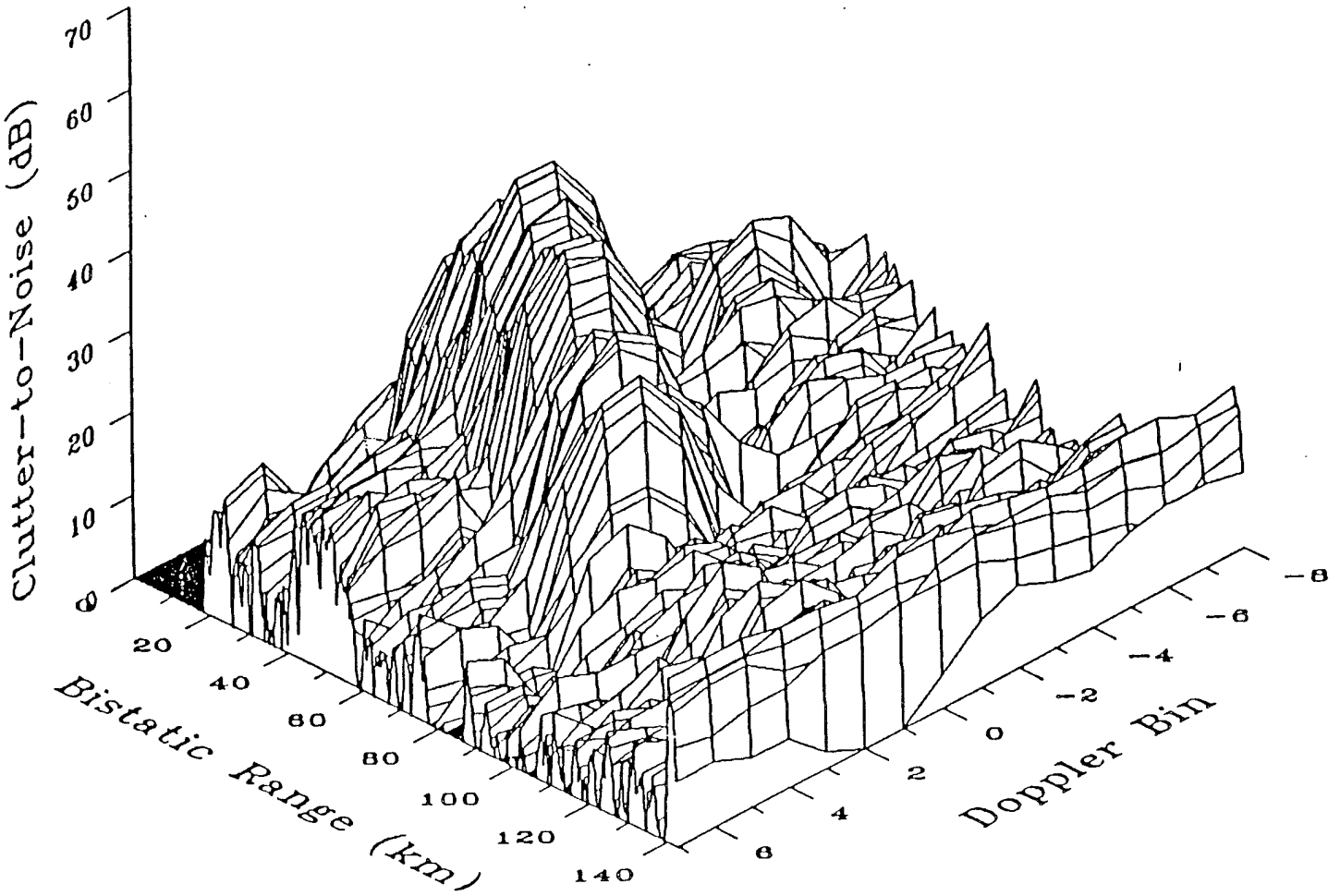

Figure 3-3. Bistatic Clutter Data

930922-03 MH

CDC NUMBER: 11218

Notice that the peak Doppler response changes somewhat with range. This is a consequence of the moving baseline geometry. In general, the Doppler of mainbeam clutter will be a function of range. It will also be a function of angle and aircraft velocity. Figure 3-4 shows contours of constant range (ellipses) and Doppler (hyperbolae) for a geometry where the receiver is located at the right-hand focus of the ellipses and moving in a roughly southwesterly direction. The transmitter is located at the other focus of the ellipses.

For this effort we are collecting data at the output of the A/D converters. Had the transmitter not been using a staggered waveform, processing would have produced plots similar to Figure 3-3. However, since a staggered PRF is transmitted, Doppler processing is not performed. Instead, non-coherent integration over 16 pulses is performed to result in a series of amplitudes corresponding to increasing bistatic range. Figure 3-5 shows a sample of processed data (CNR) collected during this effort. Figure 3-6 shows pictorially the location of the lettered portions (A, B, C, D) of the CNR plot. The direct path arrival is denoted A. The signal is received through the sidelobes of the receiver horn (hence its apparent low level). Locations B and D approximate the 3 dB beamwidth limits of the receive horn. Location C shows the transition point of terrain from Gulf (water with wave heights under 4 feet) to Everglades.

The clutter level drops off quickly after the direct path arrival as evidenced from cells 1 to 10. The terrain from cell 10 to 130 is homogeneous (Gulf-wave heights less than 4 feet). This clutter increases as the pulse approaches the front edge of the 3 dB to receive beamwidth. Antenna pattern attenuation has a more dominant effect on the received signal than the attenuation due to increasing range. However, at the coast line (transition point C) there is a significant increase in clutter level. The rougher surface of Everglades terrain scatters more energy back toward the receiver, hence the increased levels of CNR. Finally we see antenna pattern attenuation dominate the returns after point D until the return clutter signal is masked by noise around cell 200.

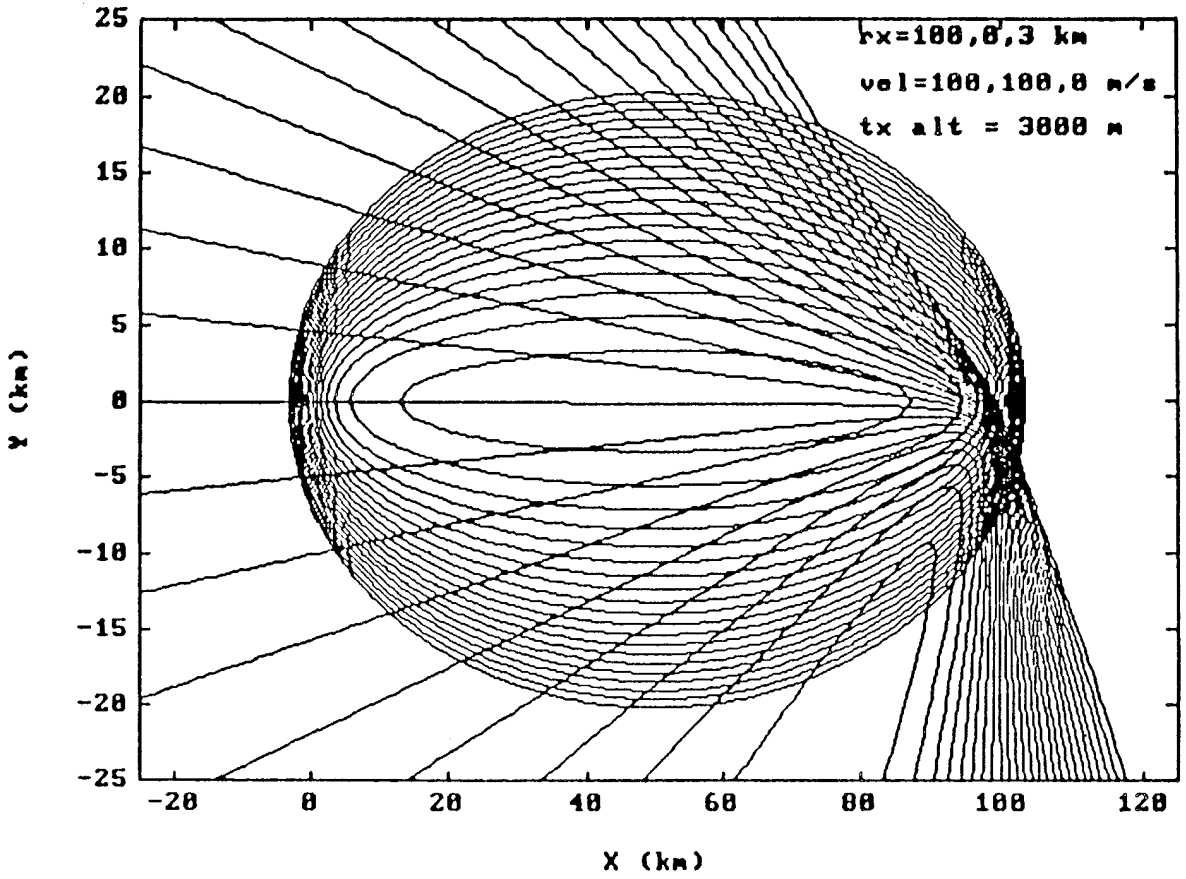

FIGURE 3-4. CONTOURS OF CONSTANT BISTATIC RANGE - DOPPLER

931020-01 MH

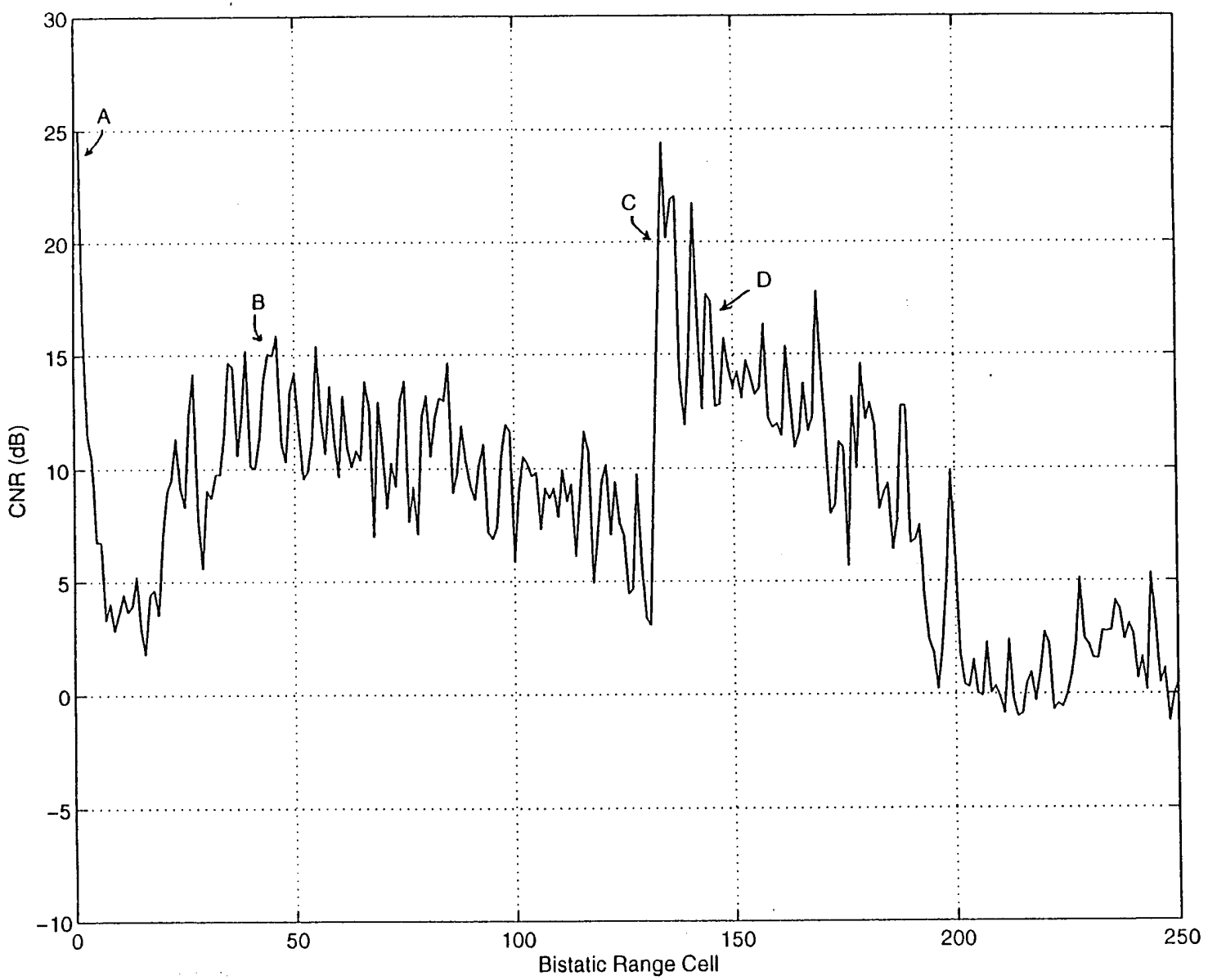

FIGURE 3-5 CUDJOE KEY TEST, GULF PROFILE 1, FILE 3, BLOCK 35, 11-10-94

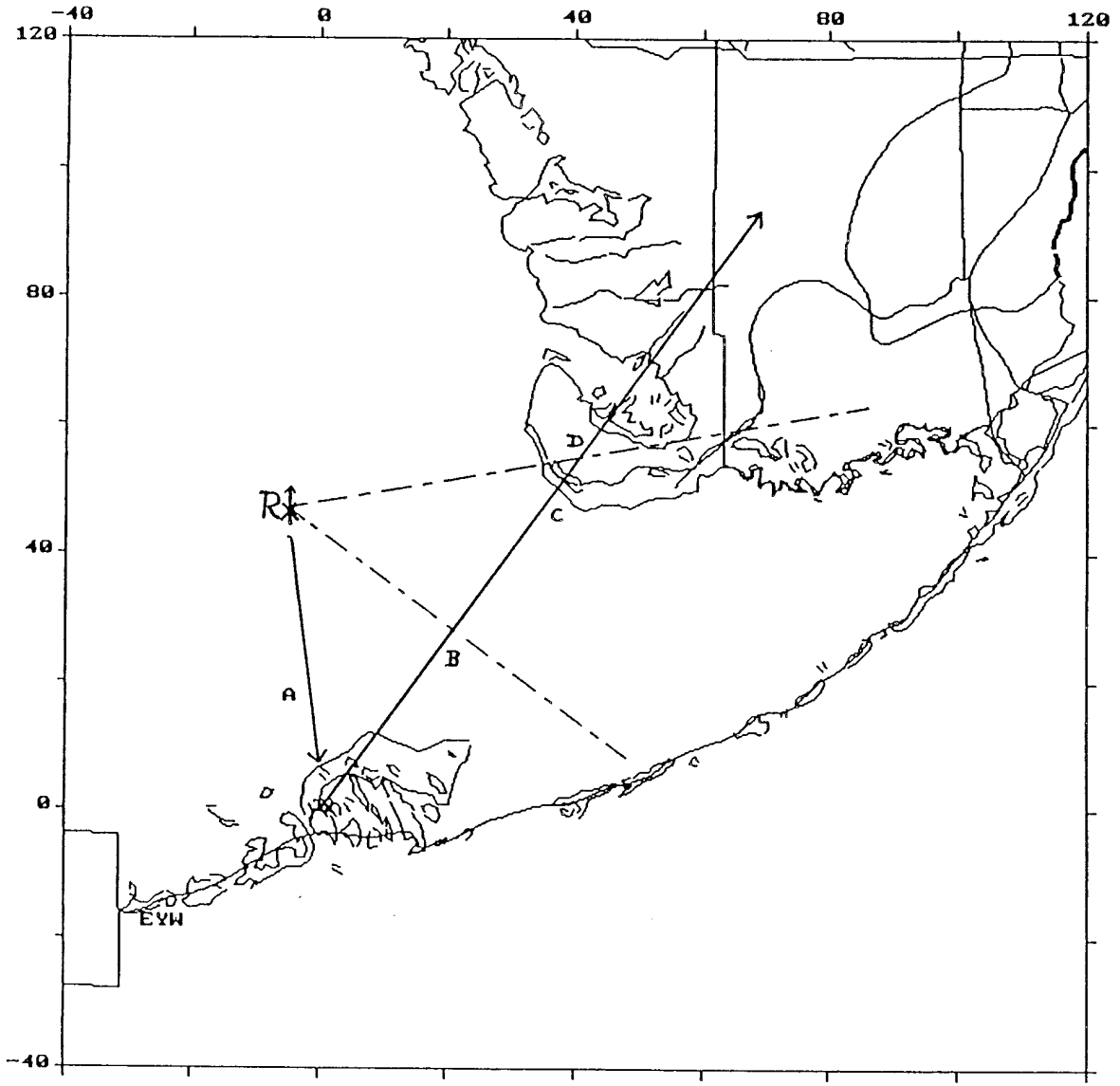

FIGURE 3-6 CUDJOE KEY TEST, GULF PROFILE 1, FILE 3, BLOCK 35, 11-10-94

4.1 TEST DESCRIPTIONS

4.1.1 GENERAL OVERVIEW

The Bistatic Clutter Data Collection Tests performed in the Florida Keys area took place November 10-13, 1994. Data were collected over a variety of terrain types; water (wave heights 0'-4' and 4'-8'), everglades, and keys. The data were collected at a variety of out-of-plane angles. Flight profiles were chosen to provide a significant amount of data from similar terrain types and angles of interest to allow statistical analyses to be performed. The tethered aerostat based at Cudjoe Key was used as the transmitter and SRC's AMBIS testbed, mounted in a Cessna 402B, was used as the receiver.

The program objective is to characterize the terrain in terms of a clutter cross section per unit area (Sigma Zero). The recorded signal levels are combined with the bistatic radar range equation to yield the clutter cross section. The area of the bistatic range cell is then computed. The cell is defined in azimuth by the dwell time and the transmitter scan rate (approximately equal to the transmitter azimuth beam width), and in range by the A/D sampling rate of the receiver. Statistics can then be computed for the data. The results are categorized by terrain type, C/N ratio, grazing angles, and out-of-plane angles.

The test scenario uses the airborne tethered transmitter and airborne moving receiver for the bistatic data collection system. The aerostat contains an S-band transmitter with a 12 second scan rate, staggered PRF, and 1.2 μsec pulse width. Three fixed receiver horns are mounted in the Cessna. Two in the nose (one centered at zero degrees relative to the nose and the second at 45 degrees), and the third horn is mounted on the equipment racks, looking out the Cessna window, centered at 112.5 degrees. Data is recorded at 750 KHz, with 256 samples collected for each PRI. The recording system is set up to collect 128 consecutive PRIs during each scan for a period of 50 scans. An onboard GPS is used to record the receiver position during the tests. Nominal heights during the testing were 10000 feet for both the transmitter and receiver.

Two flight profiles were used. The first consisted of a north-south racetrack flown over the Gulf of Mexico due north of Cudjoe Key. The second was a northwest-southeast racetrack flown over the Florida Straits to the southeast of Cudjoe Key. Multiple loops around the racetrack were flown in a clockwise direction. Terrain data collected from the Gulf profiles consists of GULF (wave heights 0'-4'), and GLADES (Everglades). Terrain data collected from the Ocean profiles consists of OCEAN (wave heights 4'-8'), and KEYS. Two flights were made of each profile; both Gulf profiles were flown on November 10; Ocean profile 1 was flown on November 11; and Ocean profile 2 was flown on November 13. The flight profiles are shown in Figures 4-1 through 4-4.

Fourteen data files were to be recorded during each profile. Ten files containing clutter data, two files containing noise data and two files of data used to compensate for the DC offset of the A/D Converters. Four files were recorded during each full loop of the racetrack, two on each leg. Since the receiver equipment required a warm-up period, the profile commenced at the point furthest away from the transmitter. The first Noise and DC Offset data files were recorded during the transition to the starting point. Eight different files were recorded during the first two racetrack loops, with the transmit angle and receive horns being varied for each file. The last inbound leg of the profile repeated the first data file collection for the ninth file and then collected direct path data in the tenth file for calibration. This required a three leg maneuver at the end of the final leg in order to ensure that the transmit beam was in the main lobe of each receive antenna. The profiles in Figure 4-1 - 4-3 display these maneuvers. Finally, second Noise and DC offset files were recorded during the Cessna's return to base.

The data files collected during the Gulf profiles contain 50 scans of data, while the files collected during Ocean profiles contain only 40 scans. This was due to the fact that the Cessna approached the US ADIZ at the southeast portion of its leg and was ordered to terminate the profile at that point. The collection time could not be lengthened by slowing the Cessna since is was already traveling close to its minimum allowable air speed. Table 4-1 displays a summary of the missions during the test.

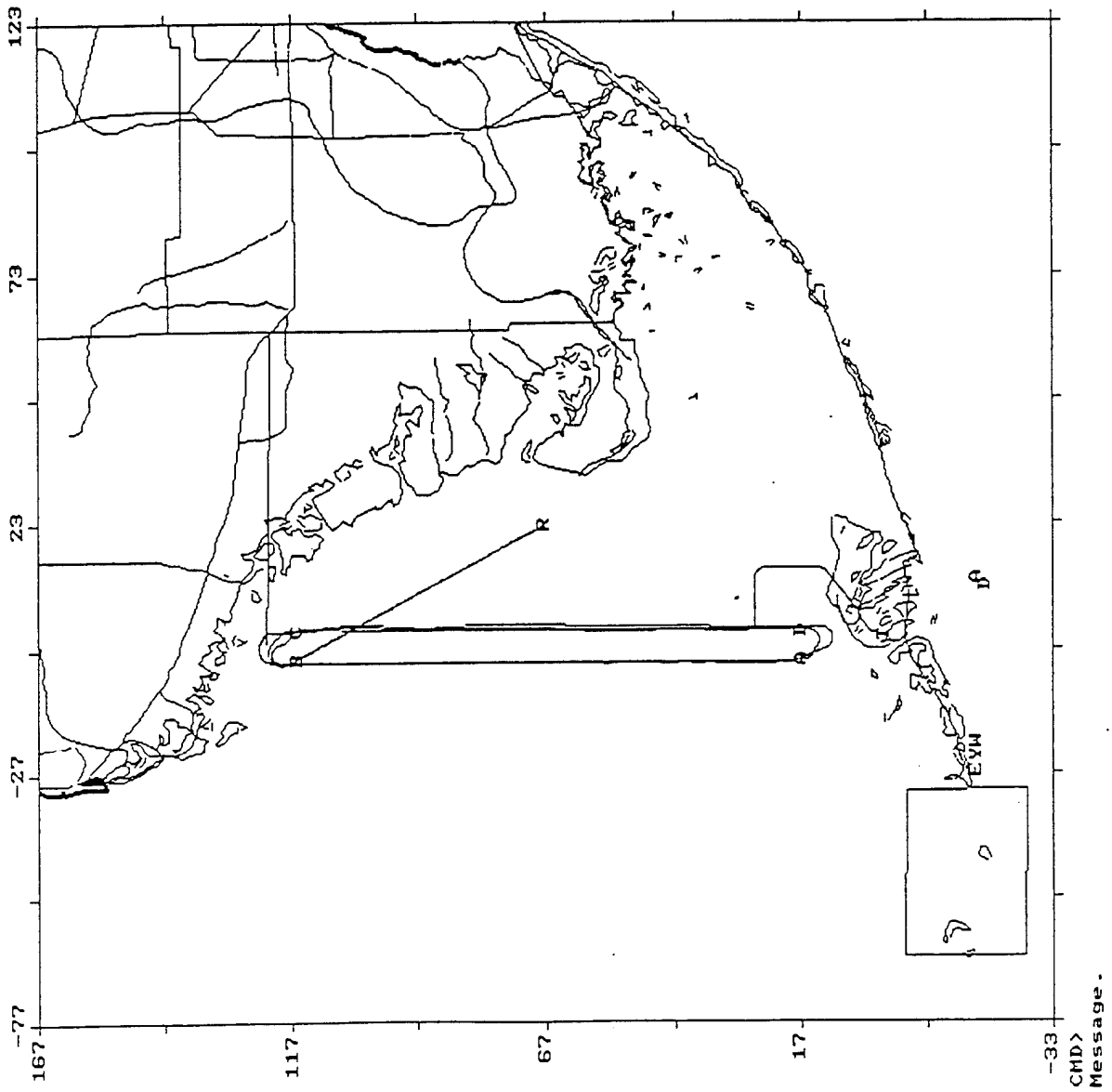

FIGURE 4-1 PROFILE FOR GULF FLIGHT 1

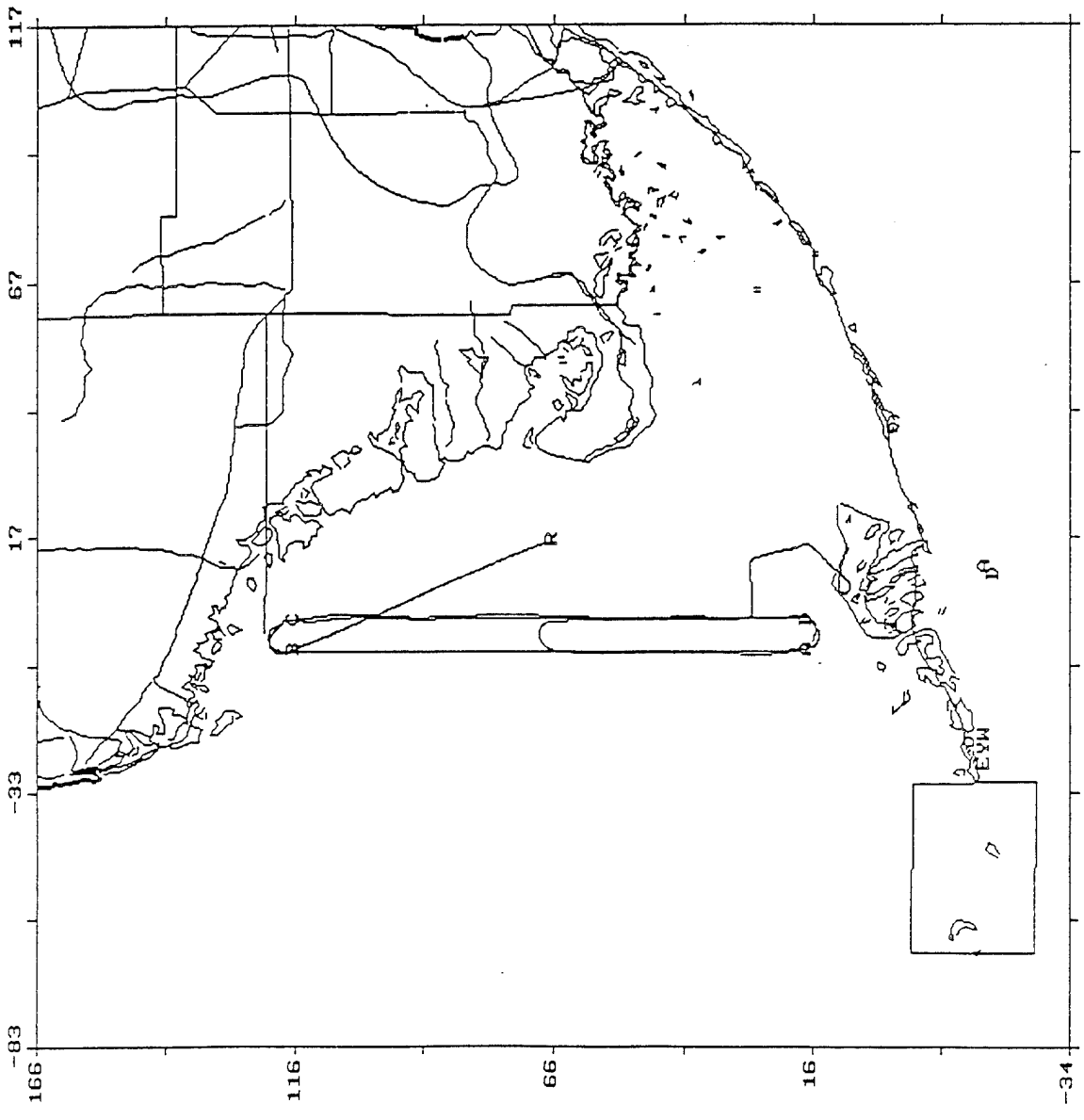

FIGURE 4-2 PROFILE FOR GULF FLIGHT 2

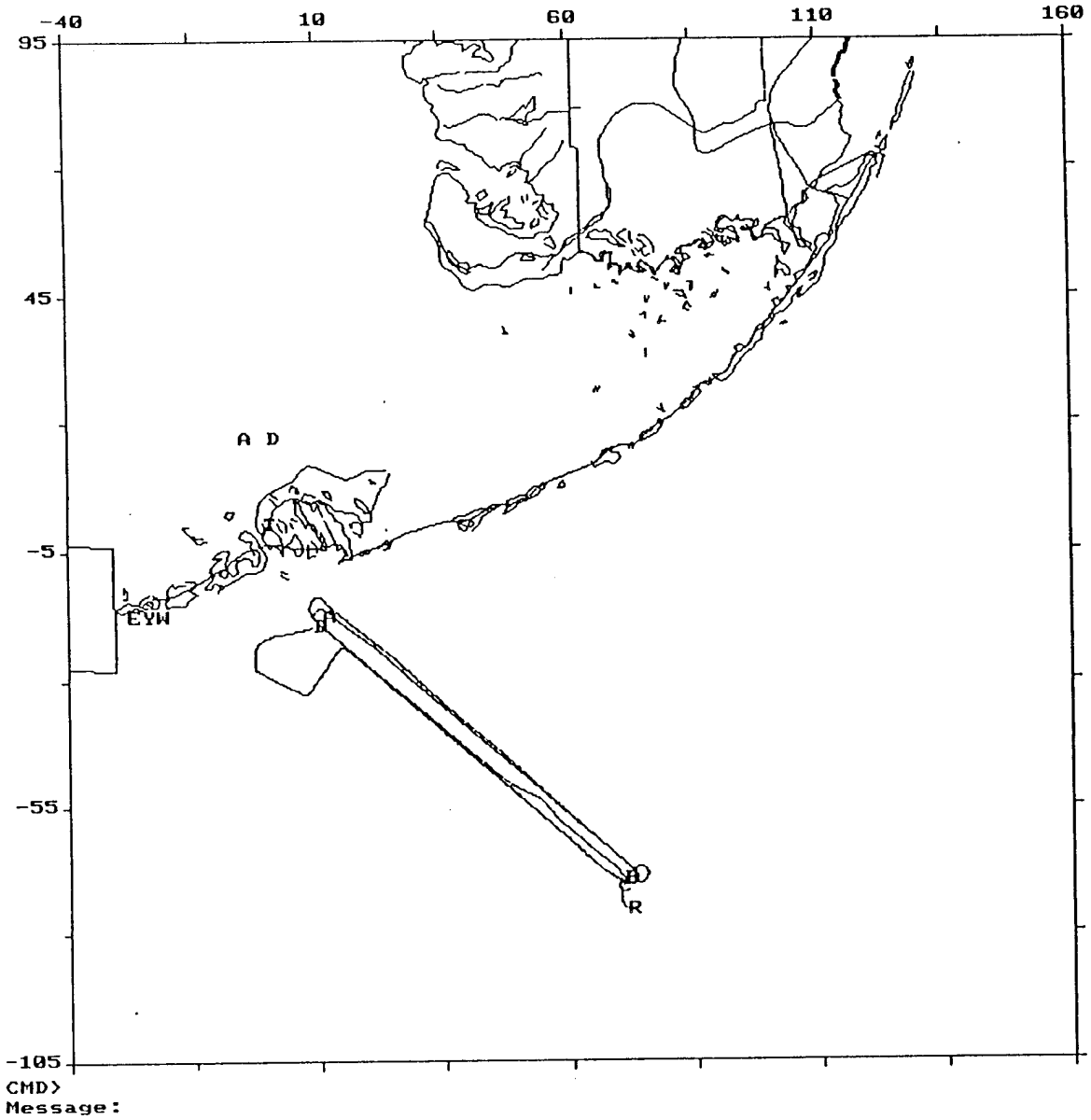

FIGURE 4-3 PROFILE FOR OCEAN FLIGHT 1

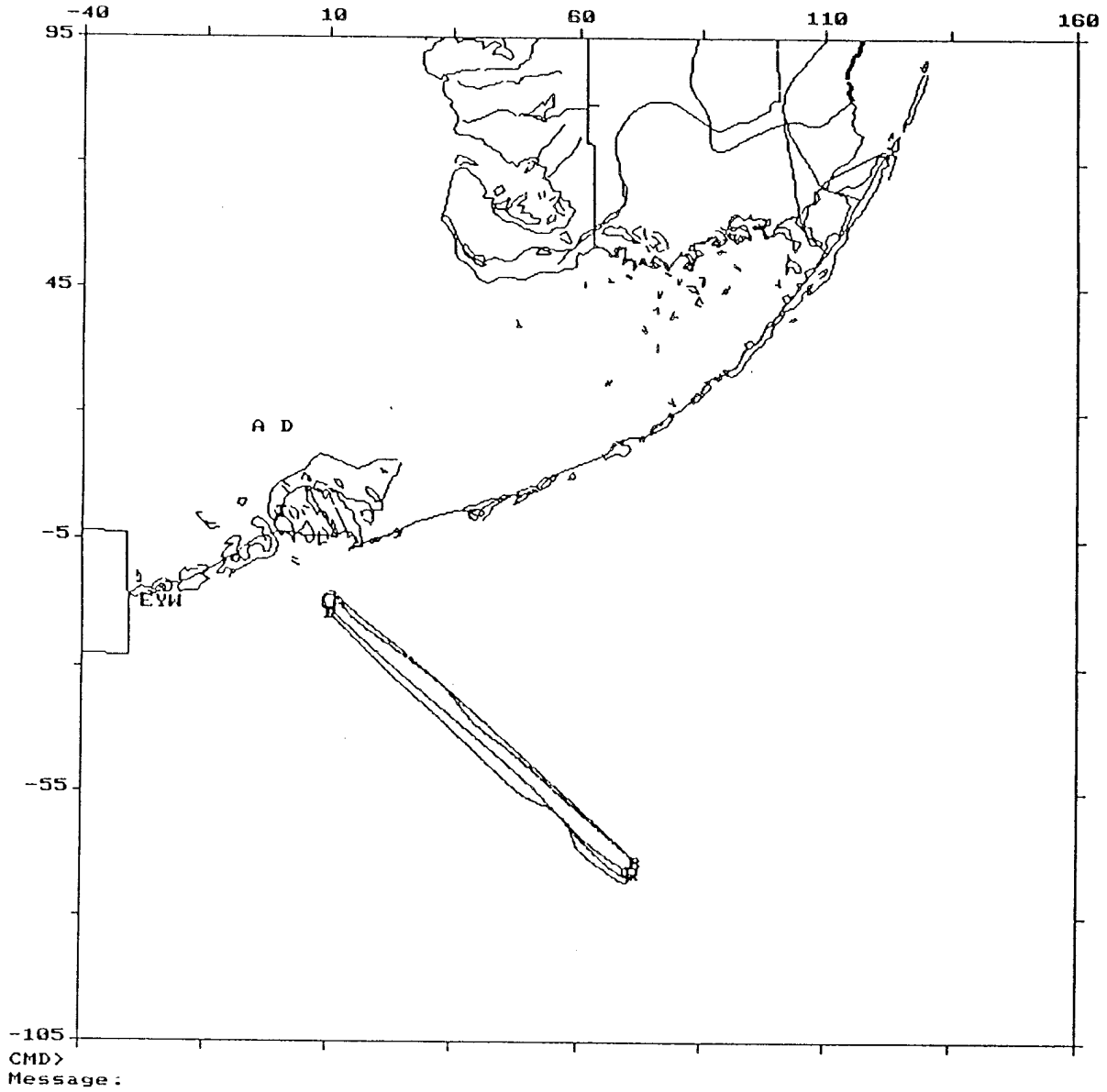

FIGURE 4-4 PROFILE FOR OCEAN FLIGHT 2

Mission	Date	File	Time	Tx Angle	Terrain	Mbytes
Gulf 1	Nov-10-1994	DC 1	15:24:52	-	-	0.125
		Noise 1	15:25:40	-	-	0.125
		DFILE1	15:40:58	345	Gulf	6.25
		DFILE2	15:53:20	310	Gulf	5.25
		DFILE3	16:05:18	40	Gulf/Glades	6.25
		DFILE4	16:17:02	30	Gulf/Glades	6.25
		DFILE5	16:30:13	330	Gulf	6.25
		DFILE6	16:41:43	320	Gulf	6.25
		DFILE7	16:54:56	20	Gulf	6.25
		DFILE8	17:06:43	10	Gulf/Glades	6.25
		DFILE9	17:19:44	345	Gulf	5.75
		DFILE10	17:37:21	DP	-	5.625
		DC 2	17:48:34	-	-	0.125
		Noise 2	17:49:12	-	-	0.125
Gulf 2	Nov-10-1994	DC 1	22:09:47	-	-	0.125
		DFILE1	22:26:34	345	Gulf	6.25
		DFILE2	22:41:14	310	Gulf	3.625
		DFILE3	22:51:58	40	Gulf/Glades	6.25
		DFILE4	23:03:32	30	Gulf/Glades	6.25
		DFILE5	23:17:40	330	Gulf	6.25
		DFILE6	23:28:59	320	Gulf	6.25
		DFILE7	23:41:37	20	Gulf	6.25
		DFILE10	00:02:15	DP	-	5
		DC 2	00:12:20	-	-	0.125
		Noise 2	00:12:57	-	-	0.125
Ocean 1	Nov-11-1994	DC 1	21:24:21	-	-	0.125
		Noise 1	21:25:04	-	-	0.125
		DFILE1	21:30:40	345	Keys/Ocean	5
		DFILE2	21:40:32	350	Ocean	5
		DFILE3	21:51:29	35	Ocean	5
		DFILE4	22:00:55	25	Ocean	5
		DFILE5	22:11:36	0	Ocean	5
		DFILE6	22:21:03	5	Keys/Ocean	5
		DFILE7	22:31:46	15	Ocean	5
		DFILE8	22:41:26	5	Ocean	5
		DFILE9	22:51:56	345	Keys/Ocean	5
		DFILE10	23:06:26	DP	-	5
		DC 2	23:17:04	-	-	0.125
		Noise 2	23:17:42	-	-	0.125
Ocean 2	Nov-13-1994	DC 1	16:36:00	-	-	0.125
		DFILE1	16:40:41	310	Keys*	5
		DFILE2	16:50:12	350	Keys/Ocean	5
		DFILE3	17:01:49	35	Ocean	5
		DFILE4	17:11:19	25	Ocean	5
		DFILE5	17:22:19	85	Keys	5
		DFILE6	17:32:10	310	Keys*	5
		DFILE7	17:43:25	15	Ocean	5
		DFILE8	17:52:59	5	Ocean	2.125

* Terrain is mostly Keys, but includes some water areas between the Keys.

TABLE 4-1 MISSION SUMMARY

4.1.2 HOST TRANSMITTER PARAMETERS

Clutter data were collected against SEEK SKYHOOK, an aerostat-borne DPS-5 radar, stationed at Cudjoe Key, Florida. SEEK SKYHOOK operates at S-band with a range unambiguous waveform with respect to clutter returns. The radar uses a staggered PRF waveform.

The aerostat is tethered to a tower and has a nominal operating height of 10,000 feet. Location is determined by adding the "blow-down" offset to the landing pad latitude and longitude. "Blow-down" is typically measured at the start of a mission and remains constant unless there is a significant change in the weather pattern. The balloon carries an IFF transponder which emits an IFF Mode 2 code of 4000.

Nominal mission times are from 9:00 am until approximately 2:00 am. The winch system which deploys and retrieves the balloon, operates at 200 feet per minute. During non-operational hours, the balloon is "stored" at 5000 feet, which yields typical deployment times of 25 minutes.

The DPS-5 antenna has an inverse cosecant-squared elevation pattern. The mechanical strut supporting the feed horn is offset from the center to generate a look-down angle of -1.0 degree. The DPS-5 has a nominal 12.0 second scan rate and a nominal azimuth beamwidth of 1.75 degrees.

The actual parameters measured while testing, are listed in Table 4-2 below.

4.1.3 TESTING DESCRIPTIONS

The discussions that follow will be divided into four sections: DC Offset Compensation, Noise Estimation, Direct Path Level Calibration, and Clutter Data Collection.

PARAMETER	VALUE
Frequency	3230 MHz
Power	1.1 MW
Gain	40 dBi
PRF	Staggered (387 Hz average)
PW	1.25 msec
BW	1.75 deg
Polarization	Vertical
Scan Rate	4.75 RPM
Location	24°42.03'N Lat 81°30.38'W Lon
Height	10,000 feet

TABLE 4-2 SEEK SKYHOOK DSP-5 PARAMETERS

Each of the four sections deals with a specific type of data collected during test flights. The detailed operation of the collection hardware is essentially the same for all the data collection. The differences occur in the election of receive horn, amount of data collected, frequency of the local oscillator and generation of triggers to start data collection. A brief discussion is warranted as an introduction to the sections that follow.

AMBIS typically records data in two channels. A reference channel which contains direct path and short delay multipath signals, and the data channel which is "blanked" for near-in returns (clutter) but then collects data for the remainder of the PRI (or a portion of it). The direct path signal is used as the reference and is correlated with the data channel. The correlation removes phase uncertainties that could arise from an unstable transmitter oscillator and provides a zero time delay reference for the data. The correlation also serves to perform pulse compression if the transmit waveform is frequency modulated.

AMBIS does not record raw I,Q data in the sum and data channels simultaneously. The procedure used during typical I,Q data recording is to first collect I,Q samples from the Reference Channel A/D Converters, then switch at an operator selected bistatic range cell and collect I,Q samples from the Data Channel A/D converters. The switch requires several clock cycles and prohibits the capability of collecting continuous range samples. Therefore, to prevent

the loss of data immediately following the direct path signal, the data was collected in a single channel, the data channel. A "synthetic" reference pulse was created from an unsaturated sample of the direct path signal data. This sample was used in all subsequent correlation processing.

4.1.3.1 DC OFFSET COMPENSATION

Files are recorded at the beginning and end of a flight for the purpose of determining the DC offset levels of the A/D converters. Each file contains 32K I,Q samples of data collected with the receiver's local oscillator turned off.

An average level for each channel (I,Q) is determined independently. The values are computed for each flight and applied to all of the data collected during that flight.

4.1.3.2 NOISE ESTIMATION

A file of noise only data was recorded at the beginning and end of each flight profile. The receive system was set up in normal operational mode, except that instead of selecting one of the three receive horns, a 50 ohm load was selected. A single dwell of 32K I,Q samples was collected. The dwell is comprised of 128 PRIs each containing 256 range (or time delay) samples. The data was corrected for DC offset, correlated with the "reference" on a PRI basis, and 16 PRIs were non-coherently integrated (staggered PRF waveform). An average of the resulting data was determined and that value set the noise level used for subsequent processing. Statistics on the noise data showed a mean of 107.4 dB.

4.1.3.3 Direct Path Calibration

Direct Path Calibration demonstrates the ability to accurately account for parameters in the bistatic system. The direct path signal collected has a signal to noise ratio defined as:

$$SN\mathbb{R}_d = \frac{P_{AV} G_T(\theta_{AZ},\theta_{EL}) A_e(\phi_{AZ},\phi_{EL})}{4\pi R_d^2 kTBN_F L L_{AT}} \qquad (11)$$

where:

P_{av} = Average Transmit Power
$G_T(\theta_{AZ}, \theta_{EL})$ = Gain Pattern of Transmit Antenna
θ_{az} = Transmit Azimuth Angle (relative to peak)
θ_{EL} = Transmit Elevation Angle
A_e = Effective Receive Aperture
ϕ_{AZ} = Receive Azimuth Angle
ϕ_{EL} = Receive Elevation Angle
R_d = Range
kT = Boltzmann's Constant x Temperature
B = Bandwidth
N_f = Noise Figure
L = System Loss
L_{AT} = Attenuator Loss

The clutter-to-noise ratio (CNR) of normal measurements is defined as:

$$CNR = \frac{P_{AV} G_T(0^o, \theta_{ELC}) \sigma_0 A_C A_e(\phi_{AZC}, \phi_{ELC})}{(4\pi)^2 R_R^2 R_T^2 kTBN_F L} \tag{12}$$

which after manipulation of Equations 11 and 12 yields:

$$CNR = \frac{SNR_d R_d^2 L_{AT} \sigma_0 A_C G_T(0^o, \theta_{ELC}) A_E(\phi_{AZC}, \phi_{ELC})}{4\pi R_R^2 R_T^2 G_T(\theta_{AZ}, \theta_{EL}) A_e(\phi_{AZ}, \phi_{EL})} \tag{13}$$

where:

θ_{ELC} = El Angle of Clutter Relative to Transmitter
ϕ_{AZC} = Az Angle of Clutter Relative to Receiver
ϕ_{ELC} = El Angle of Clutter Relative to Receiver
σ_0 = Per Unit Area Cross-Section of the Clutter
A_C = Clutter Patch Area
R_T = Range from Transmitter to Clutter
R_R = Range from Receiver to Clutter

Equation (13) shows that a number of the system parameters, which may be difficult to accurately measure or may change slowly with time, are normalized out when the direct path

calibration data are used. The flight profiles are constant enough that the direct path data can be used over the extent of the profile. Direct path measurements are made at the end of each profile in order to account for variations in any of the system parameters from flight-to-flight and from day-to-day.

Three horns are used during data collection so the profile for collecting direct path data was chosen to allow each of the horns to be aimed at the transmitter for several scans (transmitter angle wrt receiver is zero). The forward horns are centered at 0 and + 45 degrees and the side horn +112.5 degrees with respect to the nose of the aircraft.

The flight profile selected for Direct Path Calibration requires 3 maneuvers by the pilot. Each maneuver orients the plane so that the transmitter is radiating directly into the peak of a different receive horn. The data is recorded during the end of the last leg of flight towards the transmitter. The sequence of horn illumination is, horn 2 (+112.5°), horn 1 (+45°), and horn 0 (0°). Figure 4-5 shows the flight geometry.

A comparison of the theoretical and measured direct path levels was made not only as a sanity check for known system parameter values, but also as a test to determine the validity of this direct path calibration approach.

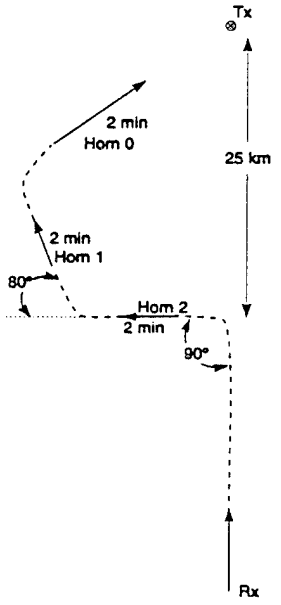

FIGURE 4-5 DIRECT PATH COLLECTION GEOMETRY

A block of unsaturated direct path data was selected from the Ocean 1 profile. The geometry for the time of that data was determined and the known values from Table 4-3 were substituted into the DP/N equation at the A/D converter output shown as,

$$DP/N = \frac{P_{pk} G_T A_e \theta_{azR}}{4\pi D^2 KTBN_f LL_{at}} \tag{14}$$

The resulting theoretical value of DP/N is 53.75 dB.

PARAMETER	VALUE (dB)
Ppk	90.4
G_T	40.0
Ae	-21.4
4π	11
D^2	90.3
kT	-174
B	57.8
N_f	5
L	12.4
Lat	50
θazR	-2.75

TABLE 4-3 DP/N THEORETICAL CALCULATION PARAMETER VALUES

The transmitter was off receive beam center by almost 18 degrees during the recording of this block. Figure 4-6 shows a loss of 2.75 dB. A plot of the raw I,Q data (Figure 4-6) shows a peak of approximately 67.0 dB. The noise level is determined to be 10.9 dB +3 dB which is included because the theoretical calculation assumes the SNR to be defined (by Skolnik)

$$SNR = \frac{A}{\sigma^2} \tag{15}$$

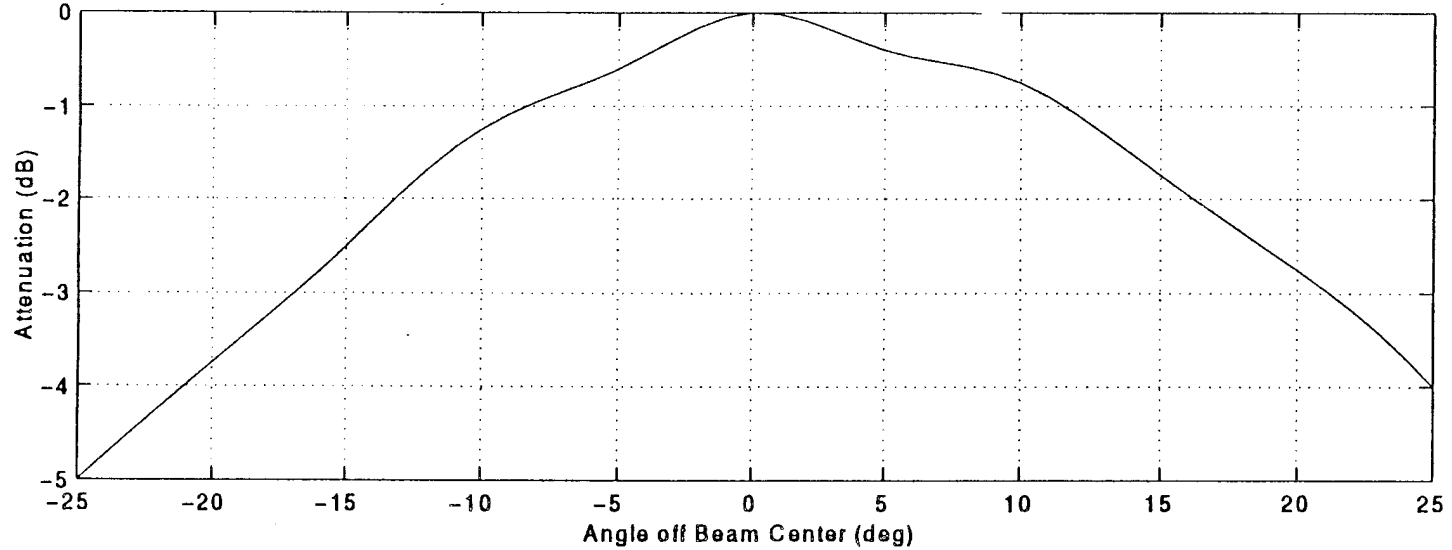

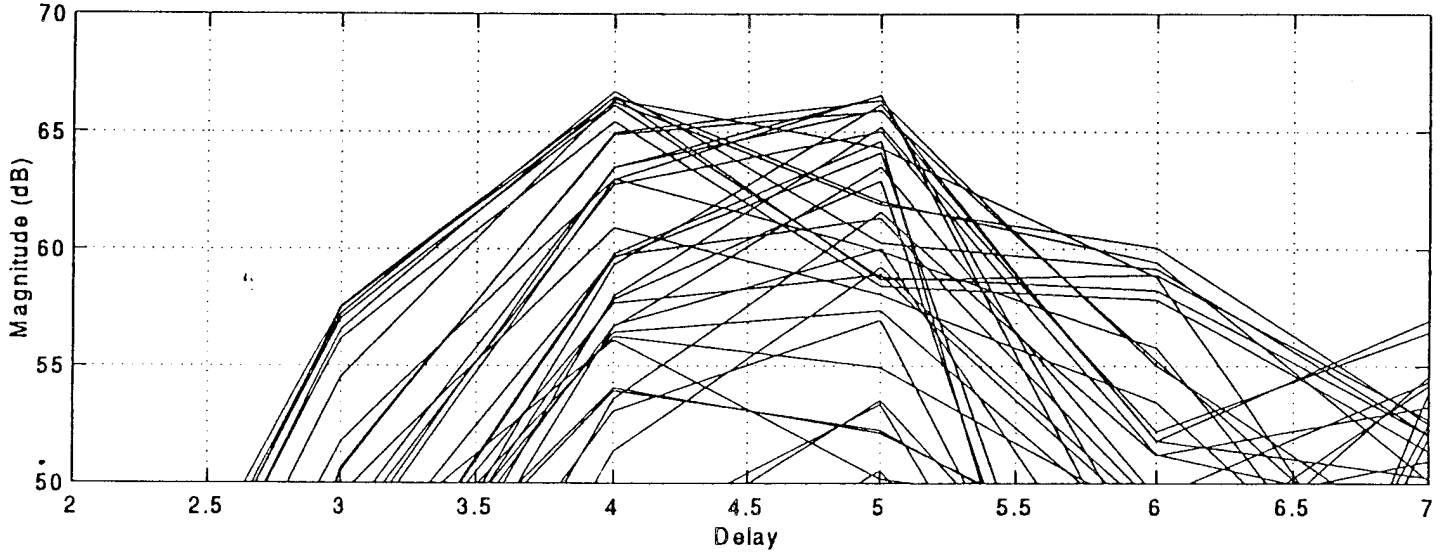

FIGURE 4-6 RECEIVE ANTENNA PATTERN AND SAMPLE DIRECT PATH DATA

where A is the peak signal power and σ^2 is the noise power spectral density. Computation of SNR from measured data assumes

$$SNR = \frac{A}{2\sigma^2} \tag{16}$$

The resulting DP/N measured value is 53.1 dB, which compares nicely with the theoretical values.

4.1.3.4 CLUTTER DATA COLLECTION

The racetrack profiles afford 2 legs of straight path flying on each loop during which clutter data can be collected. The legs are 80 to 100 km in length so 2 data files of 5 - 6¼ Mbytes each are recorded. Data were collected using a single horn, rather than pulse chasing through horns, to avoid possible switching transients as well as the loss of low bistatic range cell data for transmit angles near the baseline. Each file collected during a flight contained data from a different transmit angle. The flight was repeated to increase the amount of data available for statistical analysis.

The second gulf flight was shortened because the pilot was running out of time with which he was allowed to complete his flying for the day. A storm went through the area early in the afternoon which delayed the take-off for the second flight. Data files 8 and 9 were not collected. The second ocean flight was terminated early because a storm was entering the area and the site manager at Cudjoe Key made the decision to retrieve the balloon. Data files 9 and 10 as well as the second DC and noise files were not recorded.

Prior to the collection of any given data file, the operator selects an angular region relative to the transmitter over which data will be collected. The region is defined by a start angle (in degrees relative to the transmitter-to-receiver baseline) and a duration. A receive horn corresponding to that angle is then selected. Once the operator issues a GO command, data will be collected only in that pre-defined region on every transmitter scan. The data collection firmware is configured to record the first 256 time delay samples for each pulse. A set of data from 128 consecutive pulses is recorded (32K 32-bit samples). These samples, from a single scan, are referred to as a "block" of recorded data.

The clutter data (12-bit I,Q pairs) are stored as 16-bit integers whose upper 4 bits are tied low. The data must be sign extended and then combined to form a complex number. DC offset compensation and correlation with a stored reference waveform are then performed. The data are then non-coherently integrated over 16 pulses and an estimate of the noise level is used to generate a clutter-to-noise level for each sample collected. The bistatic range cell areas are determined and estimates of the clutter cross section per unit area (Sigma Zero) are computed.

Calculation of the Sigma Zero values accounts for antenna pattern effects, transmitter parameter variations, system losses, bistatic geometry and signal processing effects. A more detailed description of the processing is given in the following section.

Statistical analyses of the data is performed with the data being characterized in terms of terrain type, CNR levels, out-of-plane angle, transmitter grazing angle and receiver grazing angle.

At precisely the time that data collection starts for each scan, a hardware register latches the GPS time from the Time-Frequency Processor. The time required for the actual data collection is a small fraction of the entire scan time. During the remainder of the scan the GPS time is written to a buffer and the I,Q data is written to the disk. Fifty (50) blocks of data from consecutive scans are collected during the Gulf of Mexico profiles and forty (40) are collected during the profiles over the Florida Straits.

4.2 DATA REDUCTION TECHNIQUES

The goal of the data reduction process is to take sampled I,Q bistatic clutter data and generate estimates of the clutter cross section per unit area (Sigma Zero). By collecting a substantial amount of data, a statistical analysis can be performed on the resulting data.

The section provides a logical progression through the many steps required in the data reduction process. The basic data reduction process as shown in Figure 4-7 consists of an A/D converter DC offset correction, correlation of the range sweep (time delay sampled data during

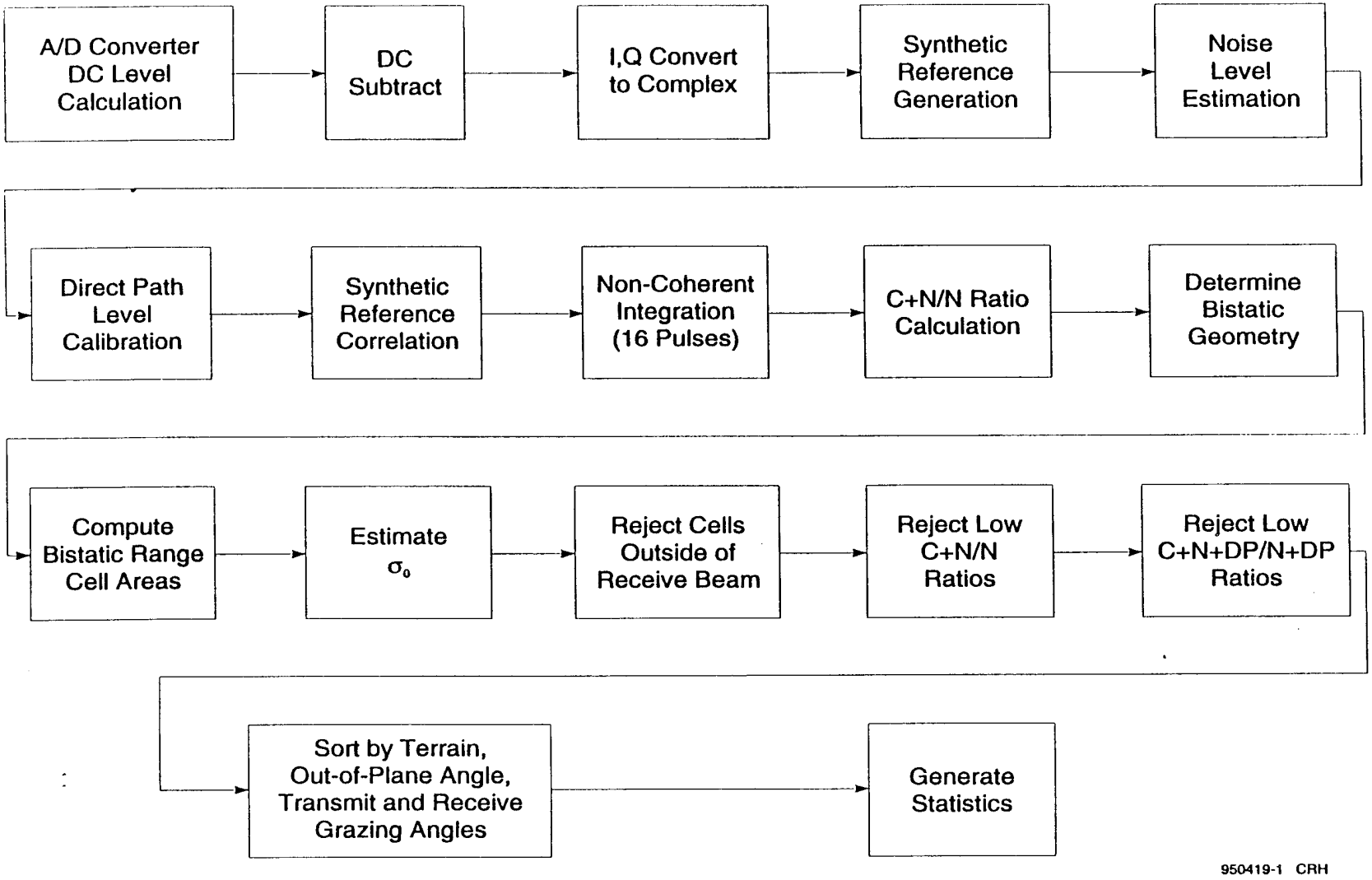

FIGURE 4-7 DATA REDUCTION PROCESSING FLOW

one transmit pulse) with a synthetic reference signal, non-coherent integration over a series of pulses (16), and conversion to a clutter plus noise-to-noise ratio (CNNR). At this point, solving the Bistatic Radar Range Equation for the clutter cross section and dividing the cross section by the clutter cell area estimate yields Sigma Zero. Once Sigma Zero is computed, all relevant terms for statistical analyses are recorded (grazing angles, out-of-plane angle, CNNR, and terrain classification). The radar range equation requires knowledge of receiver and transmitter parameters as well as the bistatic geometry. Determination of all relevant values will be described below.

As described in section 4.1.3.1, estimates of the DC offsets at the A/D converter output were computed for each flight profile. The offset correction terms are computed for each channel (I,Q) and applied independently to all of the data collected. Figure 4-8 and 4-9 show the data before and after DC Offset Compensation. The figures also show the effect in separate I,Q channels.

The data from the 12-bit A/D converters are stored as 16 bit values but not sign extended. The upper four bits are simply tied low. To properly generate complex data, the samples were sign-extended, corrected for DC offset and combined as I + jQ. The data is stored at this point in a Matlab formatted file. Each file represents a series of consecutive transmit pulses called blocks of data. There are 128 consecutive pulses in each file, with the hardware recording 256 samples (time delay or bistatic range) for every pulse.

For typical bistatic radar operation, every transmit pulse is sampled and recorded. The sampled pulse (reference) is used for correlation with the sampled time-delay data collected following that pulse. A new reference is collected for every transmit pulse. During data collection for the Cudjoe Key Tests, a separate reference was not collected for every pulse. Instead a "synthesized reference" was generated from unsaturated Direct Path signal data. This reference was stored and used for all subsequent correlation. Figure 4-10 shows the reference sample in raw form and resampled at a higher rate. Figure 4-11 is the reference sample as it was used for correlation processing. The reference sample is correlated with the raw data from each

of the 128 PRIs for every block of data collected. The location of the first peak is referred to as the zero time delay. Time delay (and hence bistatic range) progresses from that point. This allows the 128 PRIs to be properly time aligned regardless of the transmitter's PRF.

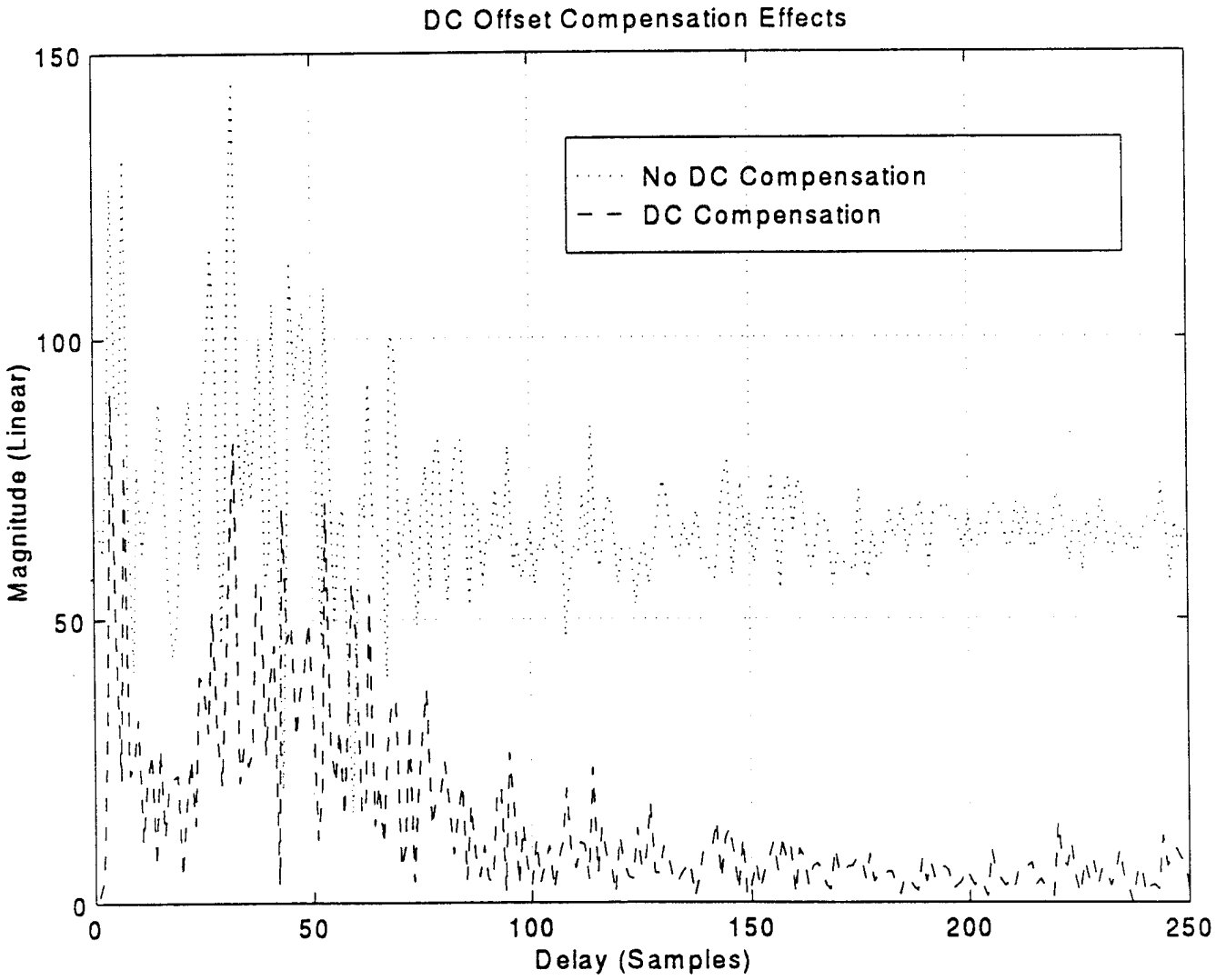

FIGURE 4-8 DC OFFSET COMPENSATION EFFECTS

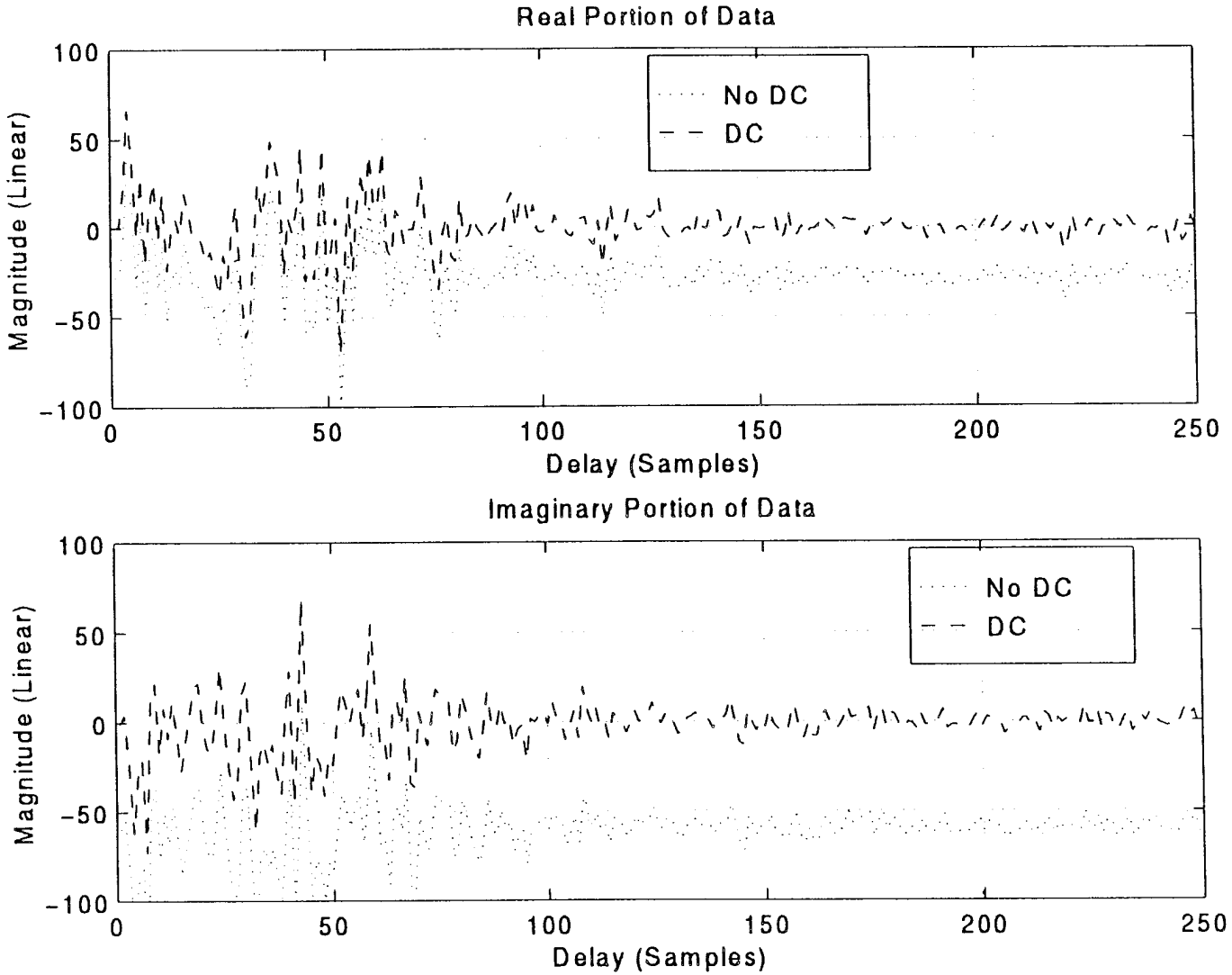

FIGURE 4-9 DC SUBTRACTION PROCESS COMPARISON

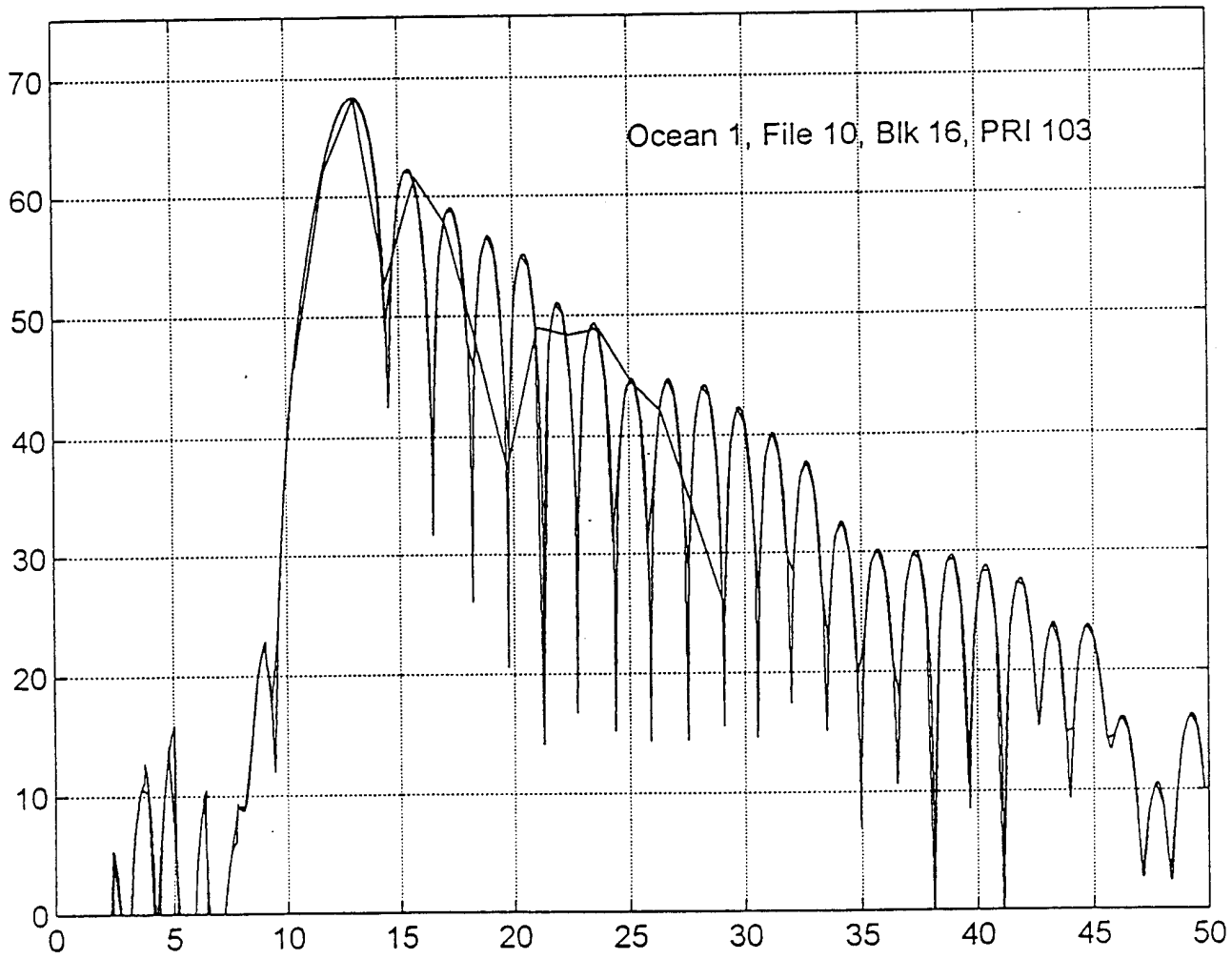

FIGURE 4-10 EXAMPLE OF RESAMPLED REFERENCE

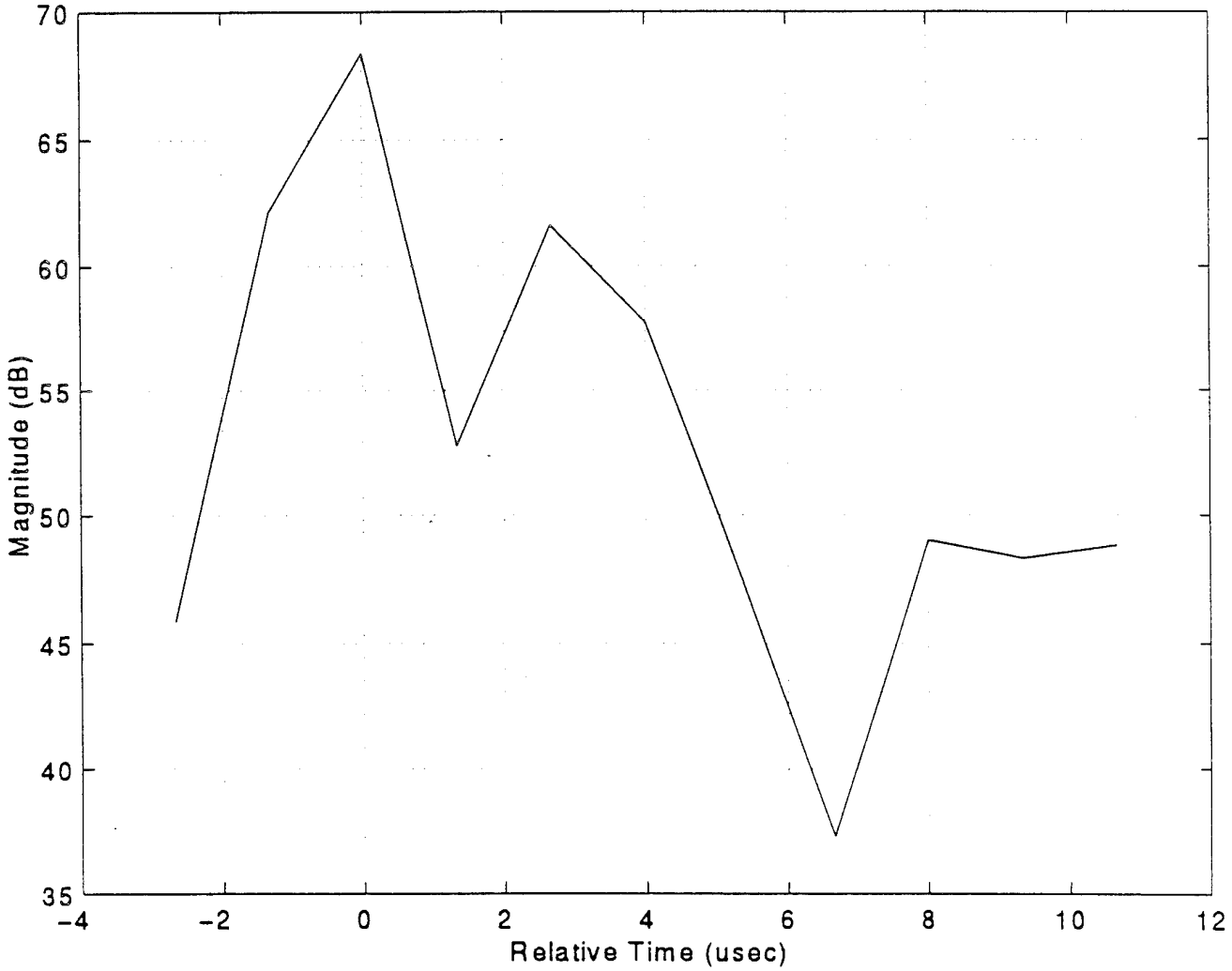

FIGURE 4-11 SYNTHETIC REFERENCE USED

Since the DPS-5 transmitter employs a staggered PRF waveform, non-coherent integration (NCI) is performed. Sixteen pulses are non-coherently integrated, so each block of data yields 8 range sweeps of NCI data. The noise estimate is used to create Clutter plus Noise to Noise Ratios (CNNR).

In order to create estimates of Sigma Zero, geometry and timing related information is required. Each data file that was recorded contains a header of timing information. The header contains the GPS time corresponding to the start of every block of data collected in the file. AMBIS records navigational data independent of the I,Q recording capability, and this data is also GPS time stamped. The I,Q data header times are matched to the closest navigation time and the receiver position in latitude and longitude is determined. The transmitter and receiver positions are used to create a set of ranges and angles for each block which represent the baseline distance and the angle from north of the receiver-to-transmitter baseline. This data is stored in a file along with the receiver and transmitter heights corresponding to the same time.

The receiver and transmitter positions are now known, as well as the transmit angle relative to the baseline. Data files containing the CNNR values corresponding to those geometries have been created. In order to compute estimates of Sigma Zero, the geometry for each block must be determined (grazing angles; receiver-to-clutter range, RR; transmitter-to-clutter range, RT) as well as the bistatic range cell areas. Increments of RT are selected along minimum and maximum transmit beam angles. The corresponding bistatic range cell (non-integerized value) is computed for each one of these RT positions. The points are interpolated to determine the cell boundaries. The minimum common cell is determined and the boundary values and corresponding RT values are saved. A flat earth with constant average terrain height is assumed. The bistatic range cell area is determined by using the four cell boundary values as the corners of a quadrilateral (X1,Y1 X2,Y2 X3,Y3 X4,Y4) and computing the enclosed area using the equations shown below.

$$
\begin{aligned}
r1 &= \text{abs}\left((X2-X1) \times (Y3-Y1) - (X3 - X1) \times (Y2 - Y1)\right)/2 \\
r2 &= \text{abs}\left((X2-X1) \times (Y4-Y1) - (X4 - X1) \times (Y2 - Y1)\right)/2 \\
r3 &= \text{abs}\left((X3-X1) \times (Y4-Y1) - (X4 - X1) \times (Y3 - Y1)\right)/2 \\
r4 &= \text{abs}\left((X3-X2) \times (Y4-Y2) - (X4 - X2) \times (Y3 - Y2)\right)/2
\end{aligned}
\qquad (17)
$$

$$
\text{area} = (r1 + r2 + r3 + r4 +)/2
$$

The geometry yields values for RT, RR and grazing angles which determine antenna pattern attenuation. The values are plugged into equation (13) and it is solved for σ_o, the estimate of clutter cross section per unit area.

A file is created at this point which contains the bistatic range cell number, estimate of Sigma Zero, Clutter + Noise to Noise Ratio, RT_{ave}, RR_{ave}, transmit grazing angle, receive grazing angle, out-of-plane angle, and bistatic angle. In addition, a file is created which contains the peak value from each PRI in a block. This value is used later in determining the clutter to direct path plus noise level validity. The calculation of Sigma Zero at this point does not account for any antenna pattern effects. It was decided that data would be saved at this point and subsequent processing would account for those effects. This is because antenna pattern data was determined from published data sheets and if rigorous measurements were made in the future, they could be easily applied to the data.

Antenna pattern effects are accounted for with regard to the receiver azimuth and elevation beam position and the transmitter elevation beam position. Since the range sweep is determined by the transmitter point angle, the assumption is made that the clutter patch is illuminated by the peak of the transmit azimuth beam. The grazing angles (TX and RX) which are computed for each cell are used to index into the arrays of elevation attenuation. The receive azimuth beam position is determined through the use of receiver and transmitter positions, receiver heading, transmit angle and horn used for data collection. Figure 4-12 shows the attenuation values for receiver azimuth and elevation beams. Figure 4-13 shows the values for transmitter elevation beams.

Processing of the data is complete at this point (with the exception of antenna pattern attenuation). The remaining work is selecting valid data based on some criteria, and performing statistical analysis on this selected data. The selection process includes the following steps:

- Reject Cells Outside The Receive Beam
- Reject Low C+N/N Ratios
- Reject Low C+DP+N/DP+N Ratios

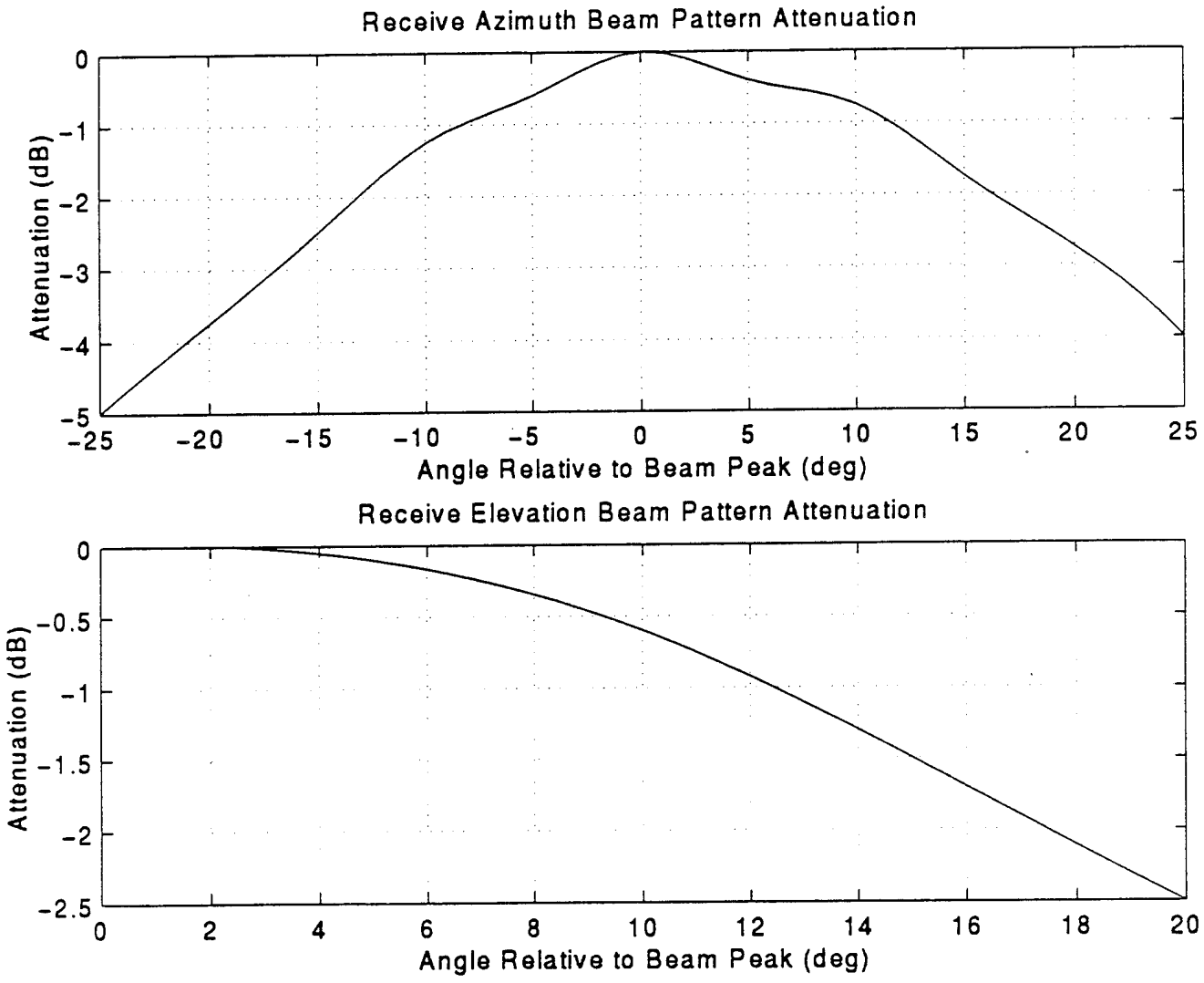

FIGURE 4-12 RECEIVER AZIMUTH AND ELEVATION BEAM PATTERN ATTENUATION

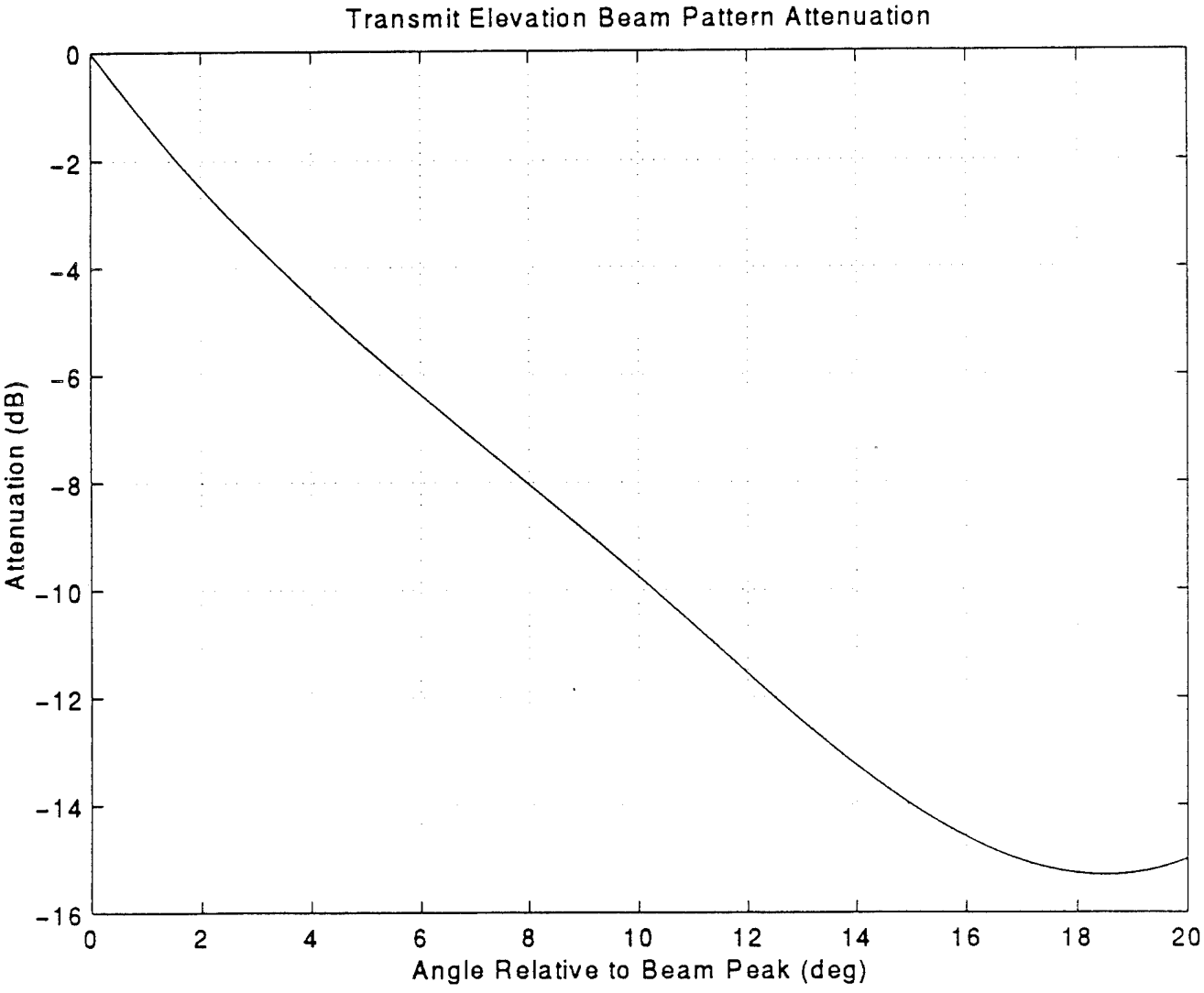

FIGURE 4-13 TRANSMITTER ELEVATION BEAM PATTERN ATTENUATION

The rejection of cells that are outside the receive beam azimuth limits is accomplished by creating a table which contains the eight pairs of bistatic range cell limits for every block in a data file. There are eight pairs because the output of the 16 pulse NCI yields eight sweeps for each block of data collected. Each pair is the minimum and maximum cell which resides within the receive beam. A comparison of all cells in a range sweep to the valid cell limits, quickly determines whether or not the data sample can be used in the statistical analysis.

As a result of the sharp frequency response in the receiver's anti-aliasing filters, there is filter ringing evidenced in the data due to strong direct path levels at time delays very close to the direct path arrival. In order to determine if the return is clutter or direct path it is necessary to determine the "typical" system response in the absence of clutter. The "typical" system response was determined from an unsaturated section of data from a direct path file. The level relative to the peak was determined along the envelope of the response at delays corresponding to the sampling rate of the system. This response is shown in Figure 4-14. The "attenuation" levels were written to a file. This file will be used with the file of peak values to assign a Validity Flag to each data sample based on the Clutter-to-Direct-Path+Noise level (CDNR).

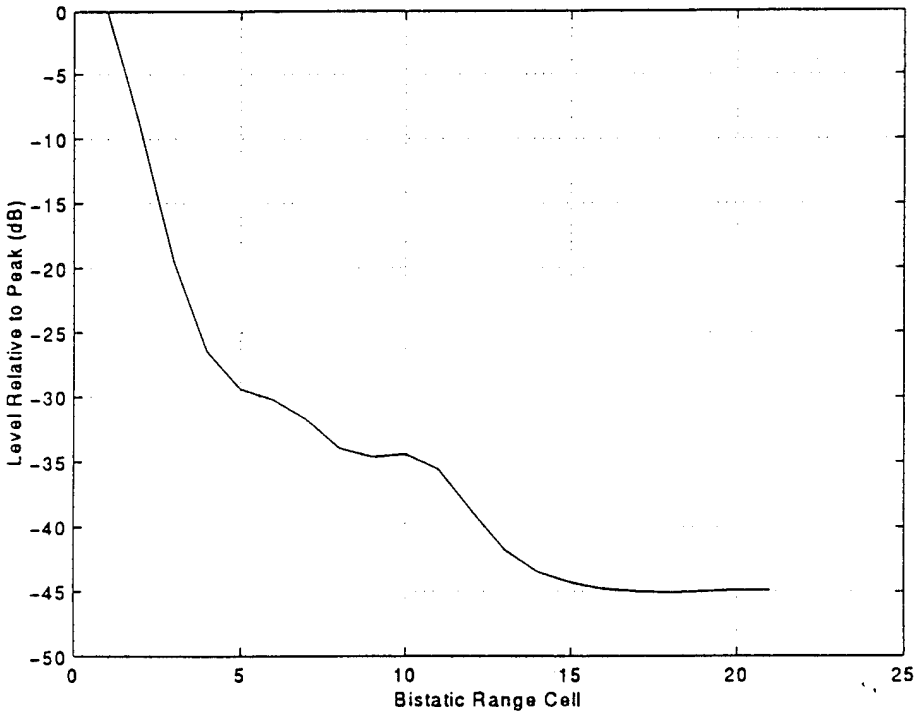

FIGURE 4-14 ATTENUATION LEVEL RELATIVE TO PEAK DUE TO FILTER RING

In addition to the CDNR Flag, a CNR Flag rejection criteria is similarly implemented. A flag system is used to represent the level of either the CDNR or CNR ratios. The values of the flags are described in Table 4-4.

Flag Value	CDNR or CNR
0	less than 5 dB
1	5 and 10 dB
2	10 and 15 dB
3	Greater than 15 dB

TABLE 4-4 VALIDITY FLAG DEFINITIONS

The threshold values were chosen through use of the plots in Figures 4-15 and 4-16. Figure 4-15 shows that if the output SNR (or CNR) exceeds 15 dB, then there is little loss in measurement accuracy when non-coherently integrating 16 pulses. However, as the output level decreases, the loss of phase information due to NCI results in a bias (minimum output SNR value).

Sigma Zero statistics are now computed on the processed data. Terrain type is one of the distinguishing characteristics therefore it is necessary to categorize the data by terrain. The data was separated into five groups; Gulf Water (wave height less than 4 feet), Ocean Water (wave heights between 4 and 8 feet), Everglades, Keys, and Keys with significant amounts of water. The data was then further separated into bins by out-of-plane angle, transmit grazing angle, and receive grazing angle. Three parameters were generated for each bin; the number of contributing samples (COUNT), the sum of the data (SUM) and the sum of the squared values of the data (SUMSQ). The mean and the standard deviation of the data in each bin is then computed from these three terms as shown below.

$$\text{MEAN} = \text{SUM} / \text{COUNT} \tag{18}$$

$$\text{ST. DEV.} = \text{SQRT}((\text{SUMSQ} - \text{MEAN} * \text{MEAN} / \text{COUNT}) / (\text{COUNT}-1).$$

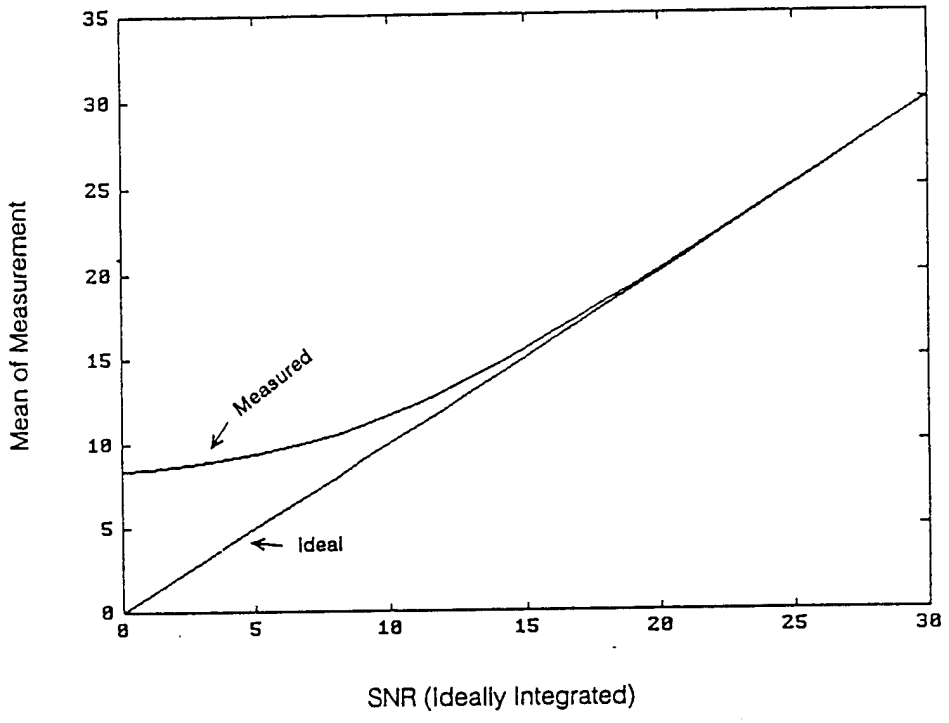

FIGURE 4-15 SNR MEASUREMENT UNCERTAINTY 16-PULSE NON-COHERENT INTEGRATION

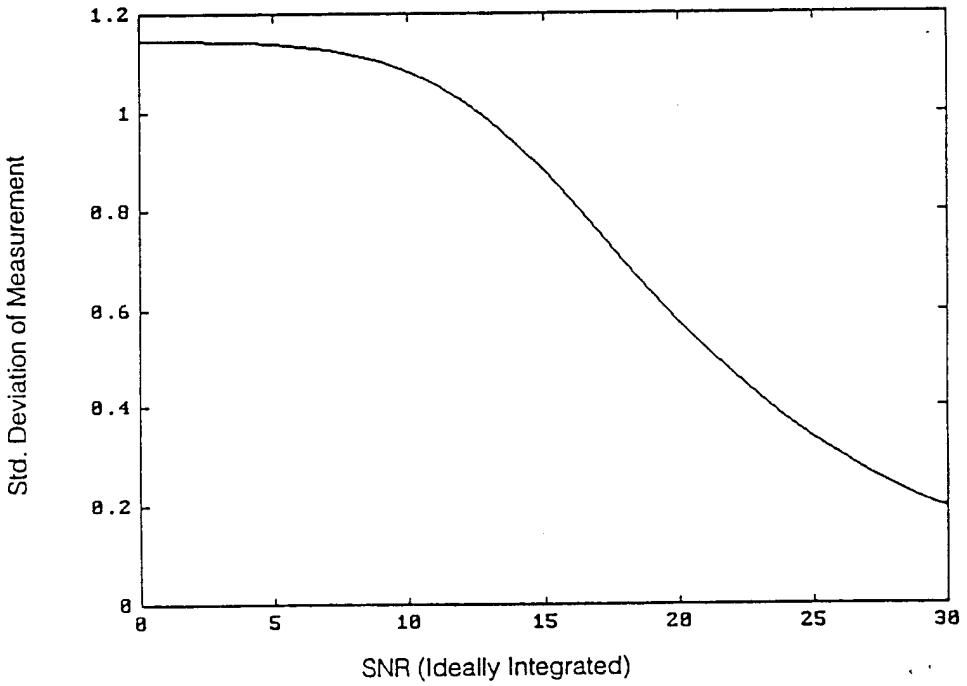

FIGURE 4-16 SNR MEASUREMENT UNCERTAINTY NON-COHERENT INTEGRATION

The data is saved in an ASCII file as blocks of numbers. Each block contains the data for each transmit and receive grazing angle for a single out-of-plane angle bin. The statistics were computed using a spreadsheet program (Quattro Pro for Windows). Outputs included plots of Sigma Zero as a function of each of the parameters independently (out-of-plane angle, transmit grazing angle, and receive grazing angle) for each terrain group. The data was also processed by validity flags. Corresponding plots were generated showing the number of samples contributing to each plot. Also a set of tables was generated which contained all the data categorized by all three parameters together.

Wave heights were obtained from a TV weather channel during the times of the flights. The days of data collection were fairly nice so wave heights never exceeded 8 feet. The classification of 0-4 feet and 4-8 feet conveniently separated the data by location (i.e., Gulf of Mexico or Florida Straits). Figures 4-17 through 4-20 show examples of flight profiles and transmit angles for data collection over various terrain types. The location (bistatic range cell) of the boundaries was determined from the geometry. Since the boundaries are not exactly known, a small buffer was set up to eliminate the data that would have some uncertainty in it's terrain classification.

The statistical analysis is performed on data which is sorted by

- Terrain Type
- Out-of-Plane (OOP) Angle
- Transmit Grazing Angle
- Receive Grazing Angle
- C+N/N Flag
- C+DP+N/DP+N Flag

4.3 TEST RESULTS

The results of the bistatic clutter data collection testing performed in the Florida Keys region are presented in graphical form in Appendix A. Plots have been generated which show the mean and standard deviation of Sigma Zero values as a function of Out-of-Plane Angle,

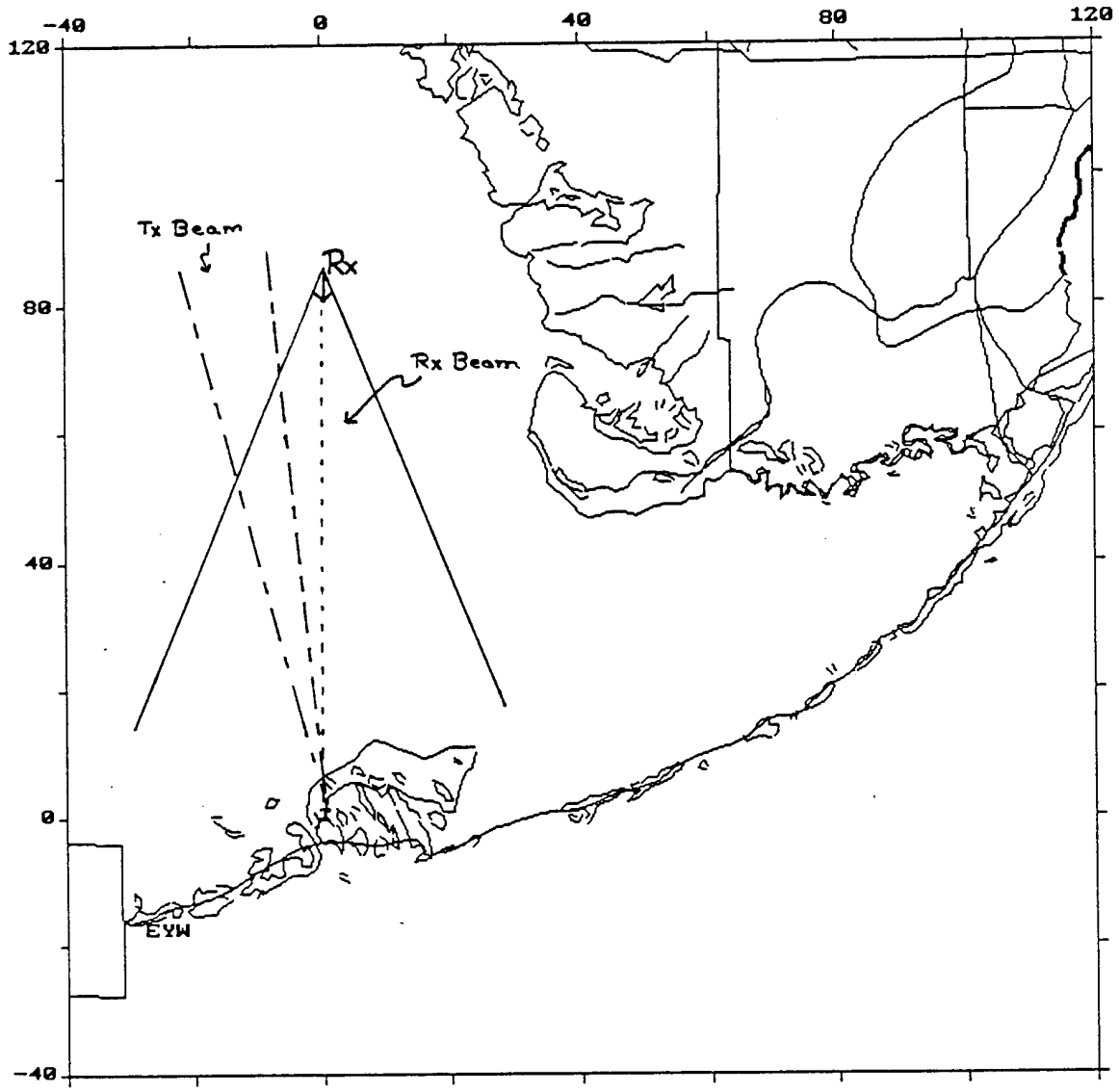

FIGURE 4-17 EXAMPLE GEOMETRY FOR GULF WATER TERRAIN COLLECTION

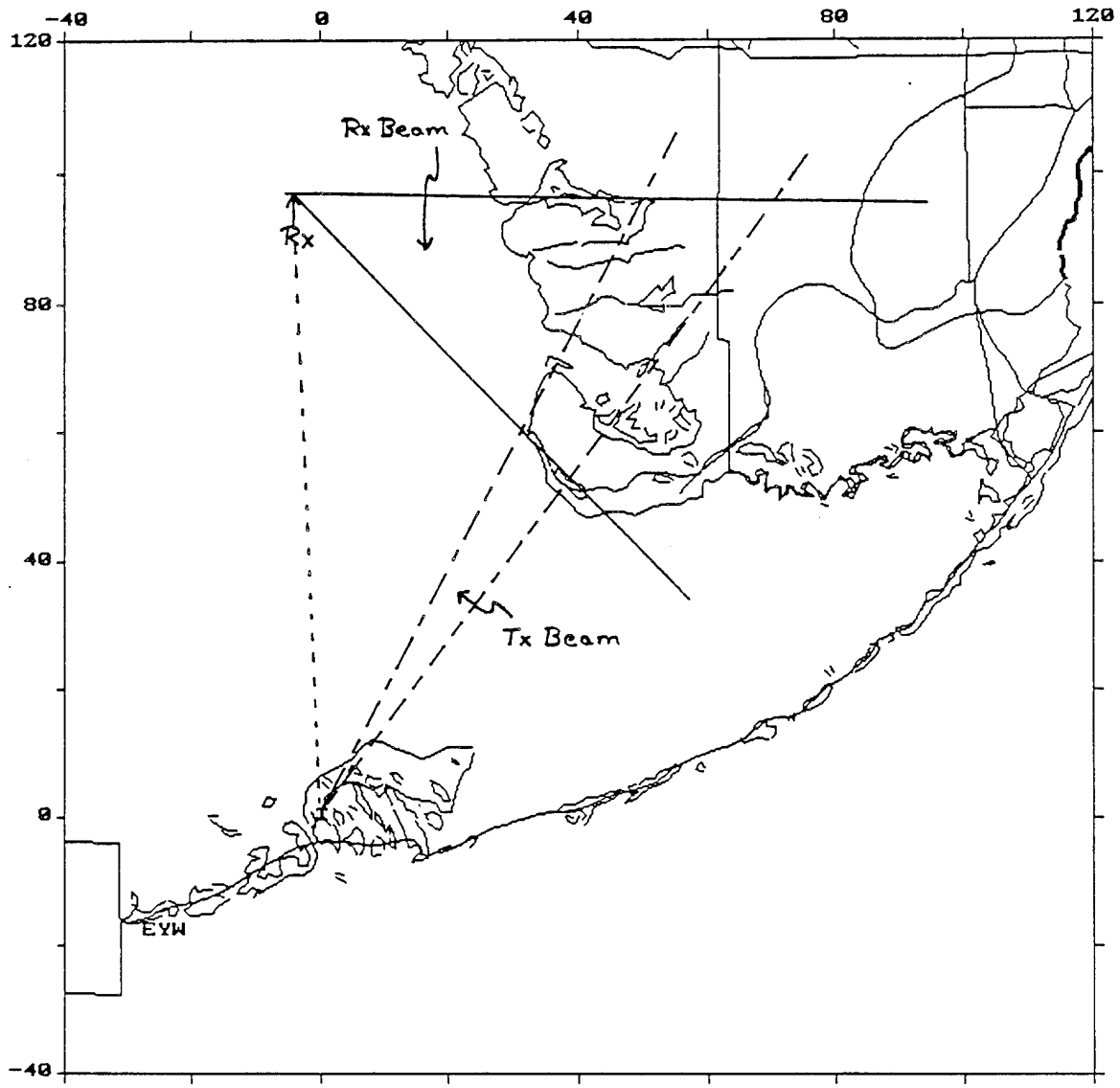

FIGURE 4-18 EXAMPLE GEOMETRY FOR EVERGLADES TERRAIN COLLECTION

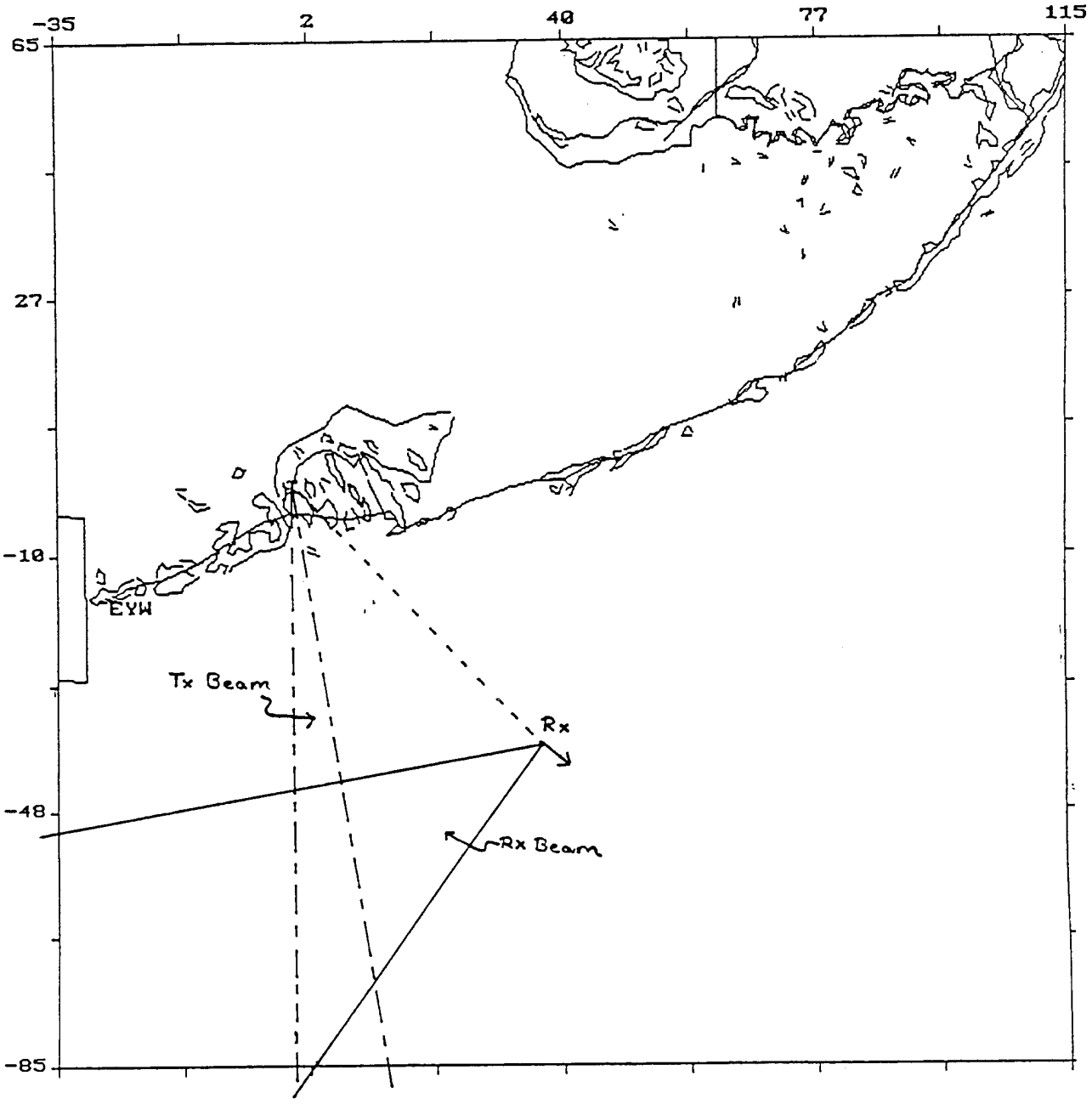

FIGURE 4-19 EXAMPLE GEOMETRY FOR OCEAN WATER TERRAIN COLLECTION

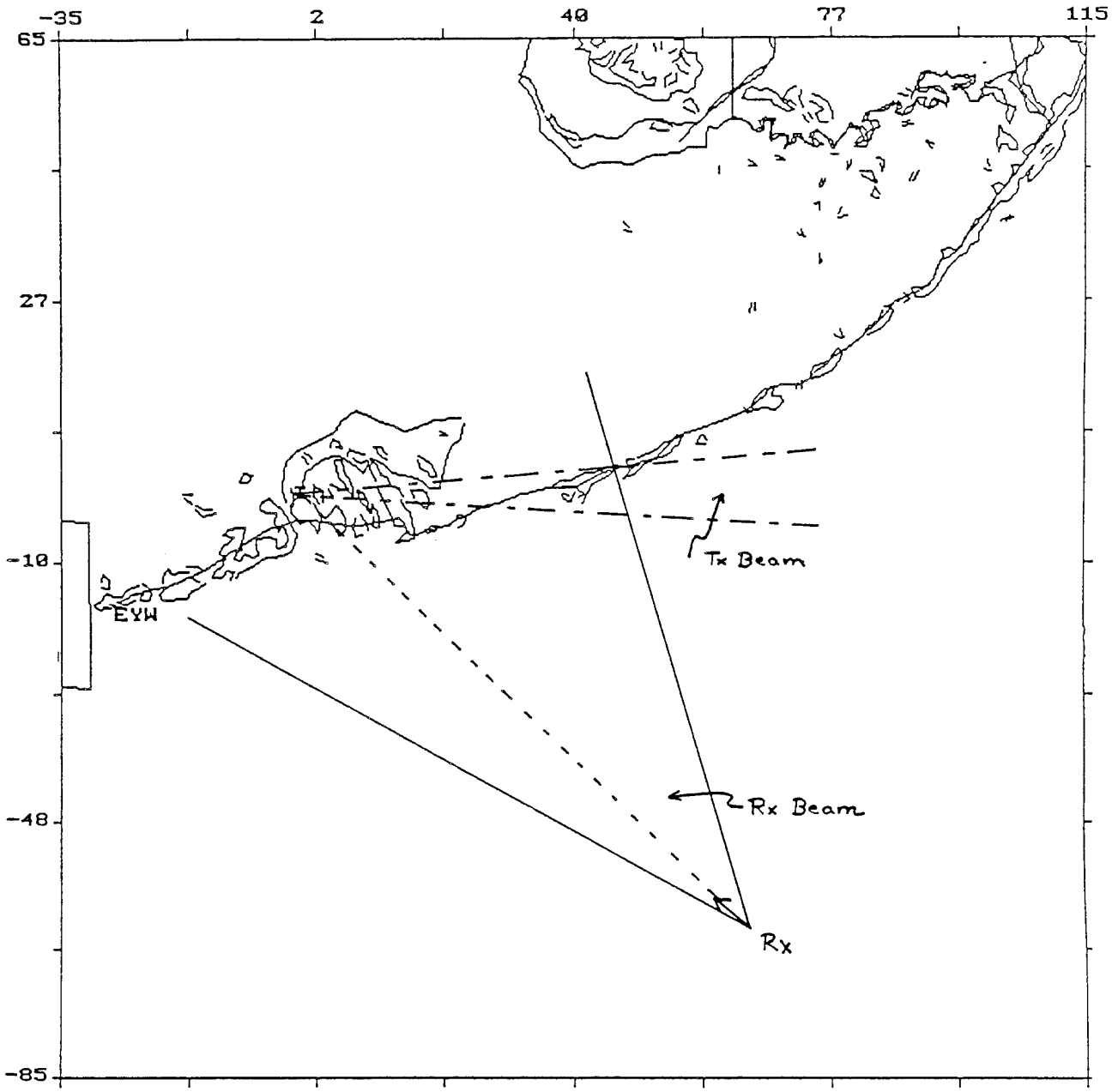

FIGURE 4-20 EXAMPLE GEOMETRY FOR KEYS & WATER TERRAIN COLLECTION

Transmitter Grazing Angle, and Receiver Grazing Angle. A line plot connects the mean values while an error bar is plotted to show the standard deviation of the measurements. A second plot is generated which depicts the number of samples which contributed to the statistics. These plots are generated for validity flag values of 2 and 3. The plots are grouped by terrain type. Figures 4-21 and 4-22 are an example of these plots. The first is sigma zero as a function of out-of-plane angle. The second is the number of samples.

These plots do not hold the other two discriminators constant when plotting sigma zero as a function of a particular discriminator. Appendix B contains a sample of Gulf terrain data with validity flags of 3, for which sigma zero is plotted versus transmit grazing angle for several constant receive grazing angles and a single out-of-plane angle. Plots are also included for sigma zero as a function of receive grazing angle for several constant transmit grazing angles and a single out-of-plane angle. The formats of the plots follow those in Figures 4-21 and 4-22.

Tables of the summarized data are found in Appendix C. The tabular form contains the statistical results depicted in the plots. The data is classified by terrain type and validity flags. Each page contains data for a single Out-of-Plane angle bin. The bin classifications are described below.

PARAMETER	RANGE/INCREMENT	BIN LABEL
Out-of-Plane Angle	0° to 180° by 10°	5, 15, 25, 35 ...
Transmit Grazing Angle	0° to 20° by 2°	1, 3, 5, 7 ...
Receive Grazing Angle	0° to 20° by 2°	1, 3, 5, 7 ...

TABLE 4-5 STATISTICAL BIN SET-UP

Figures 4-23 through 4-25 are intended to show the physical location of the data that is grouped together statistically. The figures do not show all of the data locations, but rather a respresentation of the location of data relative to the transmitter and receiver when collecting data. Figure 4-23 shows several transmitter pointing angles and the Out-of-Plane angle bin from

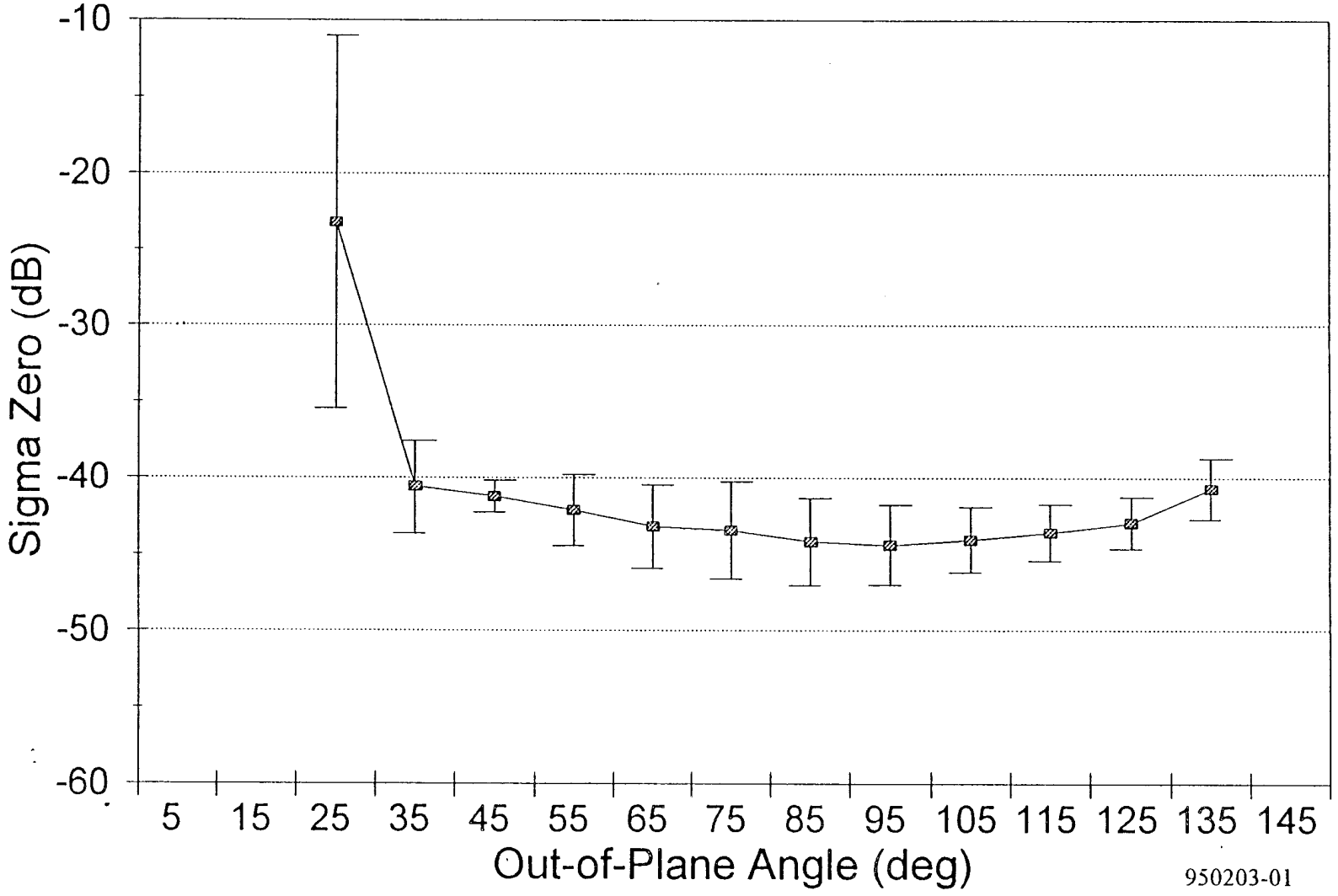

FIGURE 4-21 SIGMA ZERO FOR GULF TERRAIN - WAVE HEIGHT 0' - 4', VF = 3

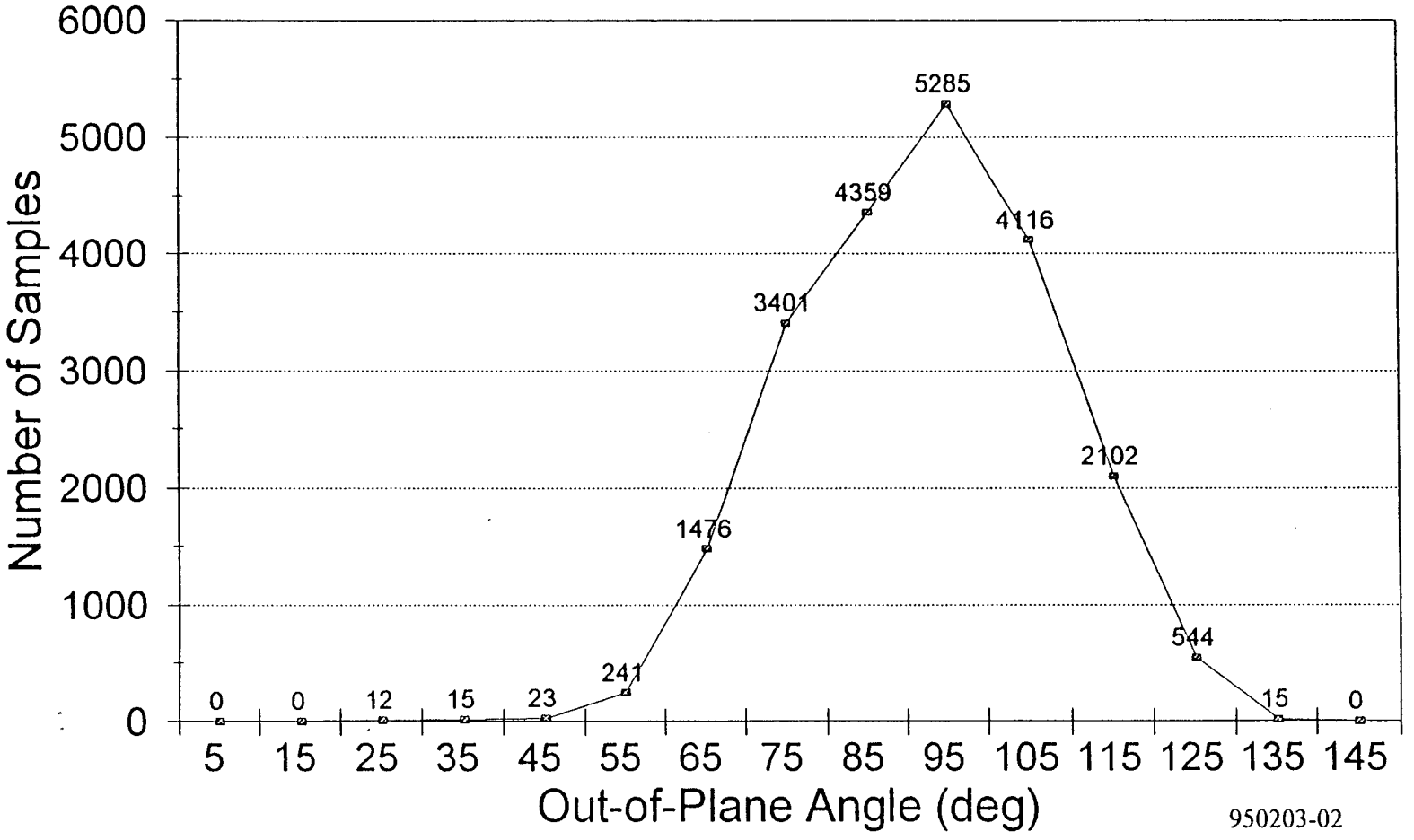

FIGURE 4-22 EXAMPLES FOR GULF STATISTICS - WAVE HEIGHT 0' - 4', VF = 3

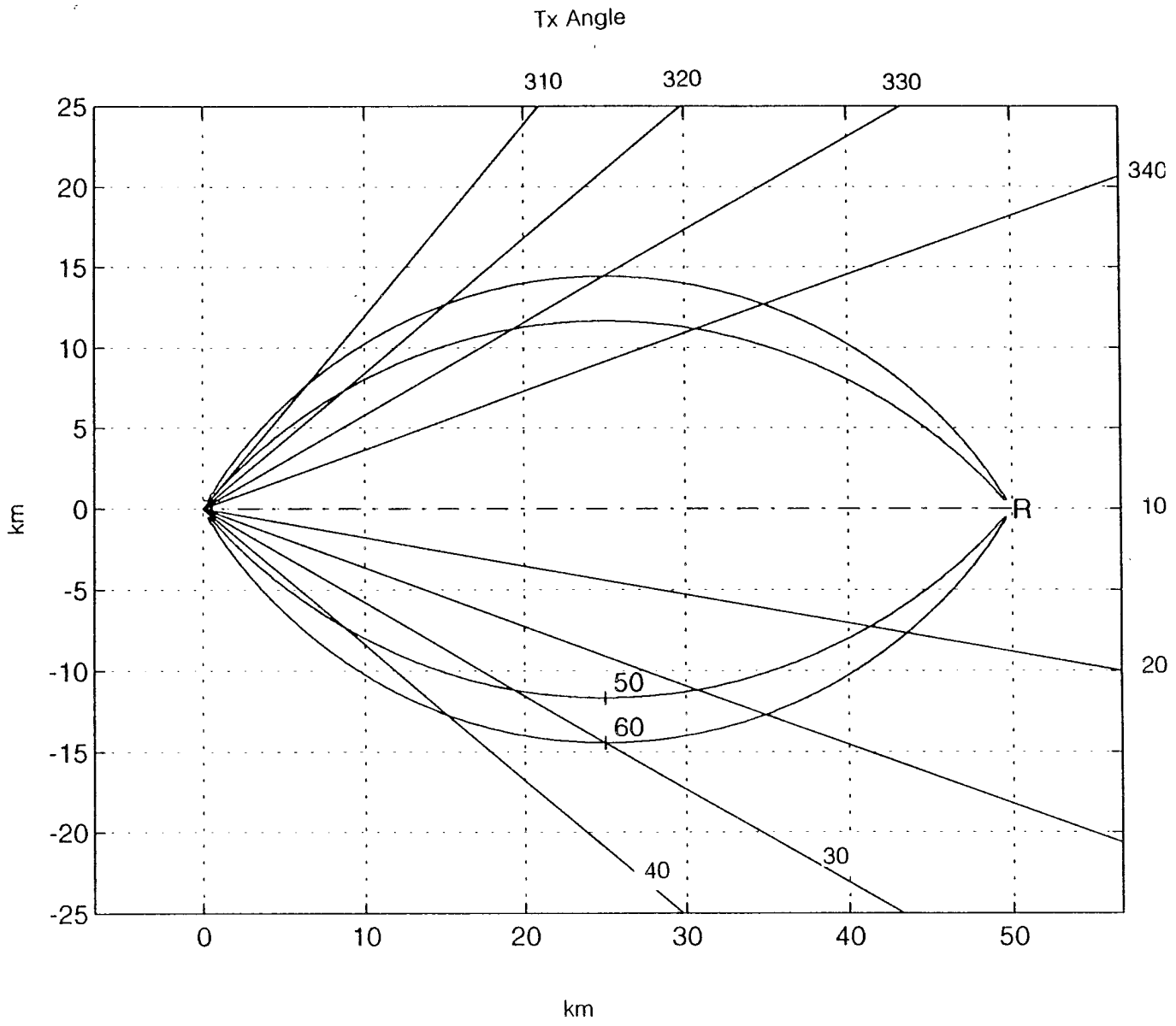

FIGURE 4-23 DATA SELECTION BASED UPON OUT-OF-PLANE ANGLE

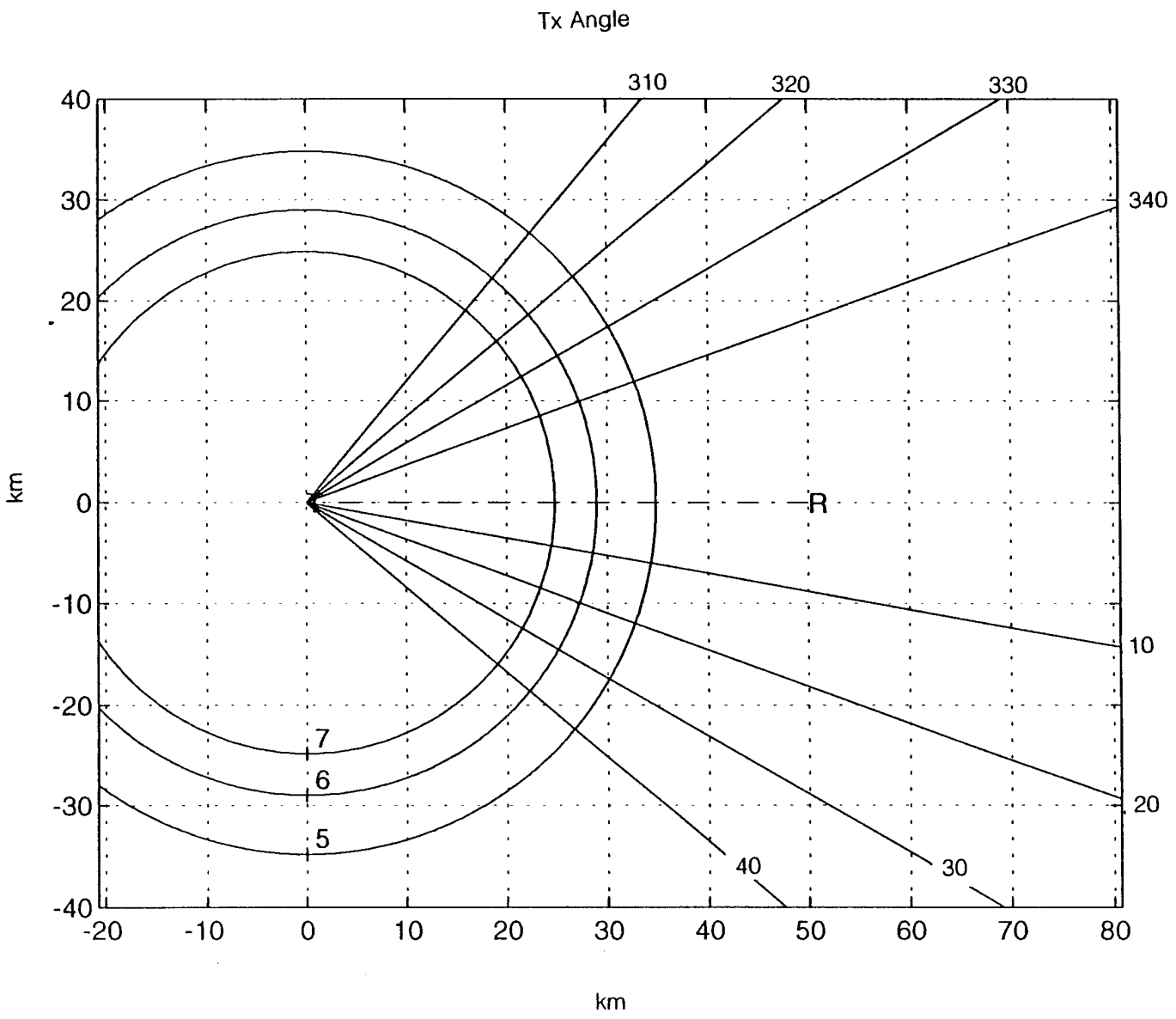

FIGURE 4-24 DATA SELECTION BASED UPON TRANSMITTER GRAZING ANGLE

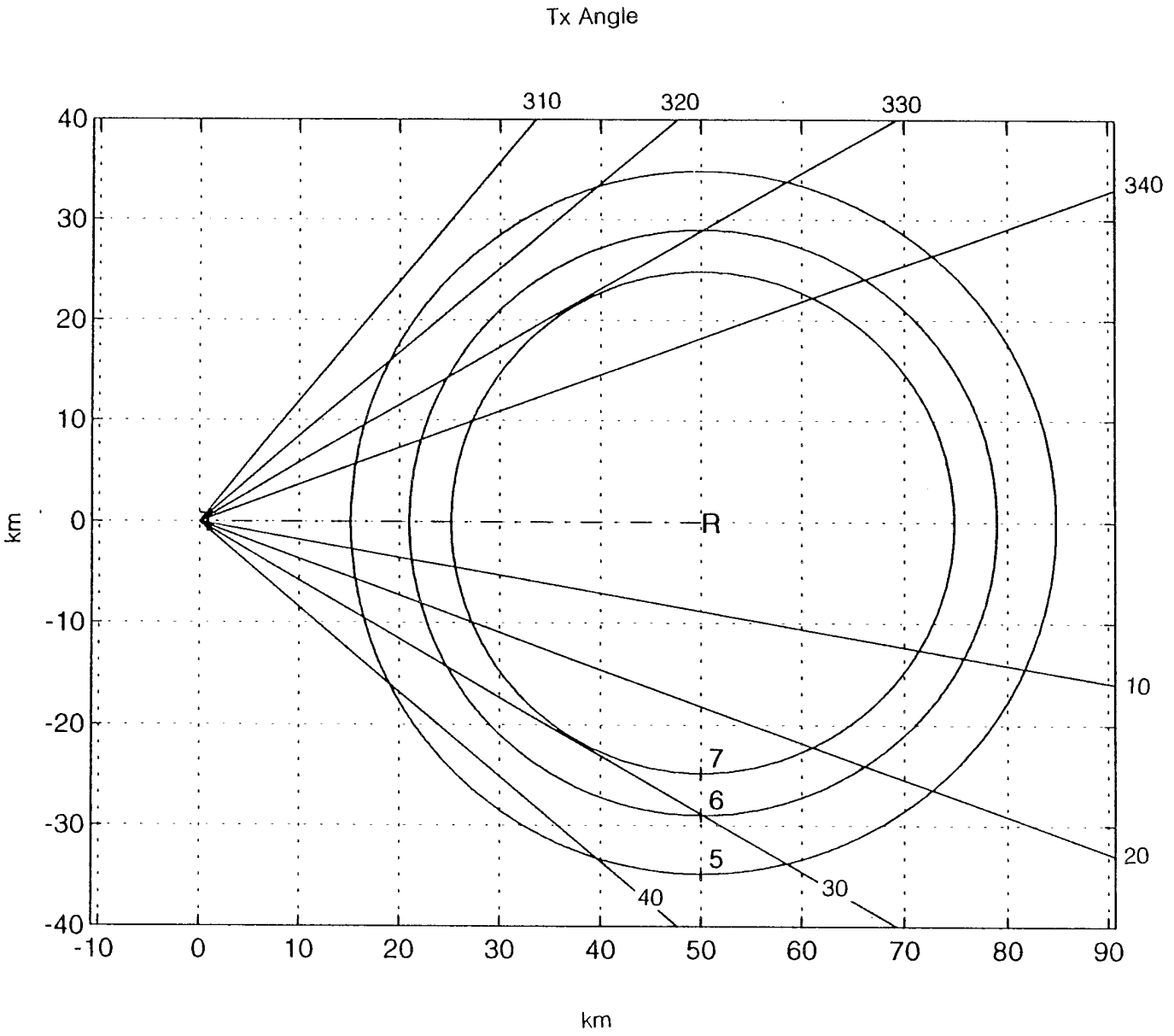

FIGURE 4-25 DATA SELECTION BASED UPON RECEIVER GRAZING ANGLE

50 to 60 degrees. The shaded areas are the data locations. Figures 4-24 and 4-25 depict the collection regions for transmit grazing angle and receive grazing angle respectively. Two degree bins are chosen for grazing angle classification. The shaded areas display the data which is grouped together.

4.4 σ_0 ACCURACY

Of primary importance in any clutter measurement program is the accuracy of the results. Estimation accuracy of σ_0 depends upon the estimation accuracy of the clutter-to-noise ratio of data as well as the estimation accuracy of the parameters of the system and environment used to calculate σ_0. Recall from section 4.1.3.3 that we are using a direct path calibration technique. Thus we have:

$$\sigma_0 = \frac{4\pi R_R^2 R_T^2 G_T(\theta_{AZ},\theta_{EL}) A_e(\phi_{AZI}\phi_{EL})}{(SNR_d)(CNR) R_d^2 L_{AT} A_C G_T(0°,\theta_{ELC}) A_e(\phi_{AZC},\phi_{ELC})} \qquad (19)$$

where:

$G_T(\theta_{AZ}, \theta_{EL})$	=	Gain Pattern of Transmit Antenna in direction of receiver
θ_{AZ}	=	Transmit Azimuth Angle (relative to peak)
θ_{EL}	=	Transmit Elevation Angle
$A_e(\phi_{AZ}, \phi_{EL})$	=	Effective Receive Aperture in direction of transmitter
ϕ_{AZ}	=	Receive Azimuth Angle
ϕ_{EL}	=	Receive Elevation Angle
R_d	=	Range from Transmitter to Receiver
L_{AT}	=	Attenuator Loss
q_{ELC}	=	El Angle of Clutter Relative to Transmitter
ϕ_{AZC}	=	Az Angle of Clutter Relative to Receiver
ϕ_{ELC}	=	El Angle of Clutter Relative to Receiver
A_C	=	Clutter Patch Area
R_T	=	Range from Transmitter to Clutter
R_R	=	Range from Receiver to Clutter

RMS uncertainties in calculating σ_0 for this test:

Transmitter - Waveform	
Tx Azimuth Pattern	1.0 dB
Tx Elevation Pattern	1.0 dB
Receiver	
Signal Processor (NCI, Quantization Error)	1.2 dB
Receive Azimuth Pattern	2.0 dB
Receive Elevation Pattern	2.0 dB
Other	
Area Illuminated	1.0 dB
Dwell Position	0.6 dB
Miscellaneous	1.0 dB
RMS Total	3.7 dB

TABLE 4-6. σ_0 CALCULATION UNCERTAINTIES AND ERRORS

TRANSMITTER PATTERN

The transmit antenna pattern has been measured and was provided to SRC. A 1 dB uncertainty has been assigned to both the azimuth and elevation dimensions to allow for altitude uncertainties, scan synchronization, errors, etc.

RECEIVER

Signal Processor

SRC modeled the signal processing function including NCI and obtained the plot of Figure 4-16 for the standard deviation of SNR estimates of various input signal levels. For the lower signal-to-noise rations, there is nearly a 1.2 dB error. There is also about a 0.1 dB error due to quantization noise.

Antenna Pattern

We estimate an uncertainty of 2.0 dB in both the elevation and azimuth patterns of the receive antennas based upon experience and upon actual measurements. It is, of course difficult to predict or measure the gain of an antenna mounted on an aircraft. Furthermore, there is some uncertainty in the orientation of the aircraft as derived from the compass or GPS which translates to gain uncertainty.

OTHER

Area Illuminated

The area calculation is based upon the area illuminated by the 3 dB antenna beam in each range gate. This is only an approximation since the antenna pattern is complex and all areas are being illuminated to some degree. A 1 dB uncertainty is assigned to the area calculation.

Dwell Position

It is thought that the clutter response in some cells may be dominated by a few or even one scatterer. In such cases, the position of the dwell in time relative to the time when the transmit beam passes by the scatterer will affect the integrated signal to noise ratio. A plot of the variation is given in Figure 4-26. The uncertainty caused by this variation is 0.6 dB. This is a worst-case estimate. In general, the clutter collected under this effort should be fairly homogeneous such that this uncertainty is much less.

Miscellaneous

1 dB of uncertainties are included for miscellaneous unknowns including the uncertainty due to SNR.

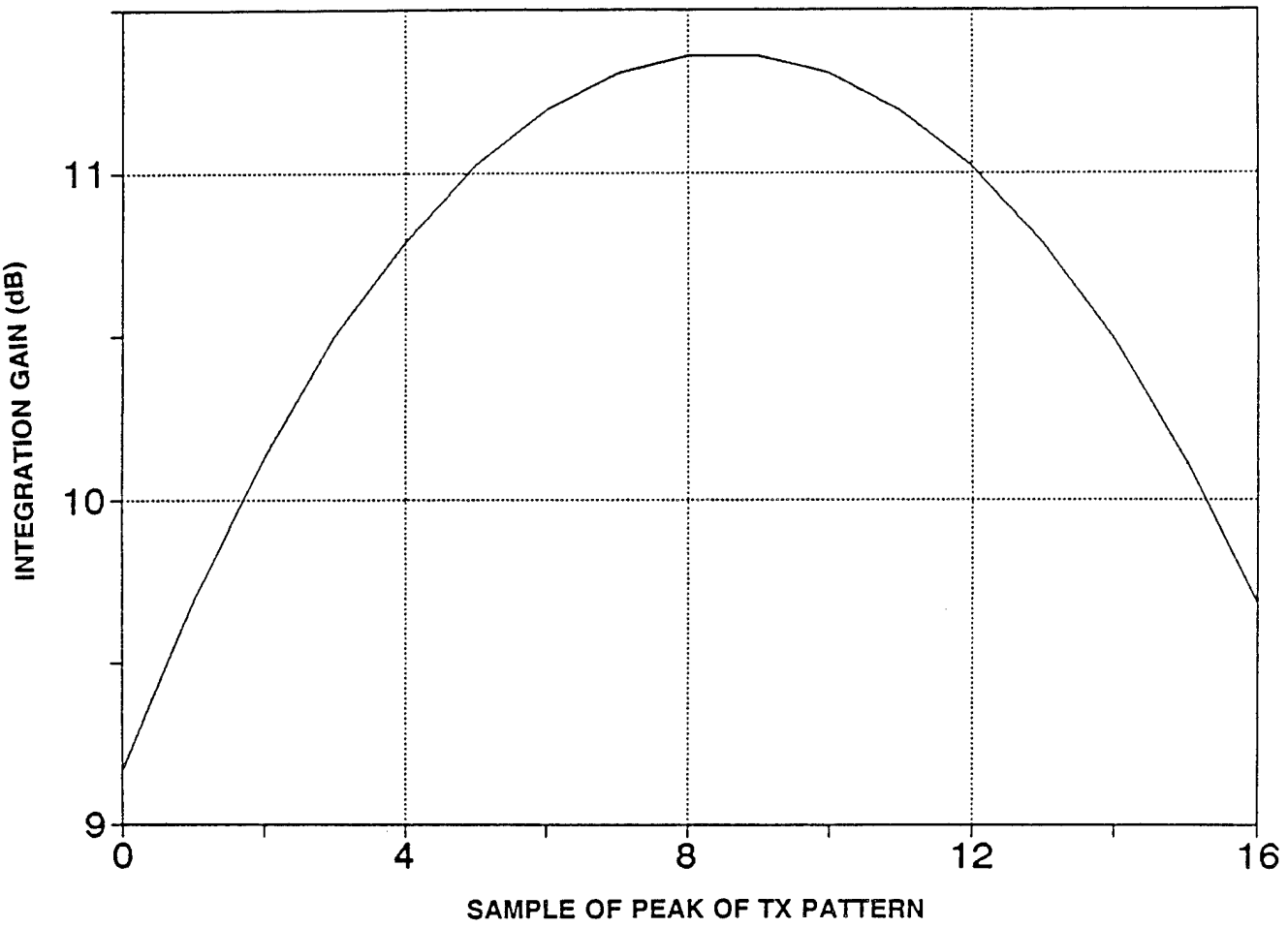

FIGURE 4-26 INTEGRATION GAIN VS. POSITION IN DWELL

We must allow an additional 1 dB of uncertainty for data with valid flag (VF) equal to 2, due to lower SNR or signal to direct path ratio. This results in an overall uncertainty of 3.8 dB rather than 3.7 dB.

Note that in some of the lower out-of-plane angle data, the standard deviations are relatively large. It is not known for certain at this time if this is due to actual fluctuation of the clutter of if there is another source of uncertainty not yet taken into account.

5.0 SUMMARY AND CONCLUSIONS

SRC has demonstrated under this and previous efforts that AMBIS is capable of collecting calibrated clutter data at both L-Band and S-Band. This clutter data is then further processed to yield estimates of Sigma Zero. The uncertainty in the data collected is primarily a function of the transmitter used. Under the first two phases of the data collection, we were limited by the altitudes of the transmitters; uncertainties in the transmitter elevation patterns, which was aggravated by low-angle multipath effects; and the relatively long pulsewidth of the Remsen radar. As a result, limitations were experienced in the maximum bistatic angles of the clutter data collected. We were also limited to low grazing angles. As a result the σ_0 uncertainties were larger than they could have been, had we been able to obtain more complete transmitter information. Testing for this effort (Phase 3) addressed these specific problems. The aerostat-based S-band transmitter has a 1.2 msec simple pulse waveform which enable uncorrupted data to be obtained at shorter time delays from the direct path. Patterns for the transmitter were obtained and the data collection was performed with an airborne transmitter (tethered) and receiver (moving). Since both receiver and transmitter operated at 10,000 feet, good direct path calibrated data could be obtained. It was possible to separate, in time delay, the direct path signal from any multipath return so as to obtain a good clean signal with which to perform direct path calibration. The σ_0 uncertainties were significantly lower during these tests, and grazing angles varied from less than 1 degree to almost 20 degrees.

Unfortunately, the terrain types over which data were collected were limited. Substantial amounts of data were collected for Gulf (wave heights under 4 feet) and Ocean (wave heights 4-8 feet) terrain types. A significant amount of data was also collected for the Everglades terrain. The Keys terrain was limited and as a result, separated into Keys and Key with Water classifications. We were unable to collect any data which could be classified as Urban. The test plan called for a flight profile in the Greater Miami area in order to collect Urban data. Air Traffic Control in Miami placed some restrictions on our flight. They wanted it restricted to weekends only (Sat, Sun) and also to a time window of 11 pm to 5 am. As it turned out, bad weather during that data collection window resulted in the aerostat being brought down and tied

to its tower. That particular profile was to collect the urban data as well as some Everglades data at low out-of-plane angles. Since the collection did not take place, the only Everglades classified data collected was during files 4 and 8 of the Gulf profiles. As a result, the data was limited in out-of-plane angle as well as transmit and receive grazing angles.

The profiles and transmitter pointing angles were chosen such that low out-of-plane angles would be obtained. However, when processing the data we became aware of "filter-ringing" in our data. The AMBIS system was designed with extremely good anti-aliasing filters. These sharp frequency response filters (for bandwidth) result in a time domain ring which is evident in the data. Valid data is considered to be 15 dB above the experienced ringing. Much of the low out-of-plane angle data is found at the short bistatic ranges (or time delays) and does not exceed the relative filter ringing level by 15 dB. Hence the low out-of-plane angle data does not satisfy the validity criteria. The lowest valid out-of-plane angle data is in the 20-30 degree range. It was hoped that this program would provide data at low out-of-plane angles to validate bistatic clutter models in the specular region. The data contained in this report does not satisfy that requirement. Some preliminary work has been done which indicates that an inverse filter can be constructed to "undo" much of the filter ringing. At least 10-15 dB of improvement can be obtained at short ranges. It is estimated that at least 10,000 - 15,000 samples of low out-of-plane clutter σ_0 data can be recovered from the existing Cudjoe Key data set by using the inverse filter technique. It is therefore recommended that this be done as a future effort.

SRC also ran a test in June-July 1994 which involved clutter data collection in the Seattle, Washington area. An airborne, moving transmitter (S-band) was combined with the AMBIS system to collect data over Bare Mountain Peaks (BMP), Vegetated Farm Land (VFL), and the Ocean. A description of the test and the reduced data will be given in a separate document.

APPENDIX A

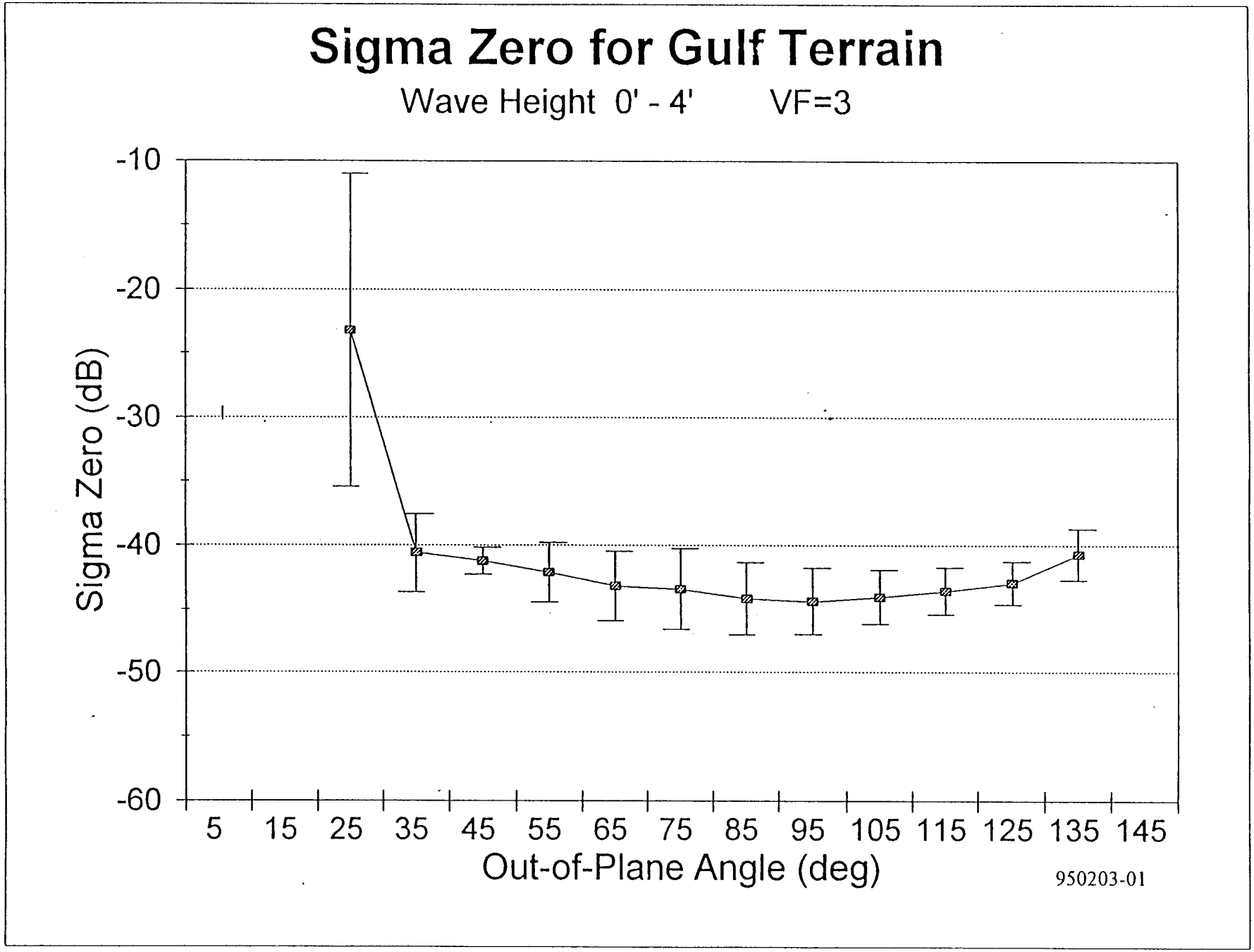
Sigma Zero for Gulf Terrain
Wave Height 0' - 4'
VF=3
Sigma Zero (dB)
-10
-20
-30
-40
-50
-60
5
15
25
35
45
55
65
75
85
95
105
115
125
135
145
Out-of-Plane Angle (deg)
950203-01

Samples for Gulf Statistics

Wave Height 0' - 4' VF=3

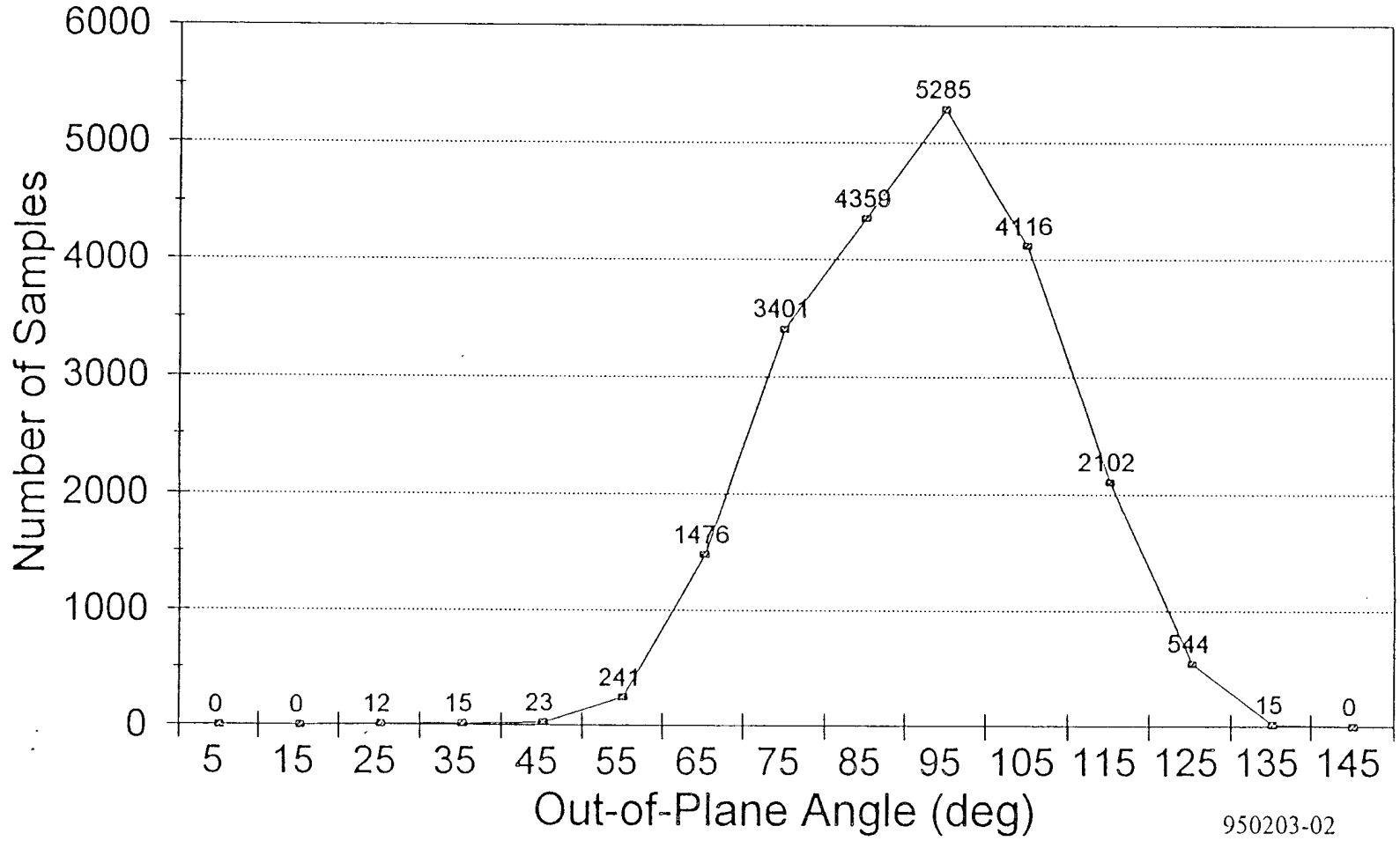

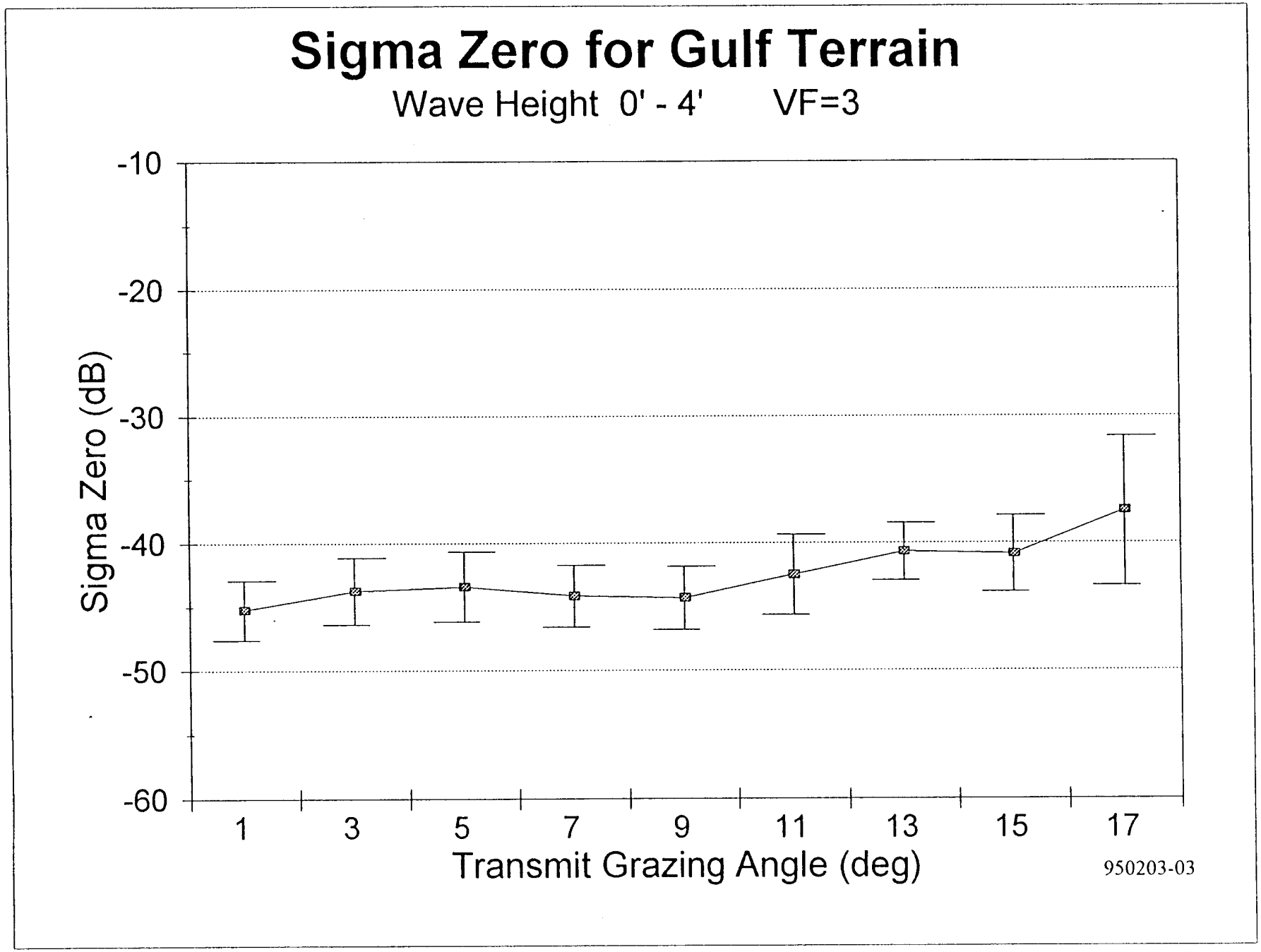
Sigma Zero for Gulf Terrain
Wave Height 0' - 4' VF=3
-10
-20
-30
-40
-50
-60
Sigma Zero (dB)
1
3
5
7
9
11
13
15
17
Transmit Grazing Angle (deg)
950203-03

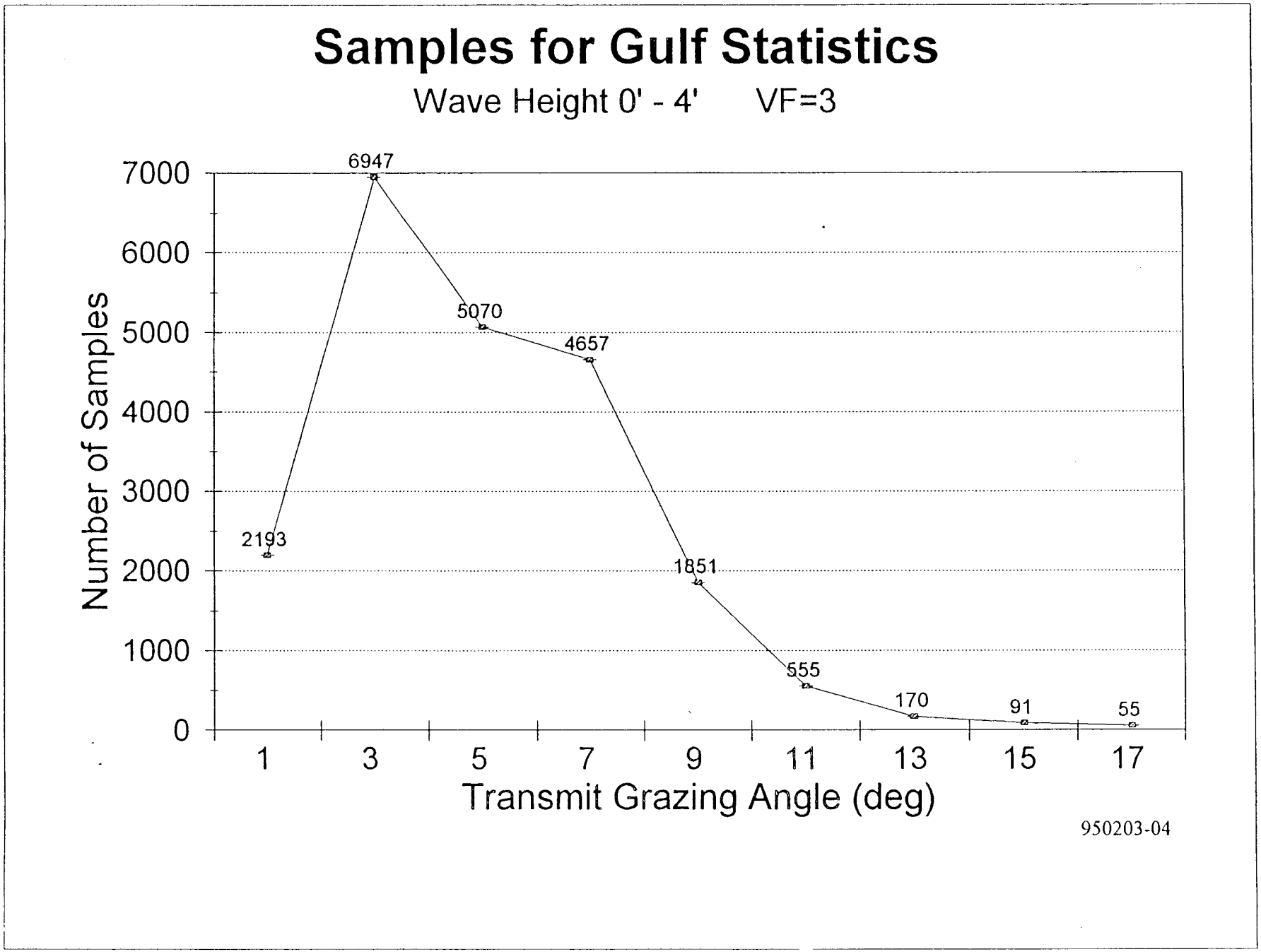
Samples for Gulf Statistics
Wave Height 0' - 4' VF=3
Number of Samples
7000
6000
5000
4000
3000
2000
1000
0
6947
5070
4657
2193
1851
555
170
91
55
1
3
5
7
9
11
13
15
17
Transmit Grazing Angle (deg)
950203-04

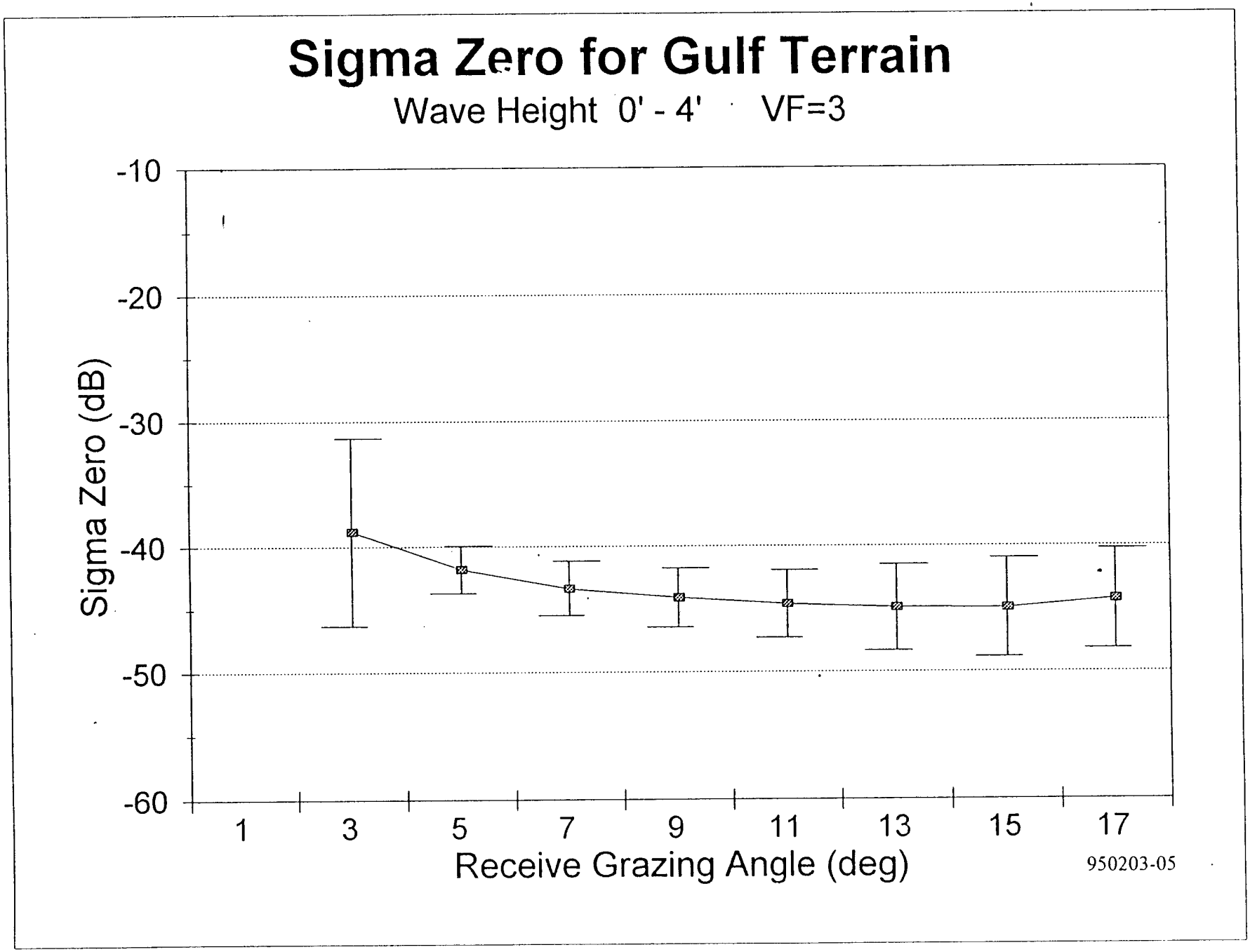
Sigma Zero for Gulf Terrain
Wave Height 0' - 4' VF=3
-10
-20
-30
-40
-50
-60
Sigma Zero (dB)
1
3
5
7
9
11
13
15
17
Receive Grazing Angle (deg)
950203-05

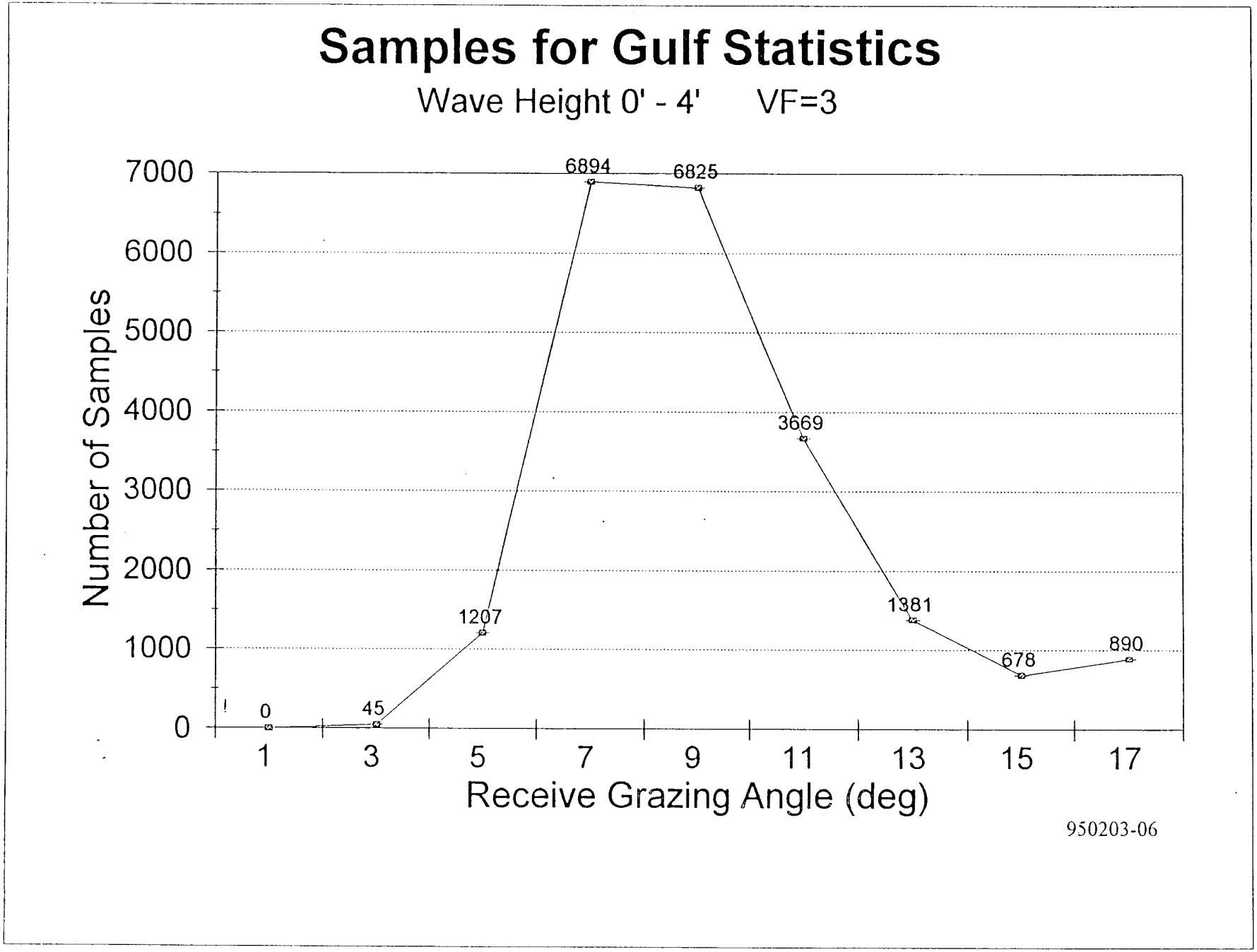
Samples for Gulf Statistics
Wave Height 0' - 4' VF=3
Number of Samples
7000
6000
5000
4000
3000
2000
1000
0
6894
6825
3669
1381
1207
890
678
0
45
1
3
5
7
9
11
13
15
17
Receive Grazing Angle (deg)
950203-06